TU

Technische Universität Wien

DISSERTATION

Hierarchically Structured (Organo-)Silica Monoliths

ausgeführt zum Zwecke der Erlangung des akademischen Grades eines Doktors der technischen Wissenschaften unter der Leitung von

Prof. Dr. Nicola Hüsing

Institut für Anorganische Chemie I, Universität Ulm

(vormals 165, Institut für Materialchemie, TU Wien)

eingereicht an der Technischen Universität Wien

Fakultät für Technische Chemie

von

Doris Brandhuber

9725245

Alserstrasse 57/12, A-1080 Wien

Wien, am 15. 12. 2005

Kurzfassung der Dissertation

Ziel dieser Arbeit war die Sol-Gel Synthese von monolithischen meso-/makroporösen (Organo-)Silica Materialien mit einer Organisation der Strukturelemente auf mehreren hierarchischen Ebenen vom molekularen bis in den makroskopischen Bereich. Dies ist ein notwendiger Schritt, um das Anwendungsfenster mesoporöser Materialien über die bereits bestehende Nutzung als beispielsweise Sorptionsmittel oder Trägermaterialien in Richtung Anwendungen im 'Life-Science'-Bereich zu erweitern. Viele Anwendungen, wie etwa die Chromatographie, Trennung (biologischer) Makromoleküle, oder Freisetzung von pharmazeutischen Wirkstoffen, verlangen nach Materialien mit sowohl kleinen als auch großen Poren, die in einer hierarchischen Weise aufgebaut sind. Zusätzlich dazu können auch chemische Modifikationen der Oberfläche oder des Netwerks der silikatischen Materialien für solche Anwendungen von Nutzen sein. Der Einbau funktioneller organischer Gruppen ermöglicht die Einführung neuer Materialeigenschaften und durch die maßgeschneiderte Poren-Chemie können die Materialien für ein breiteres Anwendungsspektrum genutzt werden.

Diese Arbeit präsentiert Materialien mit einem neuartigen hierarchischen Aufbau:

Molekulare Ebene   Organo-Silica Hybrid Netzwerk.

Nanometer Ebene   Periodisch angeordnetes Mesoporesystem.

Mikrometer Ebene   Makroporöses Gerüst.

Millimeter Ebene   Monolithische Form.

Der absolut neue Aspekt dieser Arbeit ist die hoch periodische Anordnung der Mesoporen, die sich in rein wässrigem Medium ohne weitere Zusätze wie Quellmittel oder Lösungsmittel ausbildet. Dies wurde erreicht durch spezifisches Design und Modifikation von molekularen Vorstufen im Hinblick auf maximale Kompatibilität mit der Entstehung der Mesostruktur bei der Herstellung eines monolithischen Materials: die in Sol-Gel Synthesen üblicherweise verwendeten Alkoxysilane wurden mit Glykolen substituiert. Diese neuartigen Glykol-modifizierten (Organo-)Silane wurden in einem einfachen sog. 'True Liquid-Crystal Templating'-Verfahren umgesetzt. Dieser Ansatz eröffnete Wege zur Synthese einer Vielzahl neuer Materialen mit maßgeschneiderter Porosität und Chemie des Netzwerks.

Überdies wurden die Prozessschritte, die zur Erhaltung einer monolitischen Struktur während der Trocknung und die zum Entfernen des Mesoporen-Templats nötig sind, mit einem Prozess zur chemischen Modifikation der Oberfläche kombiniert: Silylierung mit funktionellen Organosilanen. Mit der Oberflächensilylierung wird zugleich das Templat aus der Porenstruktur entfernt und die modifizierten Monolithe können einfach bei Atmosphärendruck ohne Rissbildung getrocknet werden. Die Verfahren, die im Rahmen dieser Arbeit entwickelt wurden, erlauben nicht nur eine beliebige Gestaltung der Oberflächenchemie, sondern führen reduzieren erheblich die Anzahl an Syntheseschritten, die zur Herstellung eines porösen, monolithischen Materials nötig sind.

Das letzte Kapitel ist ein Ausblick auf das hohe Anwendungspotential der in dieser Arbeit vorgestellten Materialien. Ein hierarchisch aufgebauter Monolith ist als Säulenmaterial für die HPLC ('High Performance Liquid Chromatography') in Kooperation mit einem Industriepartner getestet worden und zeigte erste, vielversprechende Ergebnisse.

Abstract

This work deals with the sol-gel synthesis of monolithic meso-/macroporous (organo-)silica materials with structural organization on several hierarchical levels from the molecular- to the macroscale. This is a necessary step forward to expanding the application window of mesoporous materials beyond the scope of their use as e.g. sorbents or support materials in the direction of applications in the life science area. For many applications, such as chromatography, separation of large molecules, or drug release, to name a few, materials with both small and large pores arranged in a hierarchical structure-in-structure fashion are desirable. Additional surface or network functionalization of the siliceous materials can provide value in such applications as well. The incorporation of functional organic groups allows the implementation of new properties and the tailored pore chemistry makes the materials viable for a broader spectrum of applications.

This work presents materials with a novel hierarchical build-up:

Molecular Level   Organo-silica hybrid framework.

Nanometer Level   Periodically ordered mesopore system.

Micrometer Level   Macroporous scaffold.

Millimeter Level   Monolithic shape.

The absolutely novel aspect of this work is the highly periodic arrangement of the mesopores, which forms in purely aqueous medium without additives such as swelling agents or co-solvents. This was achieved by specific design/modification of molecular precursors with respect to maximum compatibility with the mesostructure formation when synthesizing a monolithic material: the typically in sol-gel syntheses applied alkoxysilanes were substituted with glycols. These novel glycol-modified (organo-)silanes were applied in a simple true liquid-crystal templating approach, which opened the way to a huge variety of new materials with a tailored porosity and network chemistry.

Furthermore, the processing steps necessary to maintain a monolithic structure during drying and for removal of the template were combined with a chemical surface modification

process: silylation with functional organosilanes. Together with the surface silylation reaction, the template is removed from the porous structure and the modified monoliths can then be easily dried at ambient pressure without cracking. The processes developed in the course of this work do not only allow for a deliberate tailoring of the surface chemistry, but also significantly reduce the number of synthetic steps necessary to obtain a porous, monolithic material.

The last chapter gives an outlook on the high application potential of the materials presented in this work. A hierarchically organized monolith has been tested as column material for HPLC (high performance liquid chromatography) in cooperation with an industrial partner and showed first, very promising results.

Some part of this work has been published:

1. Brandhuber, D., Peterlik, H. & Huesing, N. Facile Self-Assembly Processes to Phenylene-bridged Silica Monoliths with Four Levels of Hierarchy. *Small* **in press** (2005).

2. Brandhuber, D., Peterlik, H. & Huesing, N. Simultaneous drying and chemical modification of hierarchically organized silica monoliths with organofunctional silanes. *Journal of Materials Chemistry* **15**, 3896-3902 (2005).

3. Brandhuber, D., Torma, V., Raab, C., Peterlik, H., Kulak, A. & Huesing, N. Glycol-Modified Silanes in the Synthesis of Mesoscopically Organized Silica Monoliths with Hierarchical Porosity. *Chemistry of Materials* **17**, 4262-4271 (2005).

4. Brandhuber, D., Huesing, N., Raab, C. K., Torma, V. & Peterlik, H. Cellular mesoscopically organized silica monoliths with tailored surface chemistry by one-step drying/extraction/surface modification processes. *Journal of Materials Chemistry* **15**, 1801-1806 (2005).

5. Brandhuber, D., Huesing, N. & Peterlik, H. Inorganic-organic hybrid hierarchically structured methyl-modified silica monoliths. *Materials Research Society Symposium Proceedings* **847**, 127-134 (2005).

to Amit

fundamental researcher

Acknowledgement

I am deeply indebted to *Prof. Nicola Hüsing* for her supportive and considerate supervision of my thesis, for challenge and help, and her continuous interest in my work, also with regard to my future career.

My sincere thanks also go to *Prof. Ulrich Schubert* for giving me the opportunity to undertake my thesis in his research group and in particular for enabling and promoting my academic career.

Special thanks go to *Prof. Herwig Peterlik* for his help and support small angle X-ray scattering and any other sort of concern, for the many productive and interesting discussions and his advice. I thank for his sedulous enthusiasm to engage in our projects and for his ideas.

My thanks go to all my colleagues and former colleagues from the group in Vienna: *Akira, Christian, Christina F.* (for being a great company and hotel room sharer), *Christoph, Claudia F., Claudia V., Denise, Didi, Dieter H., Dieter R., Dominique, Doris, Fatmir, Grace, Guido, Harald, Helmut, Jim, Maia, Melitta* (for being a reliable running and conversational partner helping me to keep physically and mentally fit), *Michael* (for training and help on the NMR instruments), *Mirka, Patrycja, Ralf* (for being really challenging and absolutely hilarious), *René, Philip, Sandra, Susan, Sorin* (my favourite flatmate), *Thomas* (for a really nice trip to Venice and Wörthersee after my first (exhausting) stay at Elettra), *Uli, Viki, Wolfgang*;

And from the group in Ulm: *Alper, Christine, Conny, Prof. Debaerdemaeker, Frau Feniuk, Jasmin, Joe, Jürgen, Herrn Opferkuch, Petra* (for doing SEM measurements), *Steffi* (for joining me for lunch, chatting, keeping a good mood during the Elettra stay and being a very bright person), *Sarah, Susan,* and *Andi* (from the Group for Macromolecular Chemistry for arranging for me to use the ultracentrifuge).

To the students who volunteered to do laboratory work for my thesis: *Ruth, Chistoph, Stefan* (for sharing a curious period of my life), *Robert, Carlos, Christian (Tontsch)* and *Markus.*

Acknoledgement

Thanks to *Dr. Johannes Bernardi* for TEM measurements, *Dr. Sigrid Bernsdorff* from the Elettra Synchrotron, Trieste/Italy, *Dr. Wolfgang Binder* for solid state NMR measurements, and *Dr. Alexander Kulak* and *Elisabeth Eitenberger* for SEM measurements.

Special thanks go to my chemist-friends: *Ellen, Georg* and *Robert;* Stammtisch-friends *Alois, Heinz* (for being a very warmhearted yet forthright friend), *Helmut, Martin, Oliver, Matthias* and *Waldl;* rest of the world friends: *Andreas* (lovely cousin, for open ear, heart and mouth), *René, Ferdi;* former flatmate-friends *Marco and Sylvester* (for participating, joining and helping me to evolve).

My final and greatest debt is to my parents for their perpetual love and support.

Special thanks also to my brothers Andi and Michael.

To Hannes for all that comes about.

List of Abbreviations and Symbols

2D	2-dimensional
AER	aerogel
a. u.	arbitrary units
BET	Brunauer, Emmett, Teller
BJH	Barrett, Joyner, Halenda
C	C-parameter (nitrogen sorption)
CP	cross polarization
cps	counts per second
d	d-spacing
D^{BJH}	BJH pore diameter
dc	degree of condensation
DNA	desoxyribonucleic acid
exp.	experimental
HMBC	heteronuclear multiple bond correlation
HPLC	high performance liquid chromatography
I	intensity
IUPAC	International Union of Pure and Applied Chemistry
LC	liquid crystal
MAS NMR	magic angle spinning NMR
MW	molecular weight
NMR	nuclear magnetic resonance
NUC	Nucleosil® 100-10
p_c	critical pressure
P_c	capillary pressure
PMO	periodic mesoporous organo-silica
ppm	parts per million
p/p_0	relative pressure
PZC	point of zero charge
R, R´	alkyl/aryl group
RO	alkoxy group
ROH	alcohol

RP	reversed phase
RT	room temperature
SANS	small angle neutron scattering
SAXS	small angle X-ray scattering
scf	supercritical fluid
S^{BET}	BET surface area
SEM	scanning electron microscopy
SP	single pulse
t	thickness
T_c	critical temperature
TDS	template displacement
TEM	transmission electron microscopy
TGA	thermogravimetric analysis
theor.	theoretical
TLCT	true liquid crystal templating
t^{gel}	gelation time
t^{wall}	pore wall thickness
UV	ultraviolet
$V^{t(ot)}$, V^{micro}, V^{meso}, V^{macro}	total-, micro-, meso-, macro- porevolume
v/v	volume fraction
w	full width at half maximum
WAXS	wide angle X-ray scattering
w/w	weight fraction
XRD	X-ray diffraction

Precursor Abbreviations:

bEt	ethylene-bridged
bEtGMS	1,2-bis[tris-(2-hydroxyethoxy)silyl]ethane
	ethylene glycol-modified ethylene-bridged silane
bPh	phenylene-bridged
bPhGMS	1,4-bis[tris-(2-hydroxyethoxy)silyl]benzene
	ethylene glycol-modified phenylene-bridged silane
EGMS	tetrakis-(2-hydroxyethyl)-orthosilicate

	ethylene glycol-modified silane
GLMS	tetrakis-(2,3-hydroxypropyl)-orthosilicate glycerol-modified silane
Me	methyl
MeGMS	tris-(2-hydroxyethoxy)methylsilane ethylene glycol-modified methylsilane
Or	organosilane
OrGMS	glycol-modified organosilane
PGMS	tetrakis-(2-hydroxypropyl)-orthosilicate glycol-modified silane
Ph	phenyl
PhGMS	tris-(2-hydroxyethoxy)phenylsilane ethylene glycol-modified phenylsilane

Surface modification agents:

ala	alaninedimethylsilyl
aza	aminopropylsilyl
azas	3-[(2,2-dimethyl-1-aza-2-silacyclopent-1-yl)dimethylsilyl]-1-propanamine
mms	(methylmethacryloyl)dimethylsilyl
mmds	(methylmethacryloyl)dimethylmethoxysilane
mps	mercaptopropylsilyl
mpts	mercaptopropyl-trimethoxysilane
phs	phenylsilyl
ptms	phenyltrimethoxysilane
rac-34	rac-3-(dimethyl(phenyl)silyl)alanineethylester
tms	trimethylsilyl
tmcs	trimethylchlorosilane
tmps	trimethylphenylsilane
cdcs	chloromethyldimethylchlorosilane
cds	chloromethyldimethylsilyl
vdcs	vinyldimethylchlorosilane
vds	vinyldimethylsilyl

Chemicals:

EG	ethylene glycol
GL	glycerol
PG	propylene glycol
P123	block copolymer Pluronic P123, $PEO_{20}PPO_{70}PEO_{20}$
PE	petroleum ether
(P)EO	(poly)(ethylene oxide)
PMMA	poly(methyl methacrylate)
(P)PO	(poly)(propylene oxide)
TEOS	tetraethyl-orthosilicate
THF	tetrahydrofurane
TMOS	tetramethyl-orthosilicate

Symbols:

δ	chemical shift (NMR)
θ	scattering angle (XRD), contact angle
λ	wavelength
γ_{LV}	liquid/vapour surface tension
q	scattering vector

Table of Contents

Table of Contents

Table of Contents

---

1 Introduction

1.1. Motivation

One of the key aims of modern chemistry is to explore and exploit the phenomenal structural and chemical complexity of matter that seems to arise spontaneously within ambient environments like that of our planet.[1-3] The ability to organize nanostructures across extended length scales is a key issue in the design of integrated materials with advanced functions. Although many approaches seek to mimic the information processing and sensing capabilities of biological nanostructures, they often lack the inherent materials-building properties typical of organisms, which are essential if nanostructures are to be organized across many length scales and used as functional materials within integrated systems. Different strategies have been developed for the long-range organization and assembly of nanostructured phases. Current approaches tend to be based on physical methods, such as patterning, rather than the spontaneous chemical assembly and transformation of building blocks across multiple length scales. Also, chemical and microfabrication methods are being combined to produce externally patterned materials,[4,5] whereas spontaneous processes associated with solvent evaporation[6,7], molecular cross-linking,[8,9] or programmed recognition[10,11] have been used to control the deposition of nanoparticle-based superlattices. Although promising, these approaches have disadvantages associated with the sequential processing and the physical fabrication, as well as limitations arising from the restricted number of superlattices available because of thermodynamic (packing) constraints on self-assembly. Indeed, structural organization in many of these systems depends on physics and crystal engineering rather than chemistry.

Rather than rationally develop a hierarchical material via sequential transformations that require intervention after each step, biomimetic approaches aim for a chemistry of organized matter based on emergent processes, in which time- and scale-dependent coupling of interactive components generate higher order architectures with embedded structure.[2] Biology is an ultimate manifestation of a universal chemical canon encompassing interactions both at the molecular and supramolecular level. Inorganic building blocks play a significant role in the self-organised assembly of many biological structures at various length-scales, however, the details of their chemical behaviour and interaction with organic compounds are still not well understood. The basis of spontaneous generation of organization is to understand

how the initial conditions and the environment engender the scale-dependent emergent behaviour needed to create hierarchical structures. This mimickes the approach of nature and it is the general philosophy behind bottom-up nanotechnology. In such cases, the embedding of structures over multiple length scales will arise as an emergent property that is not necessarily related to the smallest building blocks but is dependent on how these units evolve in time and space. Thus, different driving forces will operate at various stages along the synthesis-construction pathway such that these forces become superimposed mechanistically. For example, whereas localized molecular interactions can dominate transitions on the nanoscale, surface forces are important in determining how nanostructures become assembled at the mesoscopic level. And beyond the colloidal regime, mechanical forces, such as internal strain, can drive transformations that result in macroscopic order.

Soft chemistry-based processes (i.e., chemistry at low temperature and pressures, from molecular or colloidal precursors) offer innovative strategies to obtain tailored nanostructured materials in a biomimetic fashion.[12] The mild conditions of sol-gel chemistry provide reacting systems mostly under kinetic control.[13] Therefore, slight changes of experimental parameters (i.e., pH, concentrations, temperatures, nature of the solvent, counterions) can lead to substantial modifications of the resulting supramolecular assemblies. This may give rise to inorganic or hybrid solids with enormous differences in morphology and structure and, hence, in their properties. However, the resulting nanostructures, their degree of organization, and thus their properties certainly depend on the chemical nature of their organic and inorganic components, but they rely also on the synergy between these components. Thus, the tuning of the nature, the extent, the accessability, and the curvature of the hybrid interfaces is a key point in the design of new nanostructured materials. The growth of soft chemistry derived inorganic or hybrid networks templated by organized surfactant assemblies (structure directing agents) allowed construction of a new family of nanostructured materials in the mesoscpic scale (2-100 nm): the best example is the ever-growing family of meso-organized hybrids or mesoporous materials.[14-24]

This work deals with the sol-gel synthesis of monolithic meso-/macroporous (organo-) silica materials with structural organization on several hierarchical levels from the molecular- to the macroscale. This is a necessary step forward to expanding the application window of mesoporous materials beyond the scope of their use as sorbents, support materials, etc. in the direction of applications in the life science area. For many applications, such as

5

chromatography, separation of large molecules, or drug release, to name a few, materials with both small and large pores arranged in a hierarchical structure-in-structure fashion are desireable[21,25-30]. Ordered uniform mesopores like those of SBA-15 materials provide a high surface area and size-selectivity,[31] macropores provide access to the mesopore structure, maximize mass transport and minimize the pressure drop over the material in applications such as HPLC. Additional surface functionalization of the siliceous materials can provide value in such applications as well.[32-34] The incorporation of functional organic groups allows the implementation of new properties and the tailored pore chemistry makes the materials viable for a broader spectrum of applications, for example in catalysis, separation technologies, (bio-)immobilization, and also for sensors.

In the course of this work, materials with the following hierarchical build-up were developed:

Molecular Level   Integrating organic functionality into the amorphous silica framework either distributed within the silica network or grafted onto the surface.

Nanometer Level   Periodically ordered mesopore-system in the fashion of SBA-materials.

Micrometer Level   Macroporous framework.

Millimeter Level   Monolithic shape.

As a general principle, spontaneous self-organization, in that all structural features should evolve in a synchronized fashion under mild synthetic conditions, and also reduction of synthetic steps and chemical components were aspired. This was to be achieved by specific design/modification of the molecular precursor with respect to maximum compatibility with the mesostructure formation when synthesizing a monolithic material. Furthermore, the processing steps necessary to maintain a monolithic structure during drying and to extract the surfactant were combined with a chemical modification, therefore reducing the number of synthetic steps.

1.2. Sol-Gel Chemistry

1.2.1. Amorphous Silica Materials – Tetraalkoxysilanes

Amorphous silica from molecular alkoxide precursors $(RO)_4Si$ can be obtained by acid or base catalysed hydrolysis and condensation in alcohol-water media[13]. The most commonly used precursors are tetramethoxysilane (TMOS, R=Me) and tetraethoxysilane (TEOS, R=Et).

General reactions:

(1) $\equiv Si\text{-}OR + H_2O \equiv$ $\rightleftharpoons$ $Si\text{-}OH + ROH$ Hydrolysis

(2) $\equiv Si\text{-}OH + HO\text{-}Si \equiv$ $\rightleftharpoons$ $\equiv Si\text{-}O\text{-}Si \equiv + H_2O$

                                                        Condensation

(3) $\equiv Si\text{-}OH + RO\text{-}Si \equiv$ $\rightleftharpoons$ $\equiv Si\text{-}O\text{-}Si \equiv + ROH$
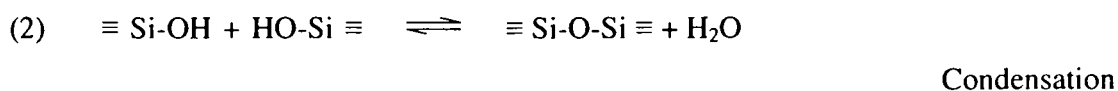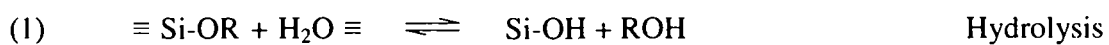
i.e. R = Me, Et

In aqueous systems, the two phase hydrolysis of TEOS is relatively slow, resulting in silicic acid that is not completely monomeric. The rate of hydrolysis is strongly dependent on the presence of an acid or base catalyst. In particular, the rate of hydrolysis correlates with the concentration of both H^+ and OH^- with a minimum at pH 7. Condensation reactions, on the other hand, are strongly influenced by the charge carried by the siliceous species. The condensation rate reveals its minimum at the point of zero charge (PZC), which is around pH 4 for monomeric silicic acid $(Si(OH)_4)$ and around pH 2.5 for pure SiO_2, i.e. it changes with ongoing condensation. Below the PZC, silica species are protonated and positively charged, whereas above the PZC, the silica species are deprotonated and negatively charged. Below the PZC, network formation is catalysed by H^+, and above the PZC, the OH^- ion is the catalyst.[35] The rate constants for the hydrolysis of each of the ethoxy groups are different, due to the inductive effects of HO- and RO-. Condensation reactions involving elimination of water and alcohol proceed concurrently. Under acidic conditions (below the PZC), the kinetics of the sol-gel reaction is governed by the condensation rate. In contrast, condensation is enhanced under alkaline conditions (above the PZC) with a control of the reaction by the hydrolysis rate. The rate of hydrolysis and condensation reactions, and therefore the overall reaction that will occur, is also highly dependent on variables such as the availability of water, the chemical

functionality of the silane, steric requirements of the alkoxy group, temperature, catalyst, reactant concentrations and the nature of the template, if one used.

Acid catalysed network formation produces linear gels with more weakly crosslinked structures than are obtained from base catalysed reactions.[36] This can be understood by a consideration of the mechanisms of the reaction.[37] Under basic conditions, the progressive increase in the rate of hydrolysis with each hydroxyl substitution creates a high concentration of growth sites and leads to highly crosslinked structures. At low pH, the electron withdrawing effect of HO- slows down the hydrolysis, thus condensation proceeds from fewer growth sites and results in linear, less crosslinked structures.

The early stage of network formation leads to the formation of ring structures, in order to maximise the number of siloxane bonds and minimise the number of uncondensed Si-OH groups[38]. The rings then link together using additional monomer to form larger three dimensional entities. These molecules condense internally, with the Si-OH groups located on the surface. The larger more dehydrated particles grow while smaller ones redissolve, depositing silica on the larger particles ('Ostwald ripening'). At higher pH, the negatively charged particles grow quickly to a temperature dependent size, but do not aggregate and coalesce due to electrostatic repulsion. At low pH the particles bear little charge and can therefore collide and aggregate to form gel networks.

The presence of structure directing agents like surfactants, lipids, block copolymers, polysaccharides, proteins, DNA etc. also influences the hydrolysis and condensation rates. In biological systems such as diatoms and sponges, the formation of solid silica structures with precisely controlled morphologies is directed by proteins and polysaccharides and occurs in water at neutral pH and ambient temperature.[39,40] Laboratory methods, in contrast, mostly rely on extreme pH conditions and/or surfactants to induce the condensation of silica precursors into specific morphologies or patterned structures.[41] TEOS is inert when mixed with water at neutral pH, but for example synthetic cysteine-lysine block copolypeptides self-assemble into structured aggregates that hydrolyse TEOS while simultaneously directing the formation of ordered silica morphologies.[42]

1.2.2. Organo-Silica Hybrid Materials – Organosilanes

Amorphous silica has been used as a host onto and into which organic functionalities have been placed for a great many years. The organic molecule may modify the mechanical

properties of the material, ease processing for various applications, or provide optical, electronic, separation, chemical, or biochemical properties.[43] The incorporation of functional organic groups allows the implementation of new properties and the tailored pore chemistry makes the materials viable for a broader spectrum of applications, for example in catalysis, for sensors or even sieving and separations.[44-46] Several pathways have been reported for the functionalization of porous silica-based systems: *Postfunctionalization* of a preformed calcined porous host via adsorption from the gas or liquid phase or *in-situ modification* directly during the synthesis by co-condensation of different silanes.[47-49]

In-Situ Modification. A route to functionalized amorphous silica materials that has been widely investigated in sol-gel chemistry involves the co-condensation of tetraalkoxysilane and organotrialkoxysilane[45,46,50-52] or organo-bridged trialkoxysilane precursors,[15,17,18,53,54] to produce hybrid inorganic-organic networks (see Figures 1.1. and 1.2). Organo-bridged silanes have the advantage that they can be used also in the pure form, as the organic moieties contribute to the build-up of the network, allowing a completely homogeneous distribution of organic moieties within the framework. In these materials, the organic moiety is covalently linked, via a non-hydrolysable Si-C bond, to a silane species that is hydrolysed to form a hybrid silica material with modified properties and reactivities (flexibility, hydrophobicity, refractive index modification, catalytic activity, etc).

The reaction rate under acidic conditions is governed by two totally different factors. The inductive effect of the alkyl group (+I effect) in alkyl-substituted alkoxysilanes increases the reaction rate, whereas bulky organic groups decrease the reaction rate because of sterical reasons. Furthermore, the chemical functionality of the substituent is of importance. For example, gelation of mixtures of organosilanes, in which the organic group contains a strongly basic constituent like an amino group ($-NH_2$) and TMOS has been found to be strongly accelerated and even taking place without addition of catalyst, as the amino group works as an 'internal catalyst'.[46] The network forming process is clearly different as both precursor species are involved in the build-up of the gel network. Sol-gel processing of mixtures of organosilanes and, for example, TMOS under base-catalyzed conditions is a two-step process in which the silica gel network is nearly exclusively built from TMOS. In the network forming stage, the organosilane acts as a co-solvent. Only in the second stage of the process the organosilane units condense on the inner surface of the then existing silica gel network.
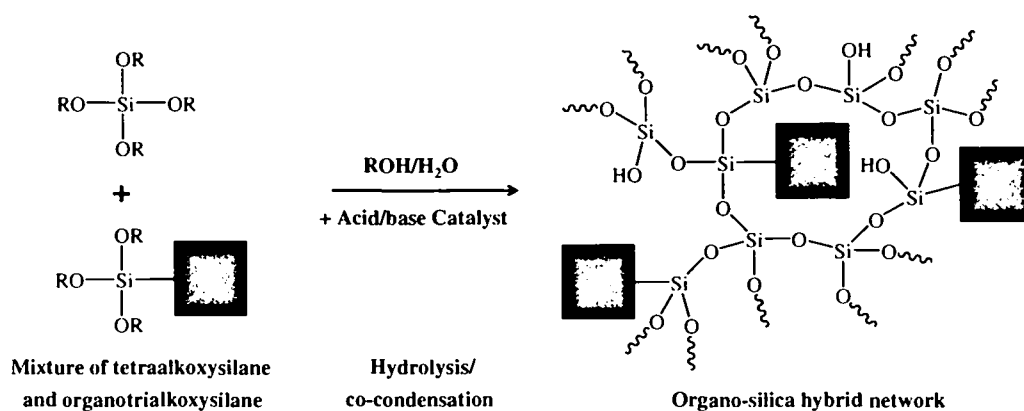
Figure 1.1. Synthesis of organo-silica hybrid materials by co-condensation of organotri- and tetraalkoxysilanes.
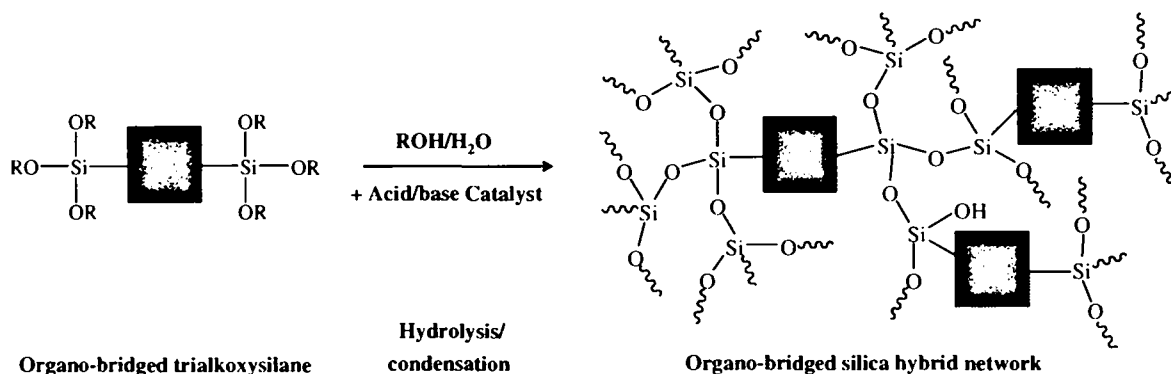
1.2. Synthesis of organo-silica hybrid materials by condensation of organo-bridged trialkoxysilanes.

Postfunctionalization (Surface Modification). For silica based systems, the inner surface of the porous host contains pendant silanol groups that are unwanted for many applications but at the same time enable easy modification of the surface properties. The purpose for modifying porous silica-based materials by organic groups is to improve the spectrum of properties without deteriorating the existing positive properties e.g., the porosity, the periodic ordering, large surface area, etc.[43] For example, unmodified silica aerogels or periodic mesoporous materials are rather hydrophilic, and by surface modification with methyl groups the material can easily be rendered hydrophobic.[55,56]

In a recent work, Jaroniec and co-workers have shown that the surface of ordered mesoporous silicas can also be modified by a direct template displacement of the wet gel powders with organosilanes (TDS process) when an ionic surfactant is used as the template, due to the replacement of electrostatic interactions by covalent siloxane bonds.[32,33]
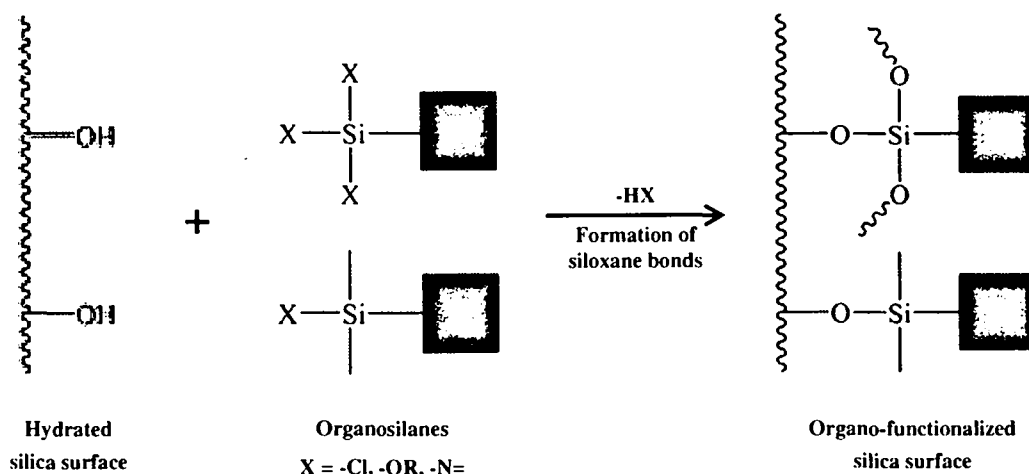
Figure 1.3. Surface functionalization of a hydrated silica material *via* pendant silanol groups using organo-chloro or -alkoxysilanes, or organosilazanes.

A wide range of organosilanes and also organosilazanes can be covalently bound onto the surface via these silanol groups: R_{4-n}-Si-X_n, with n=1-3 and R being an organic moietiy (bound via a Si-C bond) and X= -Cl, -OMe, -OEt, or -N=. The chloro-, alkoxy-, and silazane substitutes can be hydrolyzed to silanol groups and in the next step condensed with a pendant silanol group on the silica surface to form a stable siloxane bond.

1.3. Design of the Porous Structure

The deliberate design of pore sizes over length scales from Ångstroms to micrometers, of pore orientation and of the macroscopic morphology of a material has made considerable progress in recent years. Despite these advances, simultaneous control over all architectural features of an inorganic network is still a very challenging task. Maximum control of the porous structure of oxidic materials can be obtained by combining different synthetic strategies such as templating approaches or phase separation processes with sol-gel processing.

1.3.1. Supramolecular Templating – Mesoscopic Ordering

Molecular templating is well known from the synthesis of the highly organized channel structures of zeolites.[47] In addition to single molecules as templates, also supramolecular arrays of molecules such as lyotropic phases of amphiphilic surfactants or block copolymers can be used as structure-directing agents for a deliberate design of pore systems in the mesoscopic regime (Figures 1.4. and 1.5.).[14,31,47]

hydrophilic hydrophobic hydrophilic

HO O O O OH

Pluronic P123, $PEO_{20}PPO_{70}PEO_{20}$
Non-ionic block copolymer

Spherical
micelle

Cylindrical
micelle

Hexagonal liquid-
crystalline (LC) phase
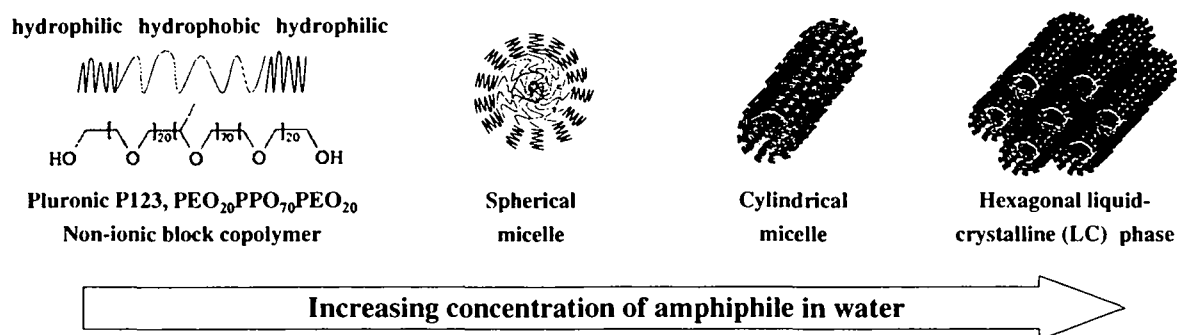
Increasing concentration of amphiphile in water

Figure 1.4. Aggregation behaviour of amphiphilic molecules in water – formation of LC phases.

Ordered mesoporous silica materials have appealing properties such as large internal surface areas and narrow pore size distributions. Amphiphilic molecules are central in the synthesis of these materials, where structures similar to the mesostructures of surfactant-water systems are formed. The amphiphiles function as scaffolds, or structure directors, for the silica network, enabling the formation of the mesoscopically ordered material. Synthesis with cationic amphiphiles, for example, cetyltrimethylammonium chloride (CTACl), have been shown to generate interesting structures such as the two-dimensional hexagonal ($p6mm$) MCM-41 material and the bicontinuous cubic ($Ia3d$) MCM-48 structure.[14,57] Other amphiphiles, for instance, non-ionic surfactants and amphiphilic block copolymers, are today also widely used as structure directors. The first synthesis of mesoporous silica using non-ionic surfactants was published in 1995.[20] Subsequently, Pluronic-type triblock copolymers, $(EO)_x$-$(PO)_y$-$(EO)_x$ (EO, ethylene oxide; PO, propylene oxide), were shown to be excellent for creating highly ordered mesostructures.[19,31]

In the scope of this work, we were applying Pluronic P123 ($EO_{20}PO_{70}EO_{20}$), which is used for the synthesis SBA-15 materials with a 2D hexagonal mesopore structure. This system was chosen due to its very intensively studied silica-surfactant mesophase assembly behavior and the resulting materials properties, which should facilitate characterization and investigation with respect to our precursor and synthesis conditions.[19,23,25,26,58-65] Using PEO/PPO-based block copolymers instead of ionic surfactants results in larger pores, which are widening the spectrum of application, especially with respect to separation/immobilization of (large) biomolecules, thicker silica walls, and a more stable material. Furthermore, they are cheaper, non toxic, and biodegradable. Different mesostructures of the inorganic material can be obtained depending on, for example, the Pluronic used, the temperature of the experiment, and the addition of additives such as alcohol or salt.[19,66-69] Zhao et al.[19] synthesized a two-

dimensional hexagonal (*p6mm*) silica now known as SBA-15 with the Pluronic polymer P123 (EO_{20}-PO_{70}-EO_{20}) and a micellar cubic (*Im3m*) material called SBA-16 with Pluronic F127 (EO_{106}-PO_{70}-EO_{106}). Several other Pluronics can also be used for formation of well ordered mesoporous silica.[66] Recently, the bicontinuous cubic *Ia3d* structure was also formed with Pluronic polymers.[67,68,70] Several groups have demonstrated that the structure of SBA-15 consists not only of large uniform and ordered channels but also of complementary micropores located in the silica wall and providing connectivity between them.[61,63,64,71] These micropores seem to be absent in the MCM-type materials. Moreover, these studies evidenced that hydrophilic poly(ethylene oxide) chains of triblock copolymers penetrate within the silica walls during the synthesis, inducing the formation of micropores upon calcination.[71] This microporosity has been shown to be controlled via the synthesis conditions (TEOS/surfactant molar ratio, aging temperature, and the presence of salt during the synthesis) as well as the thermal treatments. Materials are normally produced in the form of powders with varying morphologies ranging from spheres to fibres, and thin films.[16,65,72] Even monolithic systems of different sizes have been prepared via an approach termed as direct or true liquid-crystal templating (TLCT) applying relatively high surfactant concentrations of typically more than 30 wt% in water (Figure 1.5.).[24,73,74]

This supramolecular templating approach has not only been applied to pure silica materials, but has been extended to organosilica materials, which have been synthesized by co-condensation of organotrialkoxysilanes with tetraalkoxysilanes[50,51] and even more successfully by the use of bridged organotrialkoxysilanes[15,17,18,26,75-84] (see previous chapter). Also, silica doped with various metal oxides[49,85] and pure metal oxide frameworks[86,87] can be produced in a similar fashion.

Mixture of surfactant, tetraalkoxysilane, alcohol, and aqueous HCl (pH 1-2)

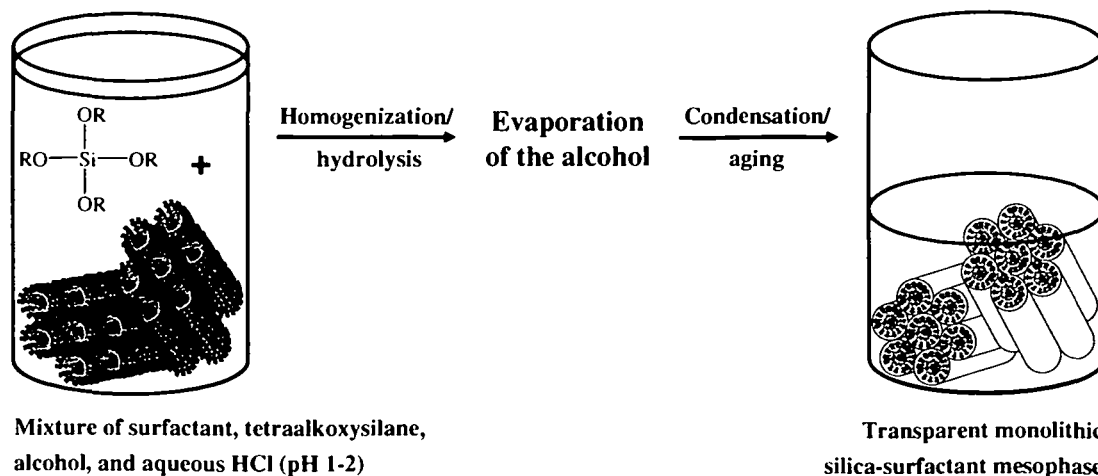Transparent monolithic silica-surfactant mesophase

Figure 1.5. True liquid-crystal templating process (TLCT).

One of the major problems related to the synthesis of monoliths is the incompatibility of many lyotropic surfactant phases with alcohols, which are inherently released upon hydrolysis and condensation of alkoxysilanes. Thus, the synthesis of materials with a high degree of mesoscopic order in combination with macroscopic morphologies such as large monoliths is still very difficult to achieve and only a limited number of examples is known from the literature.[24-26,73,74,88-91] Anderson and coworkers demonstrated a successful route to highly porous surfactant-templated silica aerogel monoliths using sol-gel processing in the presence of hexadecyltrimethylammonium bromide as structure-directing agent followed by supercritical drying with liquid carbon dioxide.[91] The resulting material showed hexagonally arranged mesopores within spherical particles, which assemble to give the monolith structure. A significant amount of pores – from interparticle packing –, which do not show any periodic ordering, contributes to the materials architecture.

1.3.2. Bi-/Multimodal Pore Systems

The situation gets even more problematic when materials with pore sizes on different length scales are desired, e.g. materials that combine small (micro- and mesopores) and large (macro-)pores. Dual or multiple templating approaches have been used for the production of materials with a bimodal pore size distribution, e.g. zeolitic nanoparticles,[92] or supramolecularly templated inorganic aggregates[92-95] in combination with colloidal particles. Gel casting has also successfully been used to create hierarchical zeolitic[96] or mesoporous[97] structures with controlled shapes. Silica spheres have also been successfully transformed into zeolitic monoliths containing interconnected macropores.[98] Furthermore, mesoporous/ macroporous silica has been prepared by coating bacterial threads with silica-surfactant mesophases.[99]

(Spinodal) Phase Separation. Other, more chemical approaches are based on phase separation strategies in combination with sol-gel processing e.g. the preparation of monolithic materials for chromatography purposes, however, no or only weak regular arrangements of the mesopores are achieved within a rather bulky network structure in the micrometer range.[30,100,101]

Nakanishi and coworkers published a series of papers in which they reported the use of water-soluble organic polymers such as poly(ethylene oxide) (PEO), to control macroscopic phase separation parallel to the sol-gel transition[30] (Figure 1.6.).

Early stages (a–c) and coarsening stages (d–f) of the
structure development process.

SEM images: Effect of increasing PEO content.
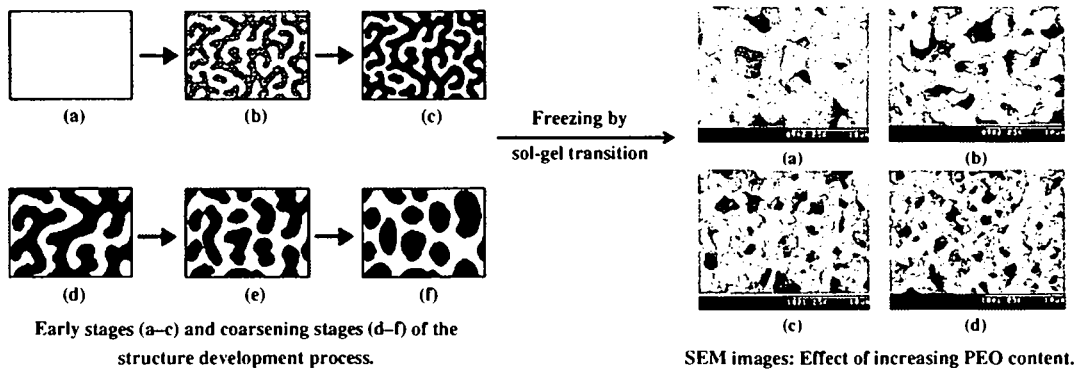
Figure 1.6. Phase separation via spinodal decomposition of a silica sol-gel mixture induced by PEO.[101]
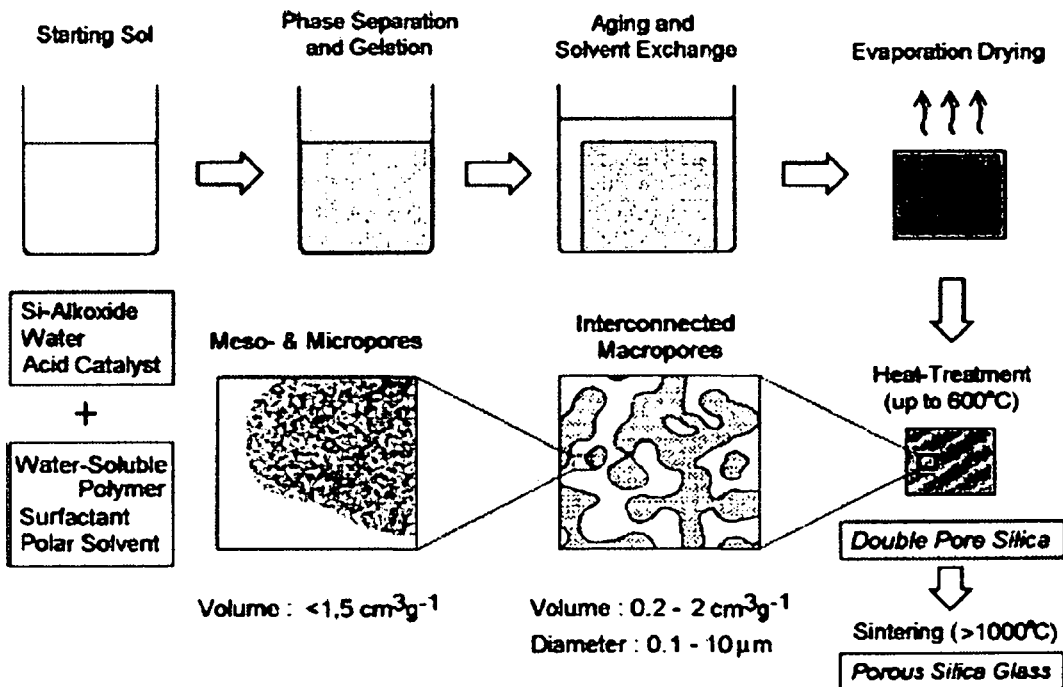
Figure 1.7. Synthesis of monolithic silica columns with a bimodal pore structure for HPLC.[30]

Lindén and Nakanishi extended this approach by applying the macroscopic, (PEO) polymer-controlled phase separation of silica particles in combination with an ionic or non-ionic surfactant as structure-directing agent in the nanometer regime.[27,102,103] The material they obtained exhibited interconnected porosity on several length scales, for which the macropore diameter is controlled via PEO-nanoparticle interactions, and the mesopore diameter by the presence of the surfactant e.g. cetyltrimethylammonium bromide or a poly(ethylene oxide)-based polymer. However, pronounced long-range ordering of the mesopores was not achieved. Only very recently, monoliths with ordered mesoporous structures in combination with macropores could be synthesized using conventional alkoxysilane precursors by applying

P123 as template in combination with 1,3,5-trimethylbenzene as swelling agent, an additive that enhances the self-organization of structure-directing agents.[25,26]

1.3.3. Meso- and Macroscopic Ordering – Ethylene Glycol-Modified Silanes

As mentioned above, one of the main problems in the synthesis of a monolithic silica-based material with a distinct long-range ordering in the mesoscopic regime is the release of alcohols due to hydrolysis and condensation reactions of the corresponding alkoxysilanes. It is well known, that the presence of methanol or ethanol is detrimental to many lyotropic phases as the solvent phase becomes more lipophilic and therefore solvatizes better the hydrophobic regions of the surfactant, which reduces hydrophobic-hydrophilic interactions. Hoffmann and coworkers hydrolyzed ethylene glycol esters of orthosilicic acid in the presence of an ionic surfactant such as tetradecyltrimethylammonium bromide and were able to show by means of small angle neutron scattering (SANS) that the structure of the surfactant aggregates is not destroyed upon mixing and gelation, thus indicating that the diol-modified silane is compatible with lyotropic surfactant species. However, they did not comment on the structure of the corresponding gels after drying.[104,105]

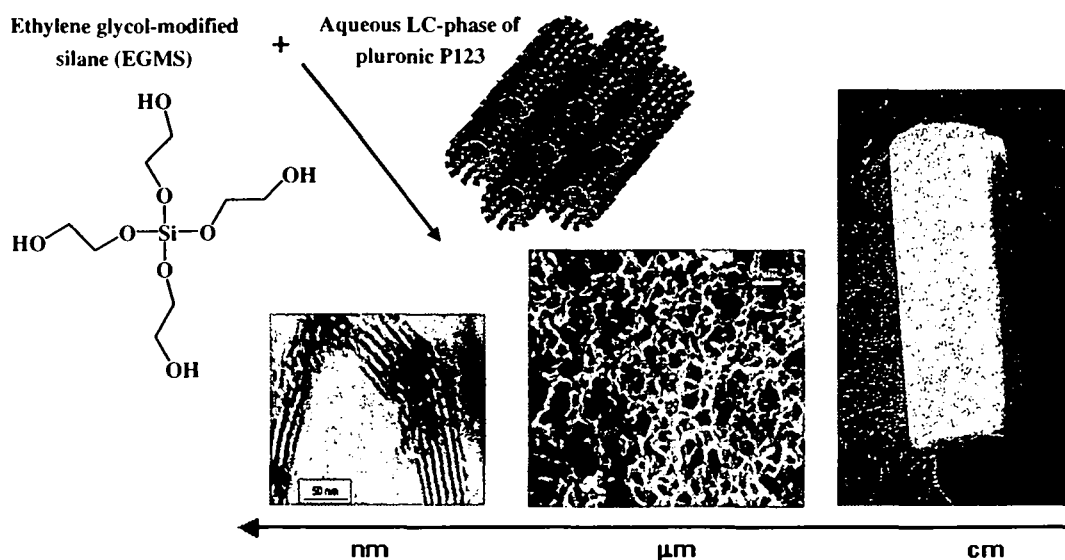**Figure 1.8.** Mesoscopically organized silica monolith with hierarchical build-up synthesized with ethylene glycol-modified silane (EGMS).

On this basis, Huesing et al. recently described the synthesis of monolithic silica gels exhibiting a hierarchical network structure with a bimodal pore size distribution (macropores in the range between 200-800 nm and periodically arranged mesopores of 8 nm in diameter)

from an ethylene glycol-modified silane in the presence of the non-ionic block copolymer surfactant Pluronic P123[59] (Figure 1.8.). Pronounced long-range ordering of the mesopores was observed in combination with macroscopic phase separation into a silica/surfactant rich phase and a solvent rich (glycol/ water) phase.

1.4. Processing of the Monoliths

Drying of large monoliths is often the most crucial step in the synthesis process, since surface tension, evolution of capillary pressure and removal of templates often results in large shrinkage or even destruction of the whole gel body.

1.4.1. Drying with Supercritical Fluids (scf)

One typical procedure to prevent cracking is drying with supercritical fluids (scf), e.g. carbon dioxide, since the building-up of a gas/ liquid interface is avoided, hence no capillary pressures evolve.[106] However, scf extraction is expensive, time consuming, and requires high temperatures/ high pressures.

The principle of supercritical drying is based on avoiding the liquid-gas tie line via the supercritical state (see Figure 1.9). Typical implementation for drying a wet gel with carbon dioxide is solvent exchange first to methanol (due to the immiscibility of liquid CO_2 and water), then to CO_2 in an autoclave at 60 bar and 10 °C. For supercritical drying, the closed autoclave is heated up to 45 °C, leading to a simultaneous increase of pressure above 100 bar and therefore preventing evaporation of the pore liquid (p_c=73.6 bar, T_c=31 °C).
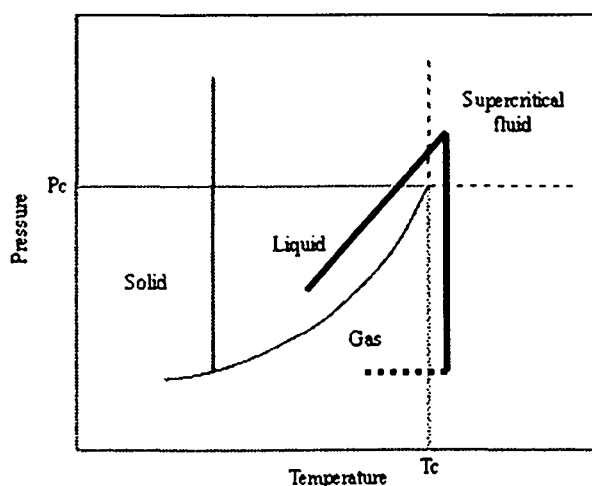

Figure 1.9. Diagram of states illustrating the principle of drying via the supercritical state to circumvent the liquid-gas tie-line.

The synthesis and drying of silica monoliths with an unique hierarchical organization of the pores composed of an extremely filigrane inorganic backbone by utilizing supercritical solvents was recently published by Huesing et al.[59] One objective of my continuing research was to find alternative routes to supercritical drying with e.g. carbon dioxide to remove the solvent and possibly the block-copolymer template but still avoid shrinkage and collapse of the pores.

Another approach for drying hierarchically organized porous monoliths has recently been presented by Mukai et al. via freeze gelation and freeze drying.[107]

1.4.2. Surface Modification

A very promising procedure for drying large silica gels relying on a simple surface modification treatment with trimethylchlorosilane was presented in the mid-nineties as an alternative to supercritical drying. The capillary pressure, P_c, generated during drying is a function of the pore fluid/vapor surface tension, γ_{LV}, the contact angle, θ; between the fluid/vapor interface and pore wall and the pore radius, a, as follows:

$$P_c = -(2\gamma_{LV}\cos\Theta)/a .$$ (1)

For a wetting fluid ($\theta < 90°$), P_c is negative, thus indicating that the fluid is in tension. The presence of organic methyl groups on the surface of the silica gel in combination with a proper selection of the final pore fluid, e.g. hexane allowed to change the contact angle to lower capillary pressures and thus dry monolithic wet silica gels without cracking.[108-111]

A similar approach also using organochlorosilanes and organoalkoxysilanes as post treatment reagents was published recently not for drying, but for the extraction of ionic surfactants from self-assembled *silica-surfactant powders* (Figure 1.10.). As the driving force for this reaction the replacement of electrostatic interactions at the inorganic-organic interface by covalent siloxane bonds, that is the formation of Si-O-SiR₃, was named.[32,33]
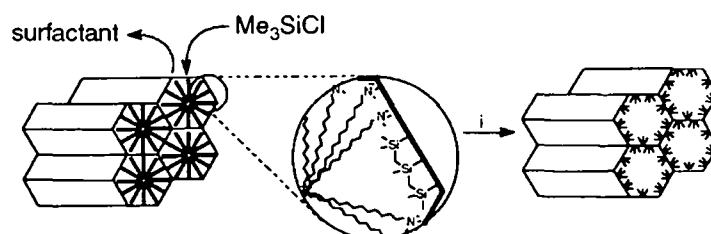
Figure 1.10. Simultaneous mesopore modification and surfactant extraction from MCM-41 by reaction with trimethylchlorosilane.[33]

1.5. Objective

The aim of this work was the sol-gel synthesis of monolithic (organo-) silica materials with hierarchical pore structures, including periodically ordered mesopores, by extending the approach of applying ethylene glycol-substituted tetraalkoxysilane (EGMS) in a true liquid-crystal templating (TLCT) approach with P123 to other glycols/polyols (Chapter 2) and to organo-trialkoxysilanes (Chapter 4). Furthermore, the original synthesis approach using EGMS under neutral conditions[59] was extended to acidic media and other synthesis compositions with the aim to optimize the periodic ordering of the mesopore structure.

Chapters 3 and 5 deal with the processing, drying and chemical modification of the wet, as synthesized monolithic (organo-)silica gels. The aim was, to investigate the process of surface-silylation with trimethylchlorosilane and subsequent drying at ambient pressure as an alternative to the expensive and time consuming method of supercritical drying with carbon dioxide. Furthermore, the silylation procedure should be extended to a variety of functional organosilanes in order to investigate the potential of this method of deliberate surface modification in combination with high surfactant extraction efficiency and facilitation of drying of large, porous monoliths.

The aim of the last chapter (Chapter 6) of this work was to investigate the potential of the materials developed in the course of this work for application as HPLC column material, which was done in cooperation with an industrial partner.

2 Porous Structure – Influence of Type of Glycol

Silica monoliths exhibiting a unique hierarchical network structure with a bimodal pore size distribution and high surface areas were prepared from three different glycol-modified silanes by sol-gel processing. Tetrakis(2-hydroxyethyl)-, tetrakis(2-hydroxypropyl)- and tetrakis(2,3-hydroxypropyl)-orthosilicate were obtained by transesterification reaction from tetraethyl-orthosilicate and the corresponding alcohols. It could be shown that for ethylene glycol- and propane-1,2-diol-modified silanes, simply the release of the corresponding diols during sol-gel processing in the presence of a block copolymeric surfactant (Pluronic P123) results in phase separation on different levels. In addition to an extraordinary cellular network structure with interconnected macropores of several hundreds of nanometer in diameter, the material exhibits a well ordered mesostructure with periodically arranged mesopores of about 6-7 nm in diameter. Interestingly, the application of glycerol-modified silanes at the given synthesis conditions results in the formation of a disordered silica mesostructure. The architectural properties and the morphology of the gel network cannot only be controlled by the choice of the glycol, but also by the amount of acid catalyst in the starting composition.

2.1. Motivation

Huesing et al. recently described the synthesis of monolithic silica gels exhibiting a hierarchical network structure with a bimodal pore size distribution (macropores in the range between 200-800 nm and periodically arranged mesopores of 8 nm in diameter) from an ethylene glycol-modified silane in the presence of the non-ionic block copolymer surfactant Pluronic P123 in pure water.[59] Pronounced long-range ordering of the mesopores was observed in combination with macroscopic phase separation into a silica/surfactant rich phase and a solvent rich (glycol/ water) phase.

The motivation of the present work was to extend this approach to synthesize monolithic silica with bi- or multimodal pore size distribution by investigating the influence of other glycols besides ethylene glycol such as propane-1,2-diol or glycerol on the gel structures formed. Because of the different properties of the alcohols e.g. their polarity, hydroxyl group content, and viscosity a distinct influence on the formation of the architectural features of the gels is expected. In addition, an optimization of the synthesis procedure with respect to catalyst concentration in order to maximize the degree of mesoscopic ordering was aspired. To simplify the following text, the term "glycol" is meant in a way that the

compound has more than one alcohol group, thus including the glycerol-prepared samples. The use of glycol-modified silanes in combination with a non-ionic block copolymer surfactant simplifies the procedures presented by Nakanishi and Lindén[25,27] as presented in the Introduction (1.2.2.) significantly, since no supplementary phase separation polymer is required to obtain macrophase-separated structures. Furthermore, this approach allows and facilitates the formation of highly ordered mesophases without the use of a swelling agent.

2.2. Results

2.2.1. Gel Synthesis

The different glycol-modified silanes were prepared by direct trans-esterification reaction of tetraethyl-orthosilicate with the corresponding diol such as ethylene glycol, propane-1,2-diol or polyol i.e. glycerol. The term glycol is used to describe all alcohols used in this work. No additional solvent or catalyst is required for this reaction and the final product is characterized by a defined silicon to glycolate molar ratio which was adjusted to 1:4.5 (EGMS), 1:4.7 (PGMS), and 1:3.7 (GLMS) in our experiments. Complete alcohol exchange was proven by ^{1}H- and ^{13}C-NMR studies, and ^{29}Si-NMR investigations showed a single peak at about -83 ppm for all different glycol-modified silanes. However, ^{29}Si-NMR results as well as ^{1}H-NMR investigations also indicate an oligomeric or polymeric character of the precursors which is due to the fact that polyols allow the formation of bridged silane species in equilibrium with non-covalently bound polyol: e.g.
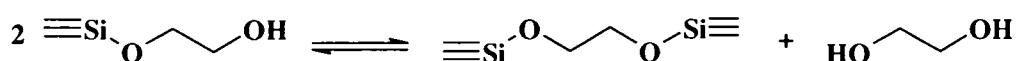
Another possibility might be bonding in a chelating fashion instead of bridging-, again resulting in free ethylene glycol molecules. In addition, hydrogen-bonding interactions pronounce this polymeric character. These factors lead to unusually long relaxation times in the ^{29}Si-NMR spectra and also to more than one signal for the hydroxy-protons in the ^{1}H-NMR spectra. However, no higher Q-species than Q^0 are present in the precursor mixture, proving that the polymeric character is due to intermolecular hydrogen-bonding and chelating/bridging glycolate species, and not due to (partial) hydrolysis and condensation of the silane.

From these glycol-modified silanes monolithic silica gels were prepared by addition of EGMS, PGMS, or GLMS to an aqueous liquid crystal (LC)-phase of 30 wt% P123 surfactant, and in

some cases hydrochloric acid in different concentrations. The concentration of P123 in water was kept constant at a ratio of P123/water = 3/7, while the acid concentration has been varied between 0-5 M HCl. Both parameters – type of glycol and acid concentration – have a strong influence on the gelation time and on the formation of the mesostructure (Tables 2.1-2.3).

Table 2.1. Synthesis conditions, gelation times and physicochemical properties of dried samples prepared from EGMS.

Samples	c_{HCl} /M	t_{gel} /min	density /g cm^{-3}	SAXS d_{100} (w) /nm	N$_2$ adsorption-desorption S^{BET} /m^2 g^{-1}	V^{N2} /cm^3 g^{-1}	D^{BJH} (w) /nm	t_{wall} /nm	Hg-porosimetry V^{Hg} /cm^{-3} g^{-1}	D^{Hg} /μm
EGMS10	0	2	0.16	11.4 (2.9)	1010	1.9	7.8 (1.4)	5.4	5.1	0.45
EGMS10	10^{-3}	3	0.15	11.2 (2.2)	740	2.3	7.0 (2.1)	5.9	--	--
EGMS10	10^{-2}	260	0.18	11.1 (1.0)	960	1.6	6.4 (0.4)	6.4	--	--
EGMS13	10^{-2}	255	0.20	11.1 (1.1)	900	1.2	6.3 (0.8)	6.5	--	--
EGMS17	10^{-2}	250	0.21	11.6 (1.1)	920	1.2	6.7 (0.7)	6.7	2.8	0.75
EGMS20	10^{-2}	245	0.26	12.0 (2.4)	910	1.1	5.7 (1.1)	8.1	--	--
EGMS10	5	120	0.56	--	830	1.1	--	--	--	--
EGMS17	5	10	0.23	11.2 (2.2)	810	1.2	5.6 (2.0)	7.3	--	--

t_{gel} corresponds to the gelation times. The specific surface area, S^{BET}, the total pore volume, V^{N2}, and pore size distributions with D^{BJH} representing the maximum were determined from N$_2$-sorption experiments. t^{wall} represents the wall thickness of the material and was calculated from the sorption experiments and small angle X-ray diffraction data as $[(2d_{100}/\sqrt{3})-D^{BJH}]$. The value inside the brackets gives the full-width at half maximum of the corresponding maximum. V^{Hg} and D^{Hg} represent the macropore volume and the -size determined by Hg-porosimetry.

Table 2.2. Synthesis conditions, gelation times and physicochemical properties of dried samples prepared from PGMS.

Samples	c_{HCl} /M	t_{gel} /min	SAXS d_{100} (w) /nm	N$_2$-sorption S^{BET} /m^2 g^{-1}	V^{N2} /cm^3 g^{-1}	D^{BJH} (w) /nm	t_{wall}/ nm	Hg-porosimetry V^{Hg} /cm^3 g^{-1}	D^{Hg} /μm
PGMS10	0	15	10.8 (5.6)	820	2.7	--	--	--	--
PGMS10	10^{-2}	2500	10.1 (1.3)	890	0.8	3.7 (0.6)	5.7	4.3	11
PGMS10	1	250	10.9 (0.9)	960	1.3	5.2 (0.7)	5.5	6.5	5.9
PGMS10	5	150	10.0 (2.2)	860	1.5	--	--	--	--

Table 2.3. Synthesis conditions, gelation times and physicochemical properties of dried samples prepared from GLMS.

Samples	c_{HCl}	t_{gel}	S^{BET}	V^{N2}
	/M	/min	/m^2 g^{-1}	/cm^3 g^{-1}
GLMS10	0	<1	--	--
GLMS10	10^{-2}	480	800	0.7
GLMS10	1	250	830	0.6
GLMS10	5	20	870	0.5

Figure 2.1 shows the gelation time (t_{gel}) as a function of pH for the different silane precursors. Gelation times under alkaline conditions were not measured because of immediate precipitation of silica from the mixture. Very short gelation times of only a few minutes can be observed at neutral pH (~6). The mixture turns white before the point of gelation. Upon increasing the HCl concentration, the gelation time remains constant until pH ~3.5. Below this value, the gelation time abruptly increases to values of above 250 min. These gels remain transparent for approximately another 250 min after gelation before macroscopic phase separation takes place and the gels turn white. The minimum in the condensation rate (long t_{gel}) is reached around pH 1.5, while further increase of the HCl concentration leads again to a decrease in the gelation times. In addition to the pH dependence, gelation is highly dependent on the SiO_2/P123 ratio, in particular under highly acidic conditions (pH = 0.7). Below 13/30, gelation times constitute around 120 min and transparent gels are obtained at pH = 0.7. Above this ratio, gelation times are much shorter (around 10 min) and white gels are formed (see also Table 2.1.).

Figure 2.1 also indicates that the type of glycol has a significant influence on the sol-gel reaction rate (tables 1-3), in particular at neutral pH and around pH 2. The gelation times (at the same pH) decrease in the following order: t_{gel}(PGMS) >> t_{gel}(EGMS) > t_{gel}(GLMS) at neutral conditions and t_{gel}(PGMS) >> t_{gel}(GLMS) > t_{gel}(EGMS) around pH 2, respectively. The reaction rate of GLMS at neutral pH was so fast that no homogeneous monolithic material could be obtained.
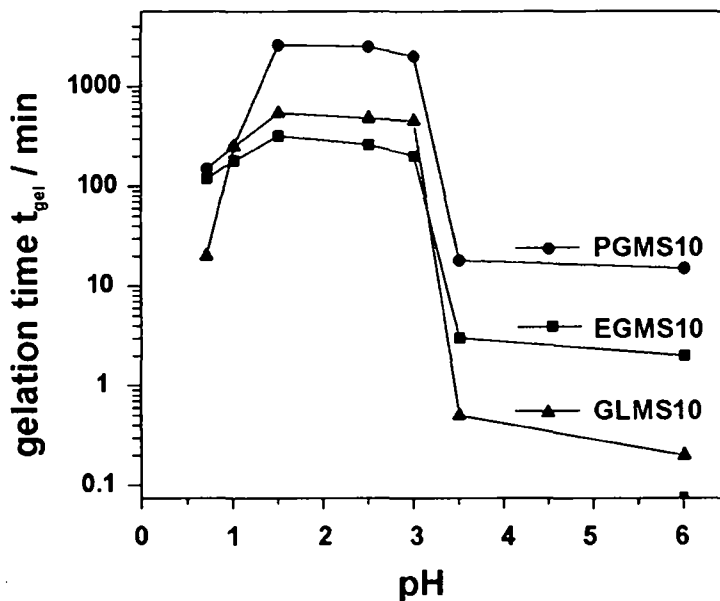
Figure 2.1. Gelation times as a function of pH of the starting solution for EGMS, PGMS and GLMS.

For all materials discussed in the following, white monolithic gel rods with diameters of 10 mm and lengths of 25 mm were obtained. The density of the dry silica gel monoliths was measured by determination of the volume and the weight of the samples, and lies in the range of 0.15-0.26 g cm^{-3}.

2.2.2. Structural Properties of the Resulting Gel Bodies

Small Angle X-ray Scattering. Small angle X-ray scattering patterns were collected for all solids after the drying step and are illustrated in Figures 2.2 and 2.3.

In general, samples with an ordered porous structure show up to four distinct Bragg diffraction peaks, which can be indexed to (100), (110), (200), and (300) associated with a *p6mm* hexagonal symmetry with a repeating unit distance of about 11 nm, indicating the formation of highly ordered 2D hexagonal mesostructures. In some samples, the (110) and (200) reflections could not be resolved well due to the broadness of the peaks. The corresponding d_{100} spacings of the dried materials from the various glycol-modified silanes can be found in Tables 2.1-2.3.
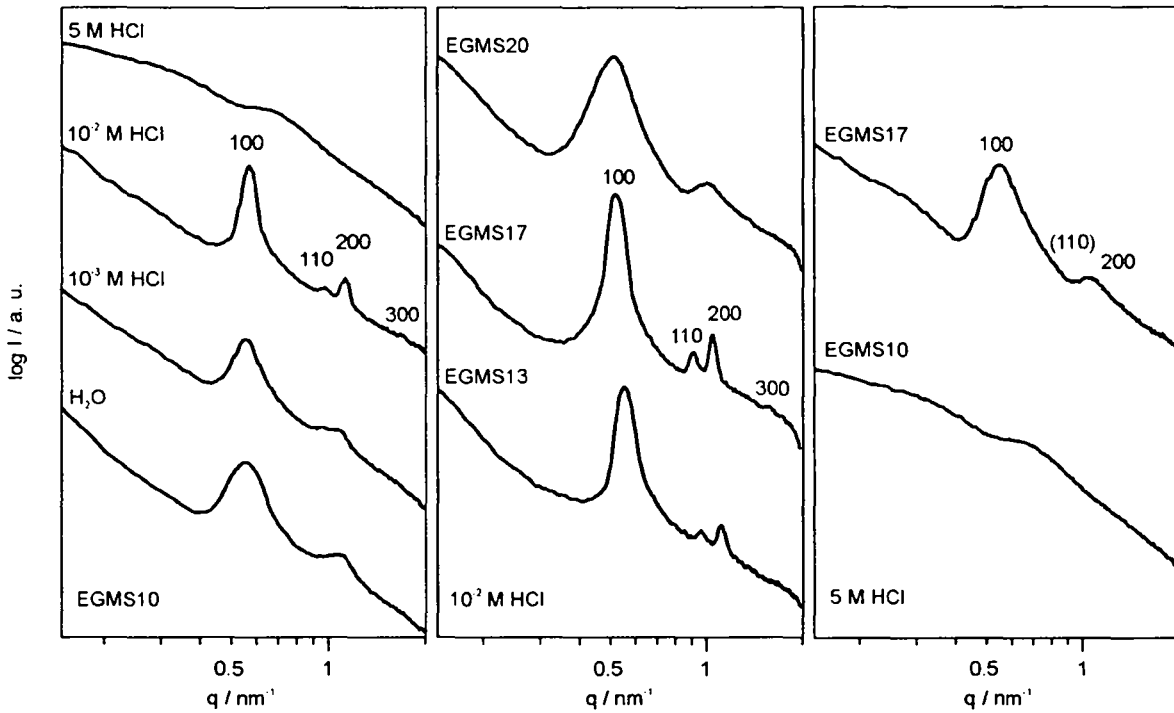
Figure 2.2. Small angle X-ray scattering profiles for dried monoliths prepared from EGMS; a) for starting composition of EGMS10 at different acid concentrations, b) at a given acid concentration of 10^{-2} M HCl with increasing amount of EGMS in the precursor sol and c) at a given acid concentration of 5 M HCl again with increasing amount of EGMS.
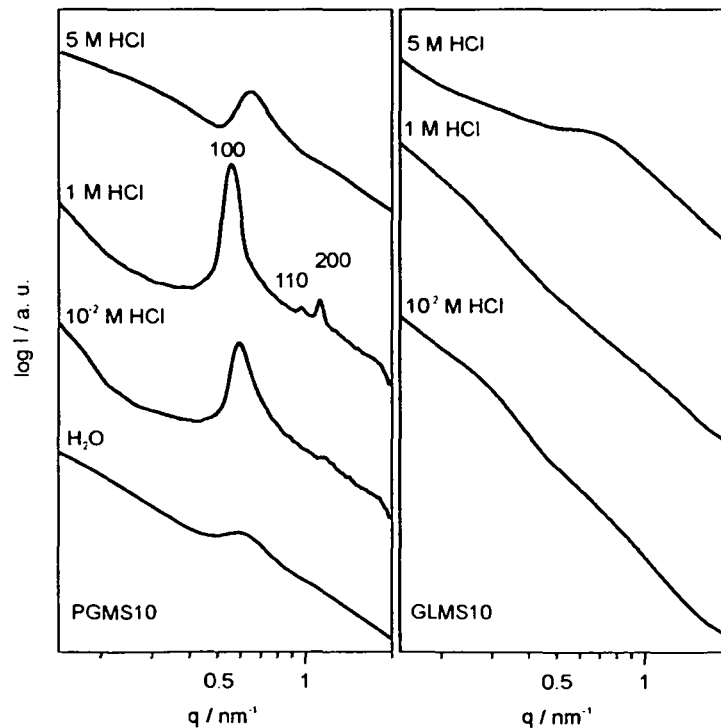

Figure 2.3. Small angle X-ray scattering profiles for dried monoliths prepared from PGMS (left) and GLMS (right) for different acid concentrations.

To compare the relative degree of mesoscopic order of the silica materials prepared with different glycol-modified silanes and different acid catalyst concentrations, the values for full-width at half maximum (w) of the (100) diffraction peak have been calculated and are included in Tables 2.1-2.3. Some general trends can be observed such that ordered, 2D hexagonal phases could be synthesized with EGMS and PGMS, but not with GLMS (Figures 2.2 and 2.3).

In addition, the degree of ordering proved to be highly dependent on the HCl concentration used and on the $SiO_2/P123$ ratio as well. For samples prepared with EGMS and PGMS, resulting in a $SiO_2/P123$ ratio of 10/30, the degree of mesoscopic order increases with HCl concentration (and gelation time) with maxima at 10^{-2} M HCl for EGMS and at 1 M HCl for PGMS, respectively. This correlation could not be observed for very high HCl concentrations (5 M).

For the EGMS samples (Figure 2.2.), it can clearly be seen that the degree of periodicity within the material depends on the acid concentration, as well as on the amount of silane and thus the silane/P123 ratio in the starting mixture. At pH = 0.7, the $SiO_2/P123$ ratio must be increased to 17/30 to obtain ordered phases at all, and at pH = 2 the optimal ratio for a maximal periodicity was also found at a ratio of 17/30, which corresponds exactly to the $SiO_2/P123$ ratio for SBA-15 materials. The latter sample prepared with EGMS and 10^{-2} M HCl shows the highest degree of ordering of all materials presented in this publication (Figure 2.2b – middle curve).

Nitrogen Sorption. Figure 2.4 shows representative examples taken from the N_2-sorption studies. The N_2-sorption isotherms of the dried materials have been used to obtain information on surface area and mesoporosity. According to the IUPAC classification, type IV isotherms could be observed for all samples. All samples revealing ordered mesostructures in the small angle X-ray scattering studies showed H1 hysteresis loops with more or less sharp adsorption and desorption branches, indicative of the uniformity of pore sizes and –shape. The relative sharpness of the desorption branches confirms the same trends as the SAXS studies. The sample prepared under neutral conditions showed the less defined step in the hysteresis loop in consistence with the SAXS results, and revealed the presence of two different types of mesopores. Non-ordered samples show H2 hysteresis loops corresponding to more complex pore systems with non-uniform pores. All samples exhibit high specific surface areas S^{BET}

between 740-1010 m^2 g^{-1} and high total pore volumes V^{N2} of 0.5-2.5 cm^3 g^{-1} (see also Tables 2.1.-2.3). The total pore volume decreases with an increasing acid concentration in the starting mixture with highest values at neutral conditions and low acid concentrations of 10^{-3} M HCl. It is anticipated that in addition to the mesopores a substantial degree of microporosity attributes to the large surface areas as it is expected for samples templated with lyotropic phases of PEO-containing block copolymers. A detailed t-plot analysis of samples prepared from EGMS can be found in Chapter 3.3.

Pore size distributions (see also Figure 2.4) of the materials with ordered mesopores have been determined using the BJH model. For comparison, the pore diameter maxima D^{BJH} are listed in Tables 2.1-2.3. The BJH method systematically underestimates pore sizes, therefore, only a comparative use of this method is appropriate. In this contribution, we are interested in changes occurring in the pore sizes due to different precursors and synthesis conditions, more than in the absolute value. The values for full-width at half maximum (w) of the pore-size distributions have been calculated in order to compare the relative uniformity of the mesopores of the silica materials prepared with different glycol-modified silanes and catalyst concentrations and are included in Tables 2.1.-2.3.
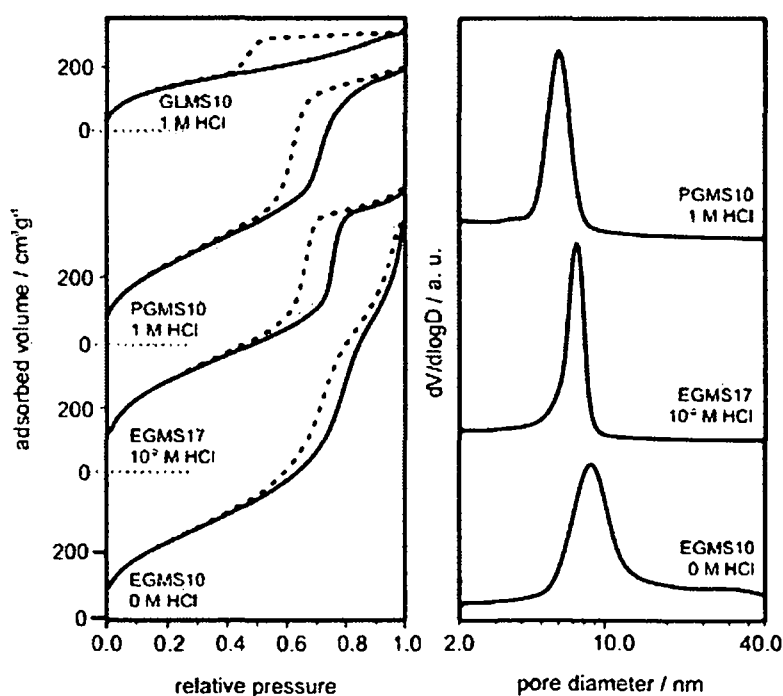

Figure 2.4. Nitrogen sorption isotherm plots and pore size distributions from the desorption branch of hierarchically organized silica monoliths prepared using EGMS, PGMS and GLMS. The pore size distribution for GLMS samples is not given due to the absence of a uniform pore size.

27

The EGMS10 sample prepared with 5 M HCl shows a H2 hysteresis loop and is therefore not considered in the discussion of the pore diameters. For the samples synthesized from EGMS a decrease in the pore diameter with increasing acid concentration is observed starting with 7.8 nm decreasing to 5.6 nm. Monoliths prepared from PGMS show the opposite trend (3.5 nm with 10^{-2} and 5.2 nm with 1 M HCl), but the number of samples was not high enough to allow further discussion. GLMS as precursor results only in disordered materials with a H2 hysteresis loop. From the d_{100} spacing and the mean pore size calculated by the BJH method, the wall thickness is calculated and found to be between 5.4 and 8 nm, which is considerably thick compared to other materials templated with non-ionic surfactants. As for the pore diameter (D^{BJH}), absolute values cannot be calculated by this method. The wall thicknesses are systematically overestimated, but again, their comparative use is appropriate. For samples EGMS10, the wall thickness increases with acid concentration from 5.4 to 6.4 nm, associated with a decrease in pore size. This trend is reversed for PGMS10 with wall thicknesses of 5.7 nm for 10^{-2} and 5.5 nm for 1 M HCl. Expectedly, higher concentration of silane in the precursor sol increases the wall thickness (up to 8.1 nm, EGMS20). In general, the results from nitrogen adsorption-desorption experiments support the data obtained by small angle X-ray scattering, especially concerning the degree of mesoscopic ordering.

Scanning– and Transmission Electron Microscopy. Representative electron micrographs of dried gel samples prepared with different silanes are exemplarily shown in Figures 2.5 and 2.6.

TEM images of EGMS17 and PGMS10 (prepared at pH = 2) confirm the well ordered 2D hexagonal mesostructures with *p6mm* symmetry also found in the SAXS experiments. The estimated repeating unit distance found in the TEM images of about 10 nm corresponds well to the ones obtained from SAXS. SEM studies reveal that parameters such as acid concentration and type of glycol-modified silane not only determine the formation of the mesostructure but also the macrophase/domain separation of the silica/surfactant phase from the solvent phase.
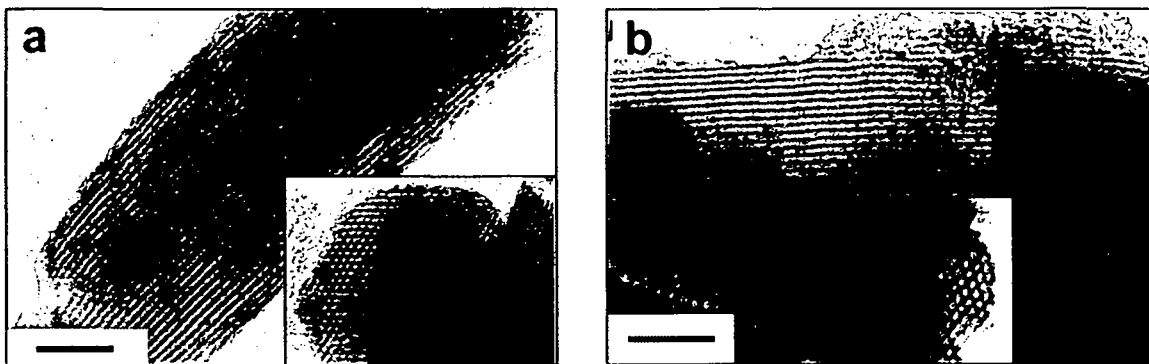
Figure 2.5. Representative transmission electron micrographs with different orientations of a 2D hexagonal mesostructure with respect to the electron beam – large pictures: perpendicular to the cylinder axis; small pictures: parallel to the cylinder axis; a – EGMS17, b – PGMS10, acid concentration 10^{-2} M HCl, scale bars correspond to 100 nm.

The SEM images reveal interconnected (open) macroporosity, but various morphologies for the different samples. The SEM images corresponding to the TEM images shown in Figure 2.5 can be found in Figure 2.6b and d. A cellular network built up from rod-shaped aggregates of 2-3 μm in length and about 0.5 μm in diameter is seen for the EGMS gel (EGMS17), while the PGMS gel (PGMS10) shows a more or less highly aggregated particulate network architecture with monodisperse particles in the range of a few micrometers. In both – EGMS and PGMS gels – influences of the acid concentration on the microstructure can be seen. For EGMS gels, the cellular morphology is visible for gels prepared in neutral conditions (EGMS10), but more pronounced and of larger dimensions for the gel with longer gelation times corresponding to a slightly higher acid concentration (Figure 2.6a and b). Increasing the acid concentration furtheron results in a particulate network structure (Figure 2.6c) with small particles of around 50 nm – for this sample no periodicity of the mesostructure is observed. Architectural changes can also be found for PGMS gels. Here the structure remains particulate throughout the given set of synthesis parameters, but with variations in the size and exact form of the particles. As mentioned, the particle sizes for the gels prepared at pH = 2 are in the range of a few microns with slightly oblated particle-morphology. With increasing acid concentration (pH = 1) first a more elongated particle shape evolves, while at pH = 0.7 smaller, monodisperse, spherical particles with diameters of 2 μm are observed (Figure 2.6d-e). The sample in Figure 2.6e shows the highest degree in mesoscopic ordering of the PGMS gels (from SAXS data), which is in good agreement with the elongated morphology and larger particle size.
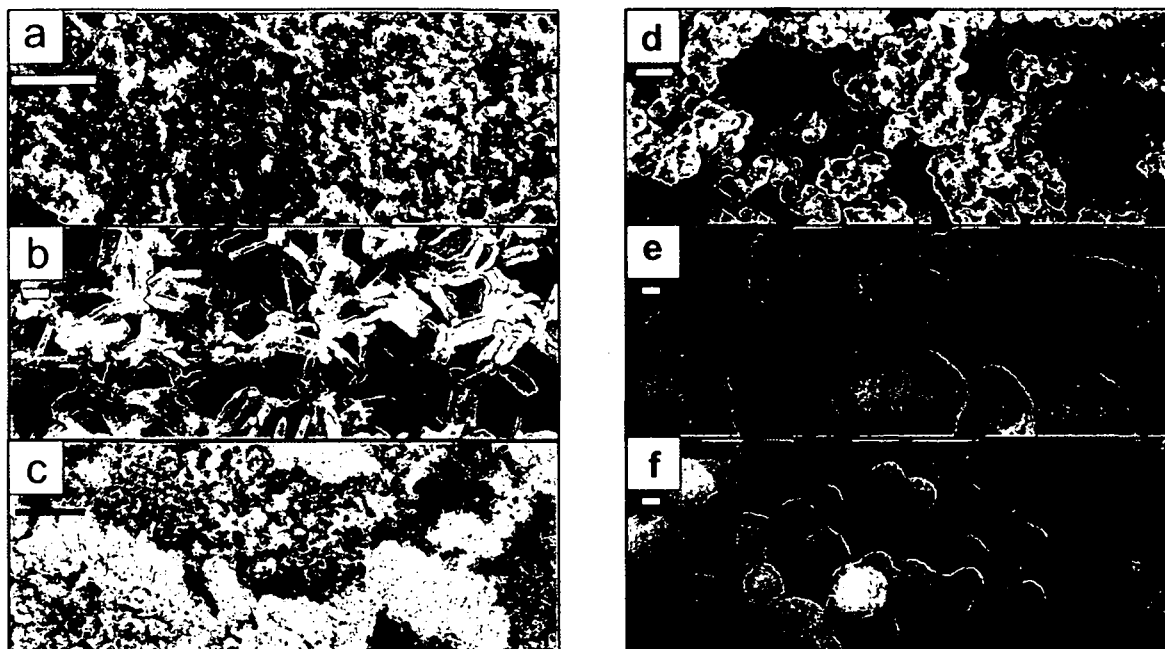
Figure 2.6. SEM images of samples EGMS10 (a/c), EGMS17 (b) and PGMS10 (d-f) prepared at different HCl concentrations: a – 0 M, b/d –10⁻² M, e – 1 M, and c/f – 5 M; scale bars: d – 10 μm, else 1 μm.

Mercury-Porosimetry. Representative intrusion curves, and mesopore- (from N_2-sorption) and macropore size distributions (from Hg-porosimetry) of samples with periodically ordered mesostructures are shown in Figure 2.7. The experiments revealed the presence of open, uniform macropores with high pore volumes V^{Hg} of ~5 cm³ g⁻¹ for all samples under investigation. The values for macropore volumes and -sizes are listed in Table 2.1 and 2.2. Samples with the same silane content of the starting mixture (EGMS10 and PGMS10) have macropore volumes between 4.3-6.5 cm³ g⁻¹. Differences arise from the shrinkage during aging and the drying process, which strongly depends on the stability of the silica network, thus on the pH conditions during network formation. Condensation rates at neutral (H_2O) and highly acidic (1 M HCl) conditions are higher than around moderate acidic conditions (10^{-2} M HCl), which is reflected in the observed macropore volumes. The macroporosity is significantly lower for sample EGMS17 (2.75 cm³ g⁻¹) due to the higher silane content in the starting mixture. The macropore size distributions are in good agreement with the SEM results and vary significantly for the different silanes and pH conditions between 0.45-11 μm. Sample EGMS10 prepared under neutral conditions (H_2O) has the smallest macropore size with 0.45 μm, on the other side of the range lies sample PGMS10 prepared under slightly acidic conditions (10^{-2} M HCl). These findings correlate well with the times of gelation which can be seen as a measure for the kinetics of phase separation. A high gelation time and

therefore late phase separation as observed for sample PGMS10 (10^{-2} M HCl) results in larger domains, and as a result also in larger particles and macropores.

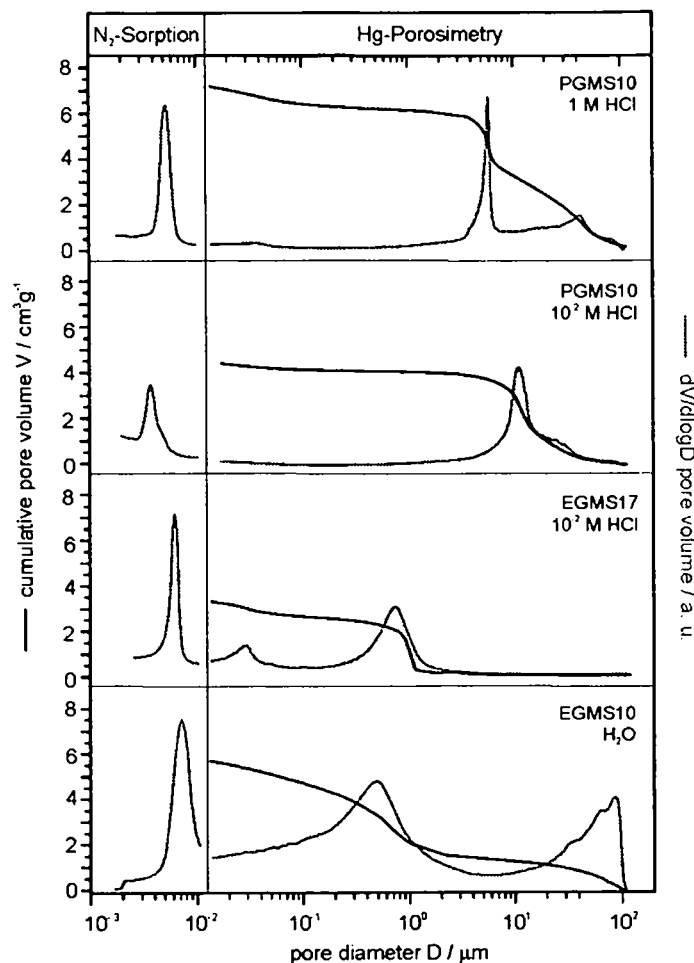**Figure 2.7.** Hg-porosimetry intrusion curves, and macropore- (Hg-Porosimetry) and mesopore- (N_2-Sorption) size distributions showing the bimodal pore structures of representative samples with periodically ordered mesostructures.

After calcination in air at 450° C for three hours, the morphology and SAXS patterns of the samples is preserved, confirming that the monolithic material is thermally stable.

2.3. Discussion

The first part of the discussion addresses the synthesis and hydrolysis/condensation behavior of ethylene glycol-, 1,2-propane diol-, and glycerol-modified silanes in the presence of Pluronic P123 under different pH conditions, while in the latter part the influence of the different glycols on the resulting materials' structure is discussed.

2.3.1. Sol-Gel Processing with Glycol-Modified Silanes

Modifications of alkoxysilanes with diols or polyols such as ethylene glycol, glycerol etc. are well known since the middle of the last century, however their application was hampered by their hydrolytic instability.[112-116] Only in recent years, interest in this type of glycol-modified silanes is increasing again due to some obvious advantages such as I) a high water solubility (no co-solvent is required to homogenize typical sol-gel solutions), II) the hydrolysis and condensation reactions can be initiated without acid or base catalysis at neutral pH by addition of water, and III) hydrolysis results in the release of a biocompatible alcohol. The latter two points were the first ones recognized as a huge advantage in the synthesis of bio-silica gels as can be seen in the application of glycerol-modified silanes for the encapsulation/ immobilization of biomolecules which are otherwise easily denatured.[117,118]

The extraordinarily high compatibility of ethylene glycol-modified silanes with lyotropic liquid-crystal phases of surfactant molecules has been demonstrated by Hoffmann in 1998.[104] These silanes are ideal candidates for true liquid-crystal templating approaches towards the synthesis of nanostructured silica monoliths, especially when non-ionic block copolymeric surfactants with polyoxyethylene units as hydrophilic moiety are used as they exhibit analogous chemical properties to the released glycols.

In addition to the work of Hoffmann, Alexandridis and coworkers identified the phase diagrams of aqueous LC-phases of similar triblock copolymer surfactants (Pluronic P105) in the presence of different alcohols such as ethanol or glycols, i.e. propylene glycol and glycerol. They demonstrated that for all investigated systems, regions of lamellar, bicontinuous cubic, hexagonal and micellar cubic lyotropic phases can be found, however, that the concentration range of stability of the different phases strongly depends on the polarity of the cosolvent.[119,120] The ethanolic system showed the largest area of an isotropic solution phase (compared to the area of liquid crystalline phases), which is present at all concentrations above 18 wt% ethanol, while for the glycols LC phases were obtained at much

higher concentrations. This corresponds very well to the results obtained in the synthesis of mesostructured silica monoliths, for which it was found that direct liquid-crystal templating approaches with tetraethoxysilane led to non-ordered materials, while removal of ethanol during gel formation resulted in periodically arranged silica structures.

Besides their interesting properties, little is known about the hydrolysis and condensation behavior of glycol-modified silanes. In our studies, the pH was varied from low values (high acid concentration) to the neutral range (using pure water). It can be seen immediately (Figure 2.1) that the modified silanes show an extraordinary condensation behavior with gel times being very low in neutral conditions, increasing towards pH = 2 and decreasing again in more acidic medium. In sol-gel systems, the typically applied tetraalkoxysilanes such as tetraethyl-orthosilicate or tetramethyl-orthosilicate are not miscible with pure water and react very slowly in the neutral regime of the pH-scale, considering hydrolysis and condensation reactions.[13] However, glycol-modified silanes are 100% miscible with water, therefore the hydrolysis reactions are very fast. Keeping this in mind, the explanation for the low gelation times at neutral pH and the maximum in the curve in Figure 1 around pH = 2 can be given based on the kinetics known for more common types of tetraalkoxysilanes at different pH. The PZC (point of zero charge) and IEP (isoelectric point) of silica and the corresponding siliceous precursors are both around pH 2-4. Above this pH, silica particles carry negative charges and condensation is catalysed by OH^- ('alkaline' conditions), below pH 2, silica carries positive charges and H^+ acts as the catalyst ('acidic' conditions). The minimum in condensation and therefore network formation rates (gelation time maximum) is normally found around this pH range and corresponds well to the trends observed in the glycol-based systems. The overall reaction rate above this pH range, especially at neutral conditions is governed by the hydrolysis rate which has a minimum at pH = 7 and increases with both the H^+ and OH^- concentration. The extremely high reaction rates found for the glycol-modified silanes can only be explained by an extremely high hydrolysis rate even under neutral conditions.

The various glycols used in this study show the same trend in the gelation times, but different reaction rates, particularly in the more neutral pH range. These observations indicate that the alcohol does have a distinct influence on the reaction kinetics, especially on the hydrolysis rates. The gelation times (at the same pH) decrease in the following order: $t_{gel}(PGMS) \gg t_{gel}(EGMS) > t_{gel}(GLMS)$ at neutral conditions and $t_{gel}(PGMS) \gg t_{gel}(GLMS) > t_{gel}(EGMS)$ around pH = 2, respectively. The reaction rate of GLMS at neutral pH was so

fast that no gels but only precipitates were obtained. The reactivity at neutral pH increases with the polarity and relative hydroxyl content of the respective glycol. Around pH 2 the lower SiO_2 content of PGMS (16%) and GLMS (16.5 %) compared to EGMS (20%) leads to lower volume fractions of SiO_2 in the overall mixture, when the mass ratio of SiO_2/P123/HCl ratio is held constant, leading to lower gelation times for PGMS and GLMS due to a lower theoretical density (higher solvent content) of the mixture. Another factor in the gelation kinetics might also be the different viscosity (v) of the respective glycols, which increases in the following order: v(PGMS) < v(EGMS) < v(GLMS). This factor might be another reason for the particularly high gelation time of PGMS around pH = 2.

2.3.2. Structural Properties of the Resulting Gel Bodies

As recently demonstrated, gels prepared from ethylene glycol-modified silanes in neutral conditions show a hierarchical network structure of a cellular silica backbone comprised of macropores in the range of 200 to 800 nm and periodically arranged mesopores with a repeating unit distance of 11 nm.[59]

At least two competing processes occur simultaneously during network formation; the first process is the sol-gel transition, thus the formation of a solid silica network, and the second, phase separation on different levels – on the one hand the formation of supramolecular aggregates of silica/surfactant assemblies which are responsible for the mesoscopic ordering, and on the other hand a macroscopic phase separation into condensed silica/surfactant and water/solvent rich domains which define the macroporous structure of the final gel. These processes cannot be viewed independently, since only the relative rates of phase separation and gel formation define the final gel structure. Nakanishi and Takahashi already showed that parameters in the synthesis procedure, which change these relative reaction rates, will have a pronounced influence on the architectural properties of the final gel, including mesoporosity, interconnected macroporosity, degree of macroscopic phase separation and thus, the morphology of the material.[30,103,121]

In the previously described system, the reactions were carried out in purely aqueous conditions, with very short gelation times. One of our working hypothesis for this work was that slower condensation rates would give the system more time to evolve and separate the different processes, especially silica condensation from mesoscopic phase separation. We therefore extended the synthesis parameters to acidic media, hoping to increase the degree of long range order in the material, by giving the mesophase more time to evolve. The small

angle X-ray scattering profiles of EGMS10 prepared under neutral and under different acidic conditions clearly indicate that the mesoscopic order is more pronounced for systems that have longer gelation times. For the PGMS systems, longer gelation times also favor long-range ordering, however, the structural features are evolved best at pH = 1, instead of pH = 2. This indicates that the processes that govern the structural mesoscopic features of the gel are very complex and highly interconnected, but nevertheless, fine-tuning of the mesostructure is possible by adjusting the experimental parameters.

Solid-phase formation from a liquid phase can be dominated either by a spinodal decomposition- or by a nucleation and growth-mechanism. The bicontinuous network morphology formed under neutral ('alkaline') conditions, with very short gelation times of only a few minutes, can be explained by a spinodal decomposition mechanism. Under acidic conditions, aggregates built of interconnected particles are formed, which can be understood by a nucleation and (particle) growth mechanism.

The particle morphology itself depends on the silane used – rod-like particles are formed in the case of EGMS, and more spherical particles in the case of PGMS. Interestingly, the macrostructure of the EGMS prepared monoliths resembles to a high degree the structure of rod-type SBA-15 material which is normally only formed at high ionic strength of the synthesis mixture.[23,122,123] Even a similar hexagonal shape of the rods can be found for our monoliths prepared at pH = 2, indicating a high degree of mesoscopic order.[124] However, the repeating unit distances are slightly higher in our material (approx. 11 nm) compared to the classical SBA-15 materials prepared from P123 (approx. 10 nm). So far, SBA-15 type of materials prepared via templating with non-ionic block copolymers such as Pluronic 123 could only be synthesized under acidic conditions, while in a neutral environment disordered and amorphous silica precipitates.[20] This was attributed to strong electrostatic and hydrogen bonding interactions due to the positive charge the siliceous species carry at pH < 2, thereby promoting cooperative self-assembly. By using ethylene glycol- and propane-1,2-diol-modified silanes as starting materials, these restrictions can be circumvented.

GLMS as starting material did not result in mesoscopically organized silica under the set of synthesis conditions used in this work. However, getting back to the work of Alexandridis, glycerol also shows a good compatibility with lyotropic LC-phases, thus it should be possible to obtain mesostructured materials from this precursor as well.

2.3. Conclusion

Different glycol-modified silanes such as the ethylene glycol, propane-1,2-diol and glycerol ester of silicic acid have been synthesized and applied in a TLCT approach with the non-ionic poly(ethylene oxide)-based block copolymeric surfactant P123 in aqueous (neutral) and acidic conditions. White, monolithic, 3-dimensional gels with a hierarchical network structure and an interconnected, multilevel pore system were obtained. The macroscopic gel morphology can be controlled by the choice of glycol to a large extent; propane-1,2-diol-modified silane results in gels with a particulate appearance and a very distinct periodicity of the mesophase, while ethylene glycol-modified silane forms a more cellular network architecture of single rods of 1-3 μm in length and 0.5 μm in diameter with a highly ordered 2D hexagonal honeycomb mesostructure. Gels prepared from the glycerol-modified silane did not show any long-range ordering under the given synthetic conditions, and exhibit particulate structures typical for silica-based sol-gel materials. For each system, the optimal synthesis parameters such as $SiO_2/P123$ ratio and acid concentration have to be fine-tuned to get optimal results with respect to long-range periodicity of the mesostructure.

The application of glycol-modified silanes in the synthesis of hierarchically structured silica monoliths is facile, rapid, environmentally benign, and does not require the presence of an additional phase separation polymer. This method can readily be extended towards organofunctional monolithic materials (see Chapter 3). Furthermore, the presented materials have great potential for several applications e.g. chromatographic or separation purposes (see Chapter 6), support materials or catalysis.

3 Monolith Processing and Surface Chemistry – Surfactant Extraction, Surface Modification and Drying

3.1. Motivation

The first crucial issue in obtaining porous materials from a template-based synthesis is the removal of the templating amphiphilic molecules embedded within the ordered structure. This is typically done after the synthesis on either the dried or the wet gels. Solvent or supercritical fluid extraction as well as treatment with sulfuric acid for a stepwise removal of the template have been applied to wet gels, whereas calcination, microwave digestion and ozone treatment are typical examples that have been performed after drying of the gels.[60,125-129]

Second, drying of large monoliths is often difficult, since surface tension and evolution of capillary pressure often result in large shrinkage or even destruction of the whole gel body. One typical procedure to prevent cracking is drying with supercritical fluids (scf), e.g. carbon dioxide, since the building-up of a gas/ liquid interface is avoided, hence no capillary pressures evolve.[106] However, scf extraction is expensive, time consuming, and requires high pressures sometimes even combined with high temperatures. Another approach for drying hierarchically organized porous monoliths has recently been presented by Mukai et al. via freeze gelation and freeze drying.[107]

The synthesis and drying of silica monoliths with a unique hierarchical organization of the pores composed of an extremely filigrane inorganic backbone by utilizing supercritical solvents was recently published by Huesing et al.[59] One objective of the continuing research was to find alternative and more simple routes to supercritical drying to remove the solvent and possibly extract the block-copolymer template but still avoid shrinkage and collapse of the pores.

A very promising procedure for drying large silica gels relying on a simple surface modification treatment with trimethylchlorosilane was presented in the mid-nineties as an alternative to supercritical drying. The capillary pressure, P_c, generated during drying is a function of the pore fluid/vapor surface tension, γ_{LV}, the contact angle, θ, between the fluid/vapor interface and pore wall, and the pore radius, a, as follows:

$$P_c = -(2\gamma_{LV}\cos\Theta)/a.$$ (1)

For a wetting fluid ($\theta < 90°$), P_c is negative, thus indicating that the fluid is in tension. The presence of organic methyl groups on the surface of the silica gel in combination with a proper selection of the final pore fluid, e.g. hexane allowed to change the contact angle to lower capillary pressures and thus dry monolithic wet silica gels without cracking[108-111].

A similar approach also using organochlorosilanes and organoalkoxysilanes as post treatment reagents was published recently not for drying, but for the extraction of ionic surfactants from self-assembled silica-surfactant powders. As the driving force for this reaction the replacement of electrostatic interactions at the inorganic-organic interface by covalent siloxane bonds, that is the formation of Si-O-SiR$_3$, was named[32,33].

In the first part of this chapter (3.2.), silylation with trimethylchlorosilanes was used to simultaneously extract the templating agent from the wet gel monoliths and facilitate a simple drying at ambient pressure of the large monoliths. This silane treatment was not only extended to non-ionic surfactant-silica systems, in which self-assembly is directed by hydrogen bonding, but also to large, mesostructured silica monoliths with very low densities and a hierarchical build-up of the porous structure. Extraction and drying with trimethylchlorosilanes is compared with other extraction/ drying procedures such as treatment with supercritical carbon dioxide, washing with ethanol or petroleum ether solutions and subsequent thermal treatments.

The next chapter (3.3.) represents an extension of the drying procedure with trimethylchlorosilane to the use of (organo)functional silanes such as vinyldimethylchlorosilane, (chloromethyl)dimethylchlorosilane, 3-mercaptopropyl-trimethoxysilane, phenyltrimethoxysilane, 3-[(2,2-dimethyl-1-aza-2-silacyclopent-1-yl)dimethylsilyl]-1-propaneamine, a cyclic silazane resulting in aminopropyldimethylsilyl groups on the silica surface, and (methylmethacryloyl)dimethylmethoxysilane. These silanes not only differ in the choice of organic functionality, but also in their reactive groups for anchoring to the silica surface. Chlorosilanes as well as alkoxysilanes, from mono- to the trialkoxy derivatives, were applied as silylation agents. In this work, full account to the degree of surface coverage with organofunctional moieties is given, as well as a discussion of the extraction efficiency with respect to removal of the block copolymer template and the influence on the structural features of the monoliths.

In the third part of this chapter (3.4.) a novel amino acid functional silane (rac-3-(dimethyl(phenyl)silyl)alanineester) was tested as surface modification agent for silica materials. The phenylsilyl moiety of this silane has been found to be exceptionally instable towards hydrolysis resulting in a silanol moiety which can be used for covalent coupling to a silica surface via a Si-O-Si bond. Silanes with amino acid functionality are not yet available for the purpose of silica surface modification though representing an interesting moiety for applications such as separation processes (HPLC), sensing, immobilization of (bio)molecules or functionalization of biomaterials. A set of porous materials with different well characterized pore structures was chosen to investigate the suitability of this silane for surface modification of porous silica materials. Furthermore the amino acid functionalized silane was compared with trimethylphenylsilane with respect to the hydrolysis of the phenylsilyl moiety.

3.2. Supercritical Drying with Carbon Dioxide vs. Ambient Pressure Drying after Surface Silylation with Trimethylchlorosilane

Large, low density silica monoliths (E10 prepared at pH 6, see Chapter 7.2.3.) with a hierarchical organisation of macro- and periodically arranged mesopores were obtained in a one-step procedure by treatment of as-synthesized wet gels with trimethylchlorosilane. This approach does not only offer the possibility to simultaneously achieve drying of the gel body and extraction of the block copolymer surfactant while preserving a monolithic body but also allows a viable access to surface modification. Monolithic gels from different drying procedures with or without extraction of the templating agent and supercritical drying in carbon dioxide are compared to the ones from treatment with trimethylchlorosilane: Drying at ambient pressure (samples TUW –d), extraction with ethanol or petroleum ether followed by ambient pressure drying (samples TUW –ed and –pd, respectively), supercritical extraction with carbon dioxide (TUW –scf), treatment of the surface with trimethylchlorosilane and subsequent ambient pressure drying (TUW –tms). In addition, all gels were subjected to calcination, these samples are denoted as –c. The choice of post-treatment and drying protocol offers the possibility to deliberately tailor the surface chemistry of these hierarchically organized silica monoliths.

Small angle X-ray scattering, nitrogen sorption, electron microscopy, thermogravimetric analysis and solid state NMR studies were applied for a detailed structural

and chemical characterization of samples from different drying procedures, thus allowing for a comprehensive comparison of the various gels.

3.2.1. Results and Discussion

This work is focussed on hierarchically organized silica monoliths with a macroporous cellular structure. The macropores are formed from single interconnected filigrane silica strands that exhibit distinct periodic ordering of the mesopores. Thus, the material after drying is highly porous, exhibits a large specific surface area and very low density, comparable to silica aerogels – however, its structural features are very different. The size of the monoliths is rather large with dimensions of 1 cm in diameter and 3 cm in height.[59]

Drying with Trimethylchlorosilane. Drying of a wet gel monolith after solvent exchange processes by successively increasing the temperature, or via supercritical fluids, e.g. carbon dioxide, should not alter the chemical features of a silica gel to a large extent. When trimethylchlorosilane is applied as reagent for drying, a surface silylation process takes places, which completely reverses the surface polarity. The material is turned from a hydrophilic, water containing system to a non-polar, hydrophobic one. The chemical reaction occurs with release of hydrochloric acid and is displayed in Scheme 3.2.1 as envisioned in a mesoporous material.
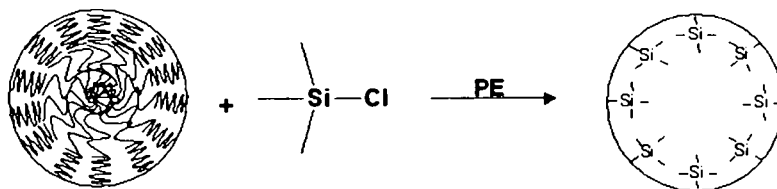
Scheme 3.2.1. Silylation of surface silanols with trimethylchlorosilane

It is not anticipated to have a 100 % conversion of silanols to trimethylsiloxy-groups due to steric considerations (umbrella effect), however a significant amount of silanols has reacted.[13]

The proposed change in surface polarity can also be observed by the behavior of the wet gels upon immersion in the trimethylchlorosilane – petroleum ether mixtures. Figure 3.2.1 shows that the P123/water/EG mixture, which was the pore fluid in the wet gel, is spontaneously expelled from the gel. An emulsion of P123/water/EG in tmcs/PE is formed in the flask which can be observed in the form of large, white (water-surfactant) droplets that become transparent after several hours.
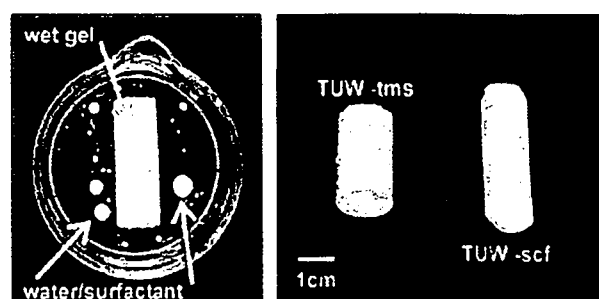
Figure 3.2.1. Photographs of the expulsion of P123/water/EG droplets from a wet gel upon immersion in a petroleum ether (PE)/trimethylchlorosilane mixture (left side) and TUW –scf and TUW –tms after the drying process (right side).

Morphology and Appearance. The sample TUW –ed showed strong cracking during the drying procedure and only smaller pieces could be obtained. All other techniques resulted in white, crack-free monoliths (Figure 3.1.1.), with TUW –d and TUW –pd exhibiting a larger shrinkage (about 9%). The structural parameters of the final materials are summarized in Table 3.2.1. For the monolithic samples, densities and linear shrinkages could be determined. The other posttreated gels (–scf and –tms) exhibit very low densities (down to 0.13 $g \cdot cm^{-3}$), while TUW –d and –pd are rather dense, in parts due to the macroscopic shrinkage, but also because the block copolymer surfactant is still present in the dried gel (vide infra). The linear shrinkage for TUW –scf and TUW –tms from the wet gel to the final dried and even calcined gel is very small with 3-4 % and 5-12 %, respectively.

Structure. The microstructure of the final dried and calcined gels was investigated by means of nitrogen sorption, small angle X-ray scattering, and electron microscopy.

Table 3.2.1. Structural parameters of the hierarchically structured monoliths from different drying procedures.

Sample	Extraction efficiency[a] (%)	Density/g cm^{-3}	Linear shrinkage (%)	Nitrogen sorption S^{BET}/m^2 g^{-1}	V/cm^3 g^{-1}	D^{BJH}/nm	$d_{10}$$^{(SAXS)}$/nm	t^{wall}/nm
TUW-d	0	0.75	9	13	0.03	—	10.9	—
TUW-c	—	0.15	11	930	1.7	8.3	9.3	2.4
TUW-ed	97	—	—	690	0.63	—	—	—
TUW-ec	—	—	—	1050	0.79	—	—	—
TUW-pd	0	0.75	9	13	0.03	—	10.9	—
TUW-pc	—	0.15	11	930	1.7	8.3	9.3	2.4
TUW-scf	96	0.13	3	1070	2.8	11.0	11.5	2.3
TUW-scf-c	—	0.18	12	940	2.0	9.2	9.7	2.0
TUW-tms	98	0.16	4	1010	2.4	10.8	11.4	2.4
TUW-tms-c	—	0.16	5	860	1.8	9.8	10.2	2.0

[a] The extraction efficiency (%) was calculated from the TGA weight loss in the range from 433-623 K.
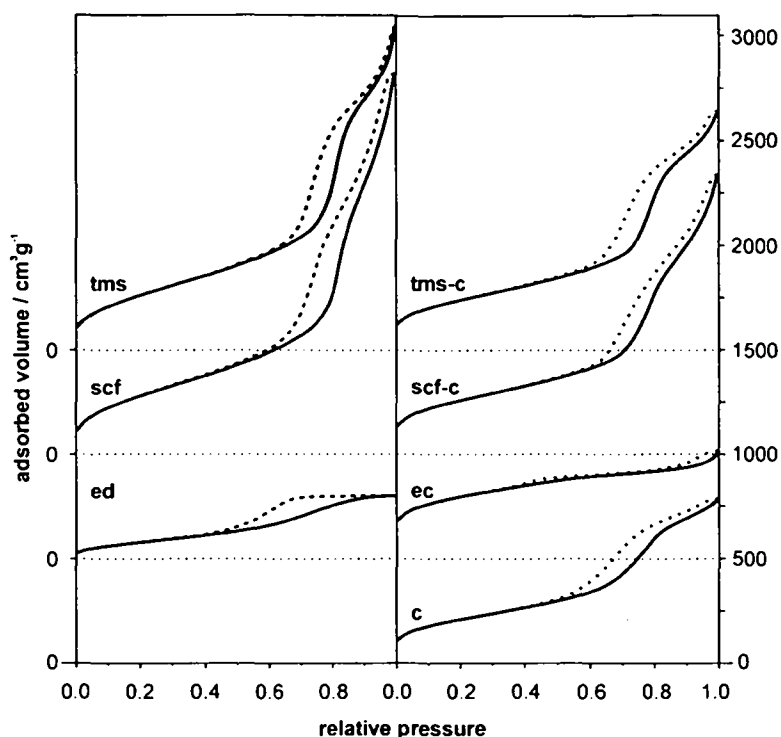
Figure 3.2.2. Adsorption – desorption isotherms from nitrogen sorption for differently dried samples: TUW – ed/ ec, TUW –scf/ scf-c, TUW –tms/ tms-c and the simply calcined sample TUW –c.

Adsorption studies showed that TUW –d and TUW –pd have very low specific surface areas, again attributable to the presence of surfactant in the pores (Table 3.2.1). Their N_2 isotherms can be classified as type II. Upon calcination, the pore volumes as well as the specific surface areas increase drastically to values of 1.7 g cm^{-3} and 930 m^2 g^{-1}. These values are analogous to the supercritically dried and trimethylchlorosilane extracted samples. Compared to TUW –scf and TUW –tms, TUW –ed as well as the corresponding calcined sample TUW –ec exhibit significantly smaller pore volumes and a type IV isotherm with H2 hysteresis loop (Figure 3.2.2). The total porosity for TUW –scf and TUW –tms amounts to 2.8 and 2.4 g cm^{-3}, respectively, thus substantially exceeding the values obtained for the extraction with petroleum ether and ethanol. TUW –scf and TUW –tms, as well as the corresponding calcined samples exhibit also high specific surface areas with values up to 1000 m^{2}g^{-1}. The type IV isotherms show a hysteresis loop that can be described as H1.

In addition to surface area and pore volume, the pore size distribution was evaluated according to the BJH model from the adsorption branch of the isotherm (Figure 3.2.3). Only for TUW –scf/scf-c and TUW –tms/tms-c monomodal pore size distributions with pore diameters (BJH) of about 9-11 nm could be observed. TUW –c and TUW –pd-c show rather

42

broad maxima of about 8 nm indicating a wider distribution of the pore sizes, while no maximum was found for the samples extracted with ethanol.
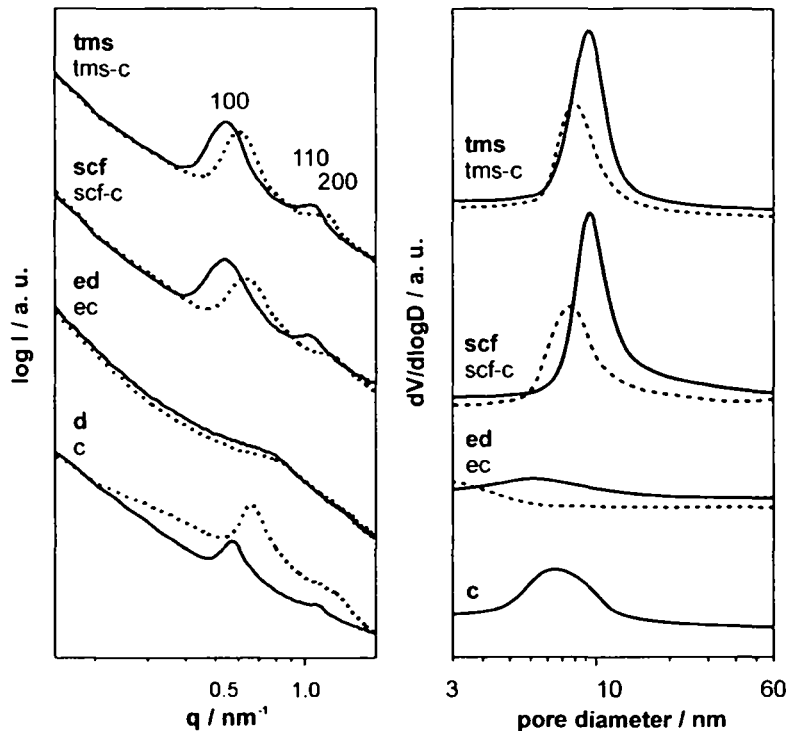
Figure 3.2.3. SAXS patterns (left) and BJH pore size distributions (right) of differently dried samples: TUW – ed/ ec, TUW –scf/ scf-c, TUW –tms/ tms-c and TUW –d/ c.

The periodic arrangement of the pores in TUW –scf and TUW –tms was also confirmed by SAXS studies (Figure 3.2.3). The patterns exhibit well-resolved reflections with d(100) spacings of about 9.3-11.5 nm and d(200) spacings of about 4.7-5.9 nm. Due to the large width of the reflections, the d(110) peak that is expected for a hexagonal packing is not resolved. However, since the structure is stable upon calcination, it can be assumed that the pores are ordered in a hexagonal pattern which is supported by TEM analysis (Figure 3.2.4). No distinct differences between the two drying techniques (scf and tmcs treatment) can be observed. Treatment with petroleum ether results in gels that are structurally comparable to TUW –d. For both, a strong decrease in the unit cell parameter compared to TUW –scf and TUW –tms is observed, indicating a shrinkage of the mesostructures during the different processing steps. This behavior was expected due to the stronger macroscopic shrinkage of the gel bodies during drying. Interestingly, treatment with ethanol results in complete loss of ordering.

The calcined samples show smaller repeating unit distances, probably due to removal of residual solvent or surfactant, thermally-driven network condensation and increased macroscopic shrinkage of the monolith bodies.
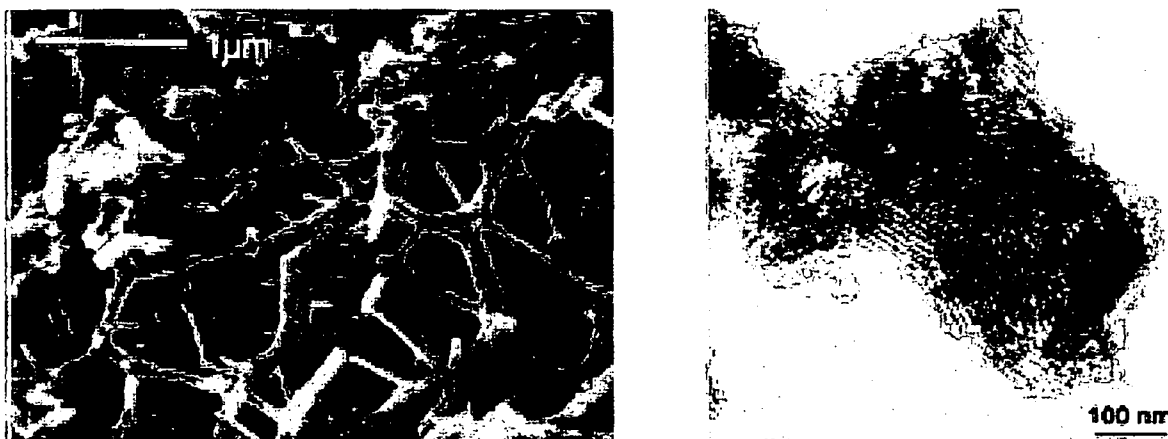
Figure 3.2.4. Scanning electron microscopy (SEM) image of TUW -tms (left) and a transmission electron microscopy (TEM) image of the same sample, clearly exhibiting mesoscopic ordering in the material.

Scanning and transmission electron microscope images of the dried and calcined gel samples show a hierarchical build-up of the network comprising a cellular silica framework with macropores of about 200-800 nm in diameter and periodically arranged mesopores of about 10 nm.[59] Figure 3.2.4 shows representative SEM and TEM images for TUW -tms. The images taken for TUW -scf and the corresponding calcined samples are very similar.

Chemical Composition. As no significant influence of the drying procedure on the macro- and mesostructure of the gels from tmcs and scf treatment was observed, the chemical composition was investigated by means of thermo-gravimetric analyses and ^{13}C solid-state NMR studies. Table 3.2.1. gives the extraction efficiencies calculated from the TGA results. The traces were interpreted as follows: the weight loss below 423 K was attributed to water, while the losses in the temperature range of 433 – 623 K were ascribed to the surfactant and to a smaller extent to loss of framework water.[60] Methyl groups in the silylated gels are known to be stable until 623 K.

For both sets of samples, TUW -scf and TUW -tms, the block copolymer surfactant is almost completely extracted from the silica gel with extraction efficiencies above 96 %. Thus, the need for calcination is eliminated altogether. This result is quite surprising, since previous publications stated significantly lower extraction efficiencies for procedures using supercritical carbon dioxide as solvent. Anderson et al. reported the loss of only 20-30 % of

hexadecyltrimethylammonium bromide surfactant.[91] The difference to our results can probably be attributed to the different templating processes, relying on a non-ionic $[S^0I^0]$ mechanism in our case, while Anderson and coworkers used a cationic surfactant in a base catalyzed silica solution, thus having a charge compensation $[S^+I^-]$ templating system. Higher extraction efficiencies (up to 93 %) could only be obtained by mixing methanol in supercritical CO_2 fluid as a modifier to increase the bulk solubility of the ionic surfactant. [128,129] However, even in Pluronic P123 templated SBA-15 $[S^0I^0]$ systems, extraction efficiencies with supercritical carbon dioxide were only in the range of 79 %.[60] Obviously, the combination of meso- and macropores in our hierarchical silica gel structure assists the extraction of surfactant. This conclusion is also supported by the TUW –ed samples, for which the extraction efficiency is as high as for the above discussed samples. Again more surfactant could be removed from the hierarchically organized gels via treatment with ethanol at room temperature than was reported by other authors.[60]

The surfactant could not be extracted with petroleum ether (PE). After treatment with PE the samples (TUW –pd) show a similar weight loss profile than TUW –d. Calcination leads in all samples to a complete removal of the templating agent.

Distinct differences in the chemical composition of the samples from the different drying techniques were proven by means of ^{13}C CP-MAS NMR (Figure 3.2.5).
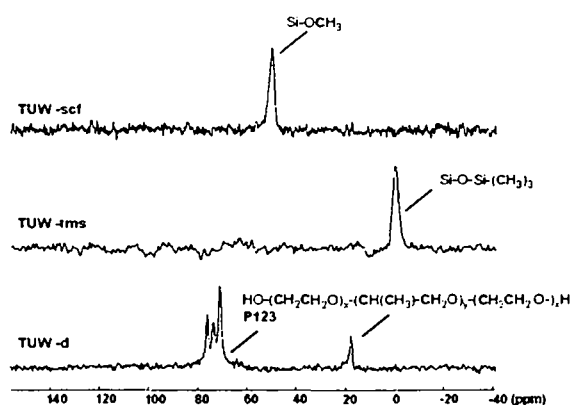
Figure 3.2.5. ^{13}C-CP MAS NMR spectra of differently dried samples (TUW –d, TUW –scf and TUW –tms).

The air-dried sample, TUW –d, clearly exhibits the expected resonances for the poly(ethylene oxide)-poly(propylene oxide) triblock copolymer surfactant at 20 ppm and 70-80 ppm for the CH_3-atoms of the PPO units and the CH_2-groups of the block copolymer backbone, respectively. Neither the sample from supercritical drying (TUW –scf) nor the sample from

trimethylchlorosilane treatment (TUW –tms) shows any resonances of the surfactant, which confirms the results from the TGA of an almost complete extraction of the surfactant from the gels. Nevertheless, the surface properties of TUW –scf and TUW –tms cannot be compared. Surprisingly, TUW –scf also shows carbon resonances at 50 ppm, which can be attributed to methoxy-units covering the surface (from the solvent exchange of water to methanol prior to supercritical drying). These gels display a non-permanent hydrophobity, since -OCH$_3$ groups are converted to silanol groups with time.

As expected, the spectrum of TUW –tms exhibits signals of the trimethylsilyl groups at 0 ppm that cover the silica surface and render the material hydrophobic. These results suggest that the surface treatment with tmcs can be extended to other functional organosilanes, thus opening novel ways to organically modified highly porous, mesostructured silica monoliths.

3.2.2. Conclusion

In conclusion, the structure and the surface properties of hierarchically organized silica monoliths can be altered significantly by the choice of post-treatment the gels are subjected to. Treatment of the wet gel with ethanol and subsequent drying will result in porous powders with high specific surface areas, but no monolithic structure can be obtained and the periodic ordering of the mesopores is completely destroyed. In contrast, gels that have been dried by thermal treatment (with or without petroleum ether washing) and simultaneous degradation of surfactant still show reflections in the small angle X-ray scattering profile, indicating at least some periodicity in the material. Here the porous structure can be preserved during the drying procedure. The best results in terms of preservation of the structural features from the wet gels to the dried ones were obtained by supercritical extraction/drying with carbon dioxide and by surface silylation with trimethylchlorosilane. Here, the high porosity with a very uniform pore size distribution and periodicity was maintained during all drying steps.

In addition, the surface chemistry can be deliberately tailored resulting in hydrophilic gels with silanol coverage of the surface via drying under ambient conditions and calcination, in permanently hydrophobic gels with trimethylsilyl groups on the surface via treatment with trimethylchlorosilane prior to drying and non-permanently hydrophobic gels with alkoxide groups on the surface via supercritical drying. Simultaneous to the surface modification, complete extraction of the non-ionic block copolymer surfactant is achieved by treatment with chlorosilanes and supercritical drying, therefore reducing the number of synthetic steps.

3.3. Ambient Pressure Drying after Surface Silylation/Surfactant Extraction with Organofunctional Silanes

Large, low density silica monoliths (E17 prepared at pH 1, see Chapter 7.2.3.) with a hierarchical organisation of macro- and periodically arranged mesopores were prepared by a true-liquid crystal templating approach with ethylene glycol-modified silane in the presence of a non-ionic block copolymer surfactant[21] and subsequent drying of the wet gels with organosilanes. In this approach the silanes serve two functions: first, the silylation reactions allow for non-destructive drying of the monolithic gels and simultaneous extraction of the block copolymer template; second, they serve as surface functionalization agent. A variety of organofunctional silanes such as trimethylchlorosilane, 3-mercaptopropyltrimethoxysilane, phenyl-trimethoxysilane, 3-[(2,2-dimethyl-1-aza-2-silacyclopent-1-yl)dimethylsilyl]-1-propaneamine, a cyclic silazane resulting in aminopropyldimethylsilyl groups on the silica surface, and (methylmethacryloyl)dimethyl-methoxysilane, has been successfully applied in the interfacial modification of the silica surface. The resulting silica monoliths were characterized with respect to their structure by small angle X-ray scattering, nitrogen sorption and electron microscopy, and with respect to their chemical composition by thermogravimetric analysis, titrations and solid state NMR studies.

3.3.1. Results and Discussion

The materials discussed here are hierarchically structured silica monoliths built up from interconnected rod-shaped particles and macropores with a pore diameter of 650 nm and a pore volume of 1.63 cm^3g^{-1} which can be obtained from drying procedures with supercritical carbon dioxide as well as from drying with the aid of trimethylchlorosilane.[21,59,130] The particles have a length of about 1-2 μm and a diameter of about 400 nm, and exhibit periodically ordered cylindrical mesopores arranged in a 2D hexagonal pattern parallel to the length of the particles (Figure 3.3.1). A third pore size level can be found in the form of micropores in the mesopore walls. All discussed samples were obtained in the form of rather large, white, crack-free monoliths after drying, with dimensions of 1 cm in diameter and 3 cm in height. Low densities and linear shrinkages were found for all samples with values around 0.2 $g·cm^{-3}$ and 15 %, respectively. The structural parameters of the final materials are summarized in Table 3.3.1.
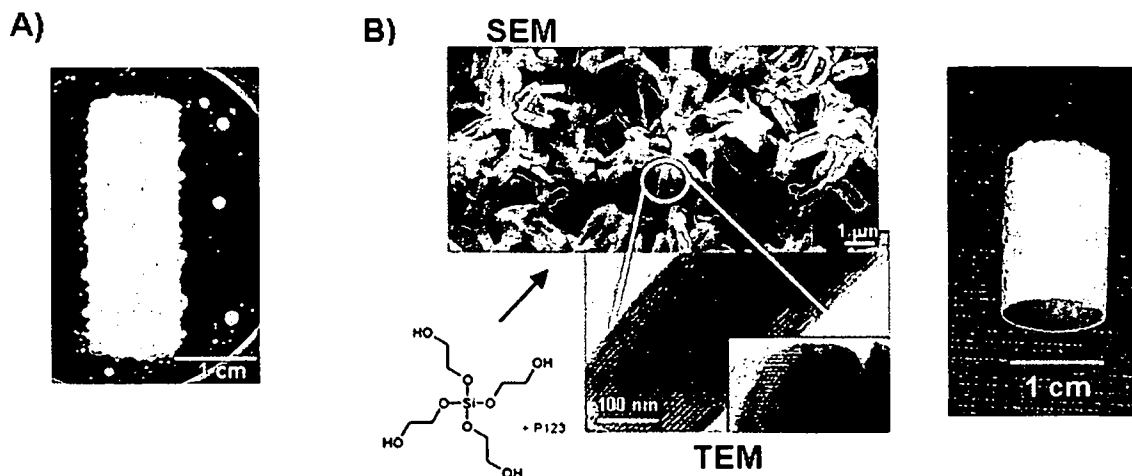
Figure 3.3.1. A) Photograph of a wet gel sample during treatment with Me₃SiCl and B) a photograph, SEM and TEM of the corresponding dried gel with trimethylsilyl-groups on the surface.

Table 3.3.1. Structural parameters of the different functionalized hierarchically organized silica gel monoliths.

Sample	SAXS pore to pore distance/nm	SAXS pore wall (silica backbone)/nm	D^{SAXS}/nm	C Value	S^{BET}/ $m^2 g^{-1}$	D_{BJH} (w^{rd})/ nm (%)	Pore wall/nm	$p^{w.al}$/ $cm^3 g^{-1}$	$p^{me.o}$/ $cm^3 g^{-1}$
tms	13.9 ± 0.1	4.5 ± 0.3	9.4 ± 0.3	41	904	10.3/(16)	3.6	0.14	0.88
phs	13.4 ± 0.1	4.5 ± 0.3	8.9 ± 0.3	62	245	8.0/(9.8)	5.4	0.04	0.18
aza	13.6 ± 0.1	2.8 ± 0.5	10.8 ± 0.5	21	447	11.4/(45)	2.2	—	0.65
mps	14.1 ± 0.1	4.8 ± 0.5	9.3 ± 0.5	52	300	8.3/(7.4)	5.8	0.03	0.31
mms	13.6 ± 0.1	4.6 ± 0.3	9.0 ± 0.3	34	401	8.7/(4.4)	4.9	0.02	0.52

Figure 3.3.2 shows schematically the different organofunctional silanes that are employed in the template displacement and functionalization reaction. Besides the different functional groups, from methyl, vinyl, chloromethyl, amino, mercapto, phenyl to methacrylate-moieties, the silanes have different reactive groups with respect to the silylation reaction, e.g. chlorosilanes, alkoxysilanes and silylamines, thus resulting in different reactivities and by-products.

The reaction of chlorosilanes (tms, vds, cds) with surface silanol functionalities occurs spontaneously and gives hydrochloric acid as the by-product, which has to be removed from the wet gel by subsequent washing procedures. In addition, the reaction is performed in an aqueous environment resulting in the formation of disiloxane species as a competing reaction. Thus, an excess of the silanes was employed.[44,130,131] Trimethylchlorosilane which has been investigated in detail as surface modification and surfactant extraction agent in the previous part of this Chapter (3.1.) serves as a reference here.
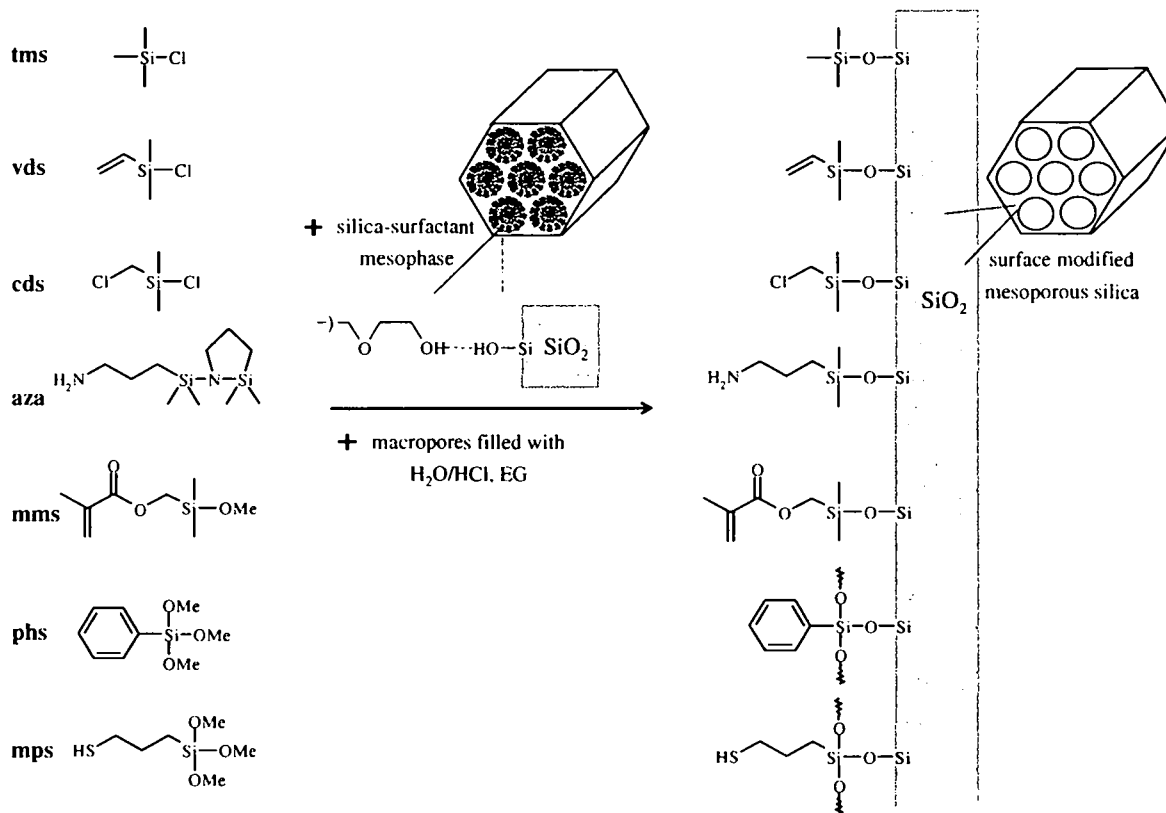
Figure 3.3.2. Schematic illustration of the pool of organofunctional silanes employed for template displacement and surface functionalization of the hierarchically structured silica monoliths.

Vds and *cds*: ^{13}C-CP MAS NMR and TGA experiments showed quite intense peaks of residual surfactant and low surfactant extraction efficiencies (around 93 %), respectively. As the organic moieties are sensitive to oxidation at elevated temperatures it was not possible to further remove the surfactant by thermal treatment at 200 °C and still preserve the functional groups. Determination of the double-bond content of vds by reaction with bromine and subsequent iodometric titration of unreacted bromine also showed a low surface coverage with vinyl groups of 0.8 $mmol \cdot g(SiO_2)^{-1}$ (in comparison, for mms a surface coverage of 2.35 $mmol \cdot g(SiO_2)^{-1}$ has been determined by the same method). As these silanes did not allow for a one-step process of simultaneous surface modification and surfactant extraction they are not further included in the discussion of the structural and chemical parameters.

For alkoxysilanes (*mms, phs, mps*) the reactivity towards surface silylation reactions is drastically reduced compared to chlorosilanes. Here, the silanes are employed in the pure form. For alkoxysilanes one of the reaction products is alcohol, which is removed during

drying. Nevertheless, extensive washing with alcohol is performed, since the trialkoxysilanes display not only surface silylation reactions, but also non-surface bonded, small oligomers are formed which should be removed prior to drying. It is worth mentioning that methacryloyloxyfunctional silanes bearing a methylene spacer between organic function and silicon atom, such as mms, were found to exhibit exceptionally high hydrolysis rates compared to the ones with a propylene spacer, which makes them interesting candidates for surface functionalization reactions.[132]

The reaction of the wet gel silica surface with 3-[(2,2-dimethyl-1-aza-2-silacyclopent-1-yl)dimethylsilyl]-1-propaneamine (aza) is a silazane-based silylation reaction. In contrast to other commercially available silazanes,[133] which release ammonia upon the silylation reaction, aza does not generate any by-products – in a ring-opening reaction the cyclic azasilane reacts with the hydroxyl groups on the silica surface at low temperatures to give two mono-functional aminopropyldimethylsilyl-groups. The reactions of cyclic azasilanes are known to be very rapid at room temperature. Treatment of the wet gel monoliths with higher concentrations of aza then 3% results in dissolution of the silica backbone, due to the basicity of the amino functionality. Therefore, aza/PE solutions with small amounts of aza are employed in the silylation reaction.

Structure. The microstructure of the final dried materials was investigated by means of nitrogen sorption, small angle X-ray scattering studies, and electron microscopy.

The periodic arrangement of the pores after the treatment with the organofunctional silanes was confirmed by SAXS studies (Figure 3.3.3). All patterns show up to four distinct Bragg diffraction peaks, which can be indexed to (10), (11), (20), and (21) associated with a 2D hexagonal symmetry (p6mm) with an interplanar d_{10} spacing of about 12 nm. In some samples, the (21) reflection is not visible due to the form factor. The repeating unit distance itself does not show any influence on the functionality applied. However, the reflections of aza exhibit a higher half-width, probably due to dissolution and rearrangement reactions of the silica network induced by the high basicity of the amino-groups resulting in smaller aggregates. In contrast, the mps-modified samples display a noticeable higher intensity and smaller half-width of the Bragg reflections compared to the other functionalities, indicating a high degree of mesostructural ordering in the final dried material.
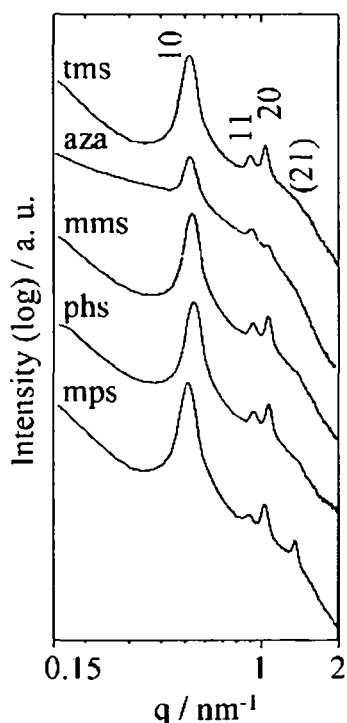
Figure 3.3.3. Small angle X-ray scattering patterns for the materials studied; from bottom to top: *mps, phs, mms, aza* and *tms* modified silica gel monoliths.
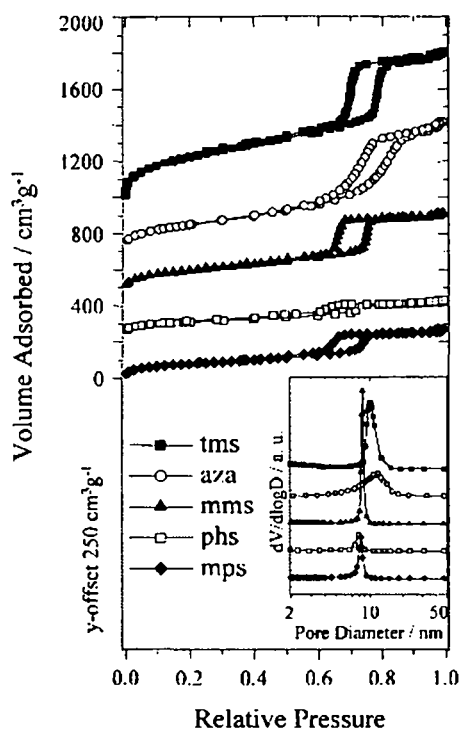
Figure 3.3.4. Nitrogen sorption isotherms for the modified silica gels; the insert shows the differential pore size distribution for the same samples calculated from the nitrogen adsorption branch of the isotherm.

Nitrogen adsorption/ desorption studies (Figure 3.3.4.) were performed to get insight into the pore structure of the functionalized silica gel monoliths. Mesoporous silica materials templated with triblock copolymers such as SBA-15 are known to have not only large, uniform and ordered channels which can easily be seen by nitrogen sorption but also complementary micro- and (small) mesopores located in the silica wall. It has been evidenced that the hydrophilic poly(ethylene oxide) chains of the template penetrate within the silica walls during the synthesis to result in micro- and (small) mesopores upon calcination.[71]

Samples modified with organodimethyl-silanes (*tms, aza, mms*): Silylation reactions with trimethylchlorosilane, the aza-cycle and the methylmethacryloyl)dimethylmethoxy-silane should result preferentially in the reaction with the silica surface and as side-reaction, the formation of dimeric species is anticipated. Ad-/desorption isotherms of all samples could be classified as type IV with H1 hysteresis loops. Specific surface areas (S^{BET}, see also Table 3.3.1) are high with values of 401 and 447 $m^2 \cdot g^{-1}$ for the samples *mms* and *aza*, respectively, and significantly higher for sample tms (904 $m^2 \cdot g^{-1}$). The difference can be explained by the

contribution of smaller pores in the pore wall to the total surface area in case of sample tms, which is manifested in a higher increase of the adsorbed nitrogen volume at very low relative pressure. The larger organosilyl-moieties in samples aza and mms fill up or block these pores which reduces the surface area by almost 500 $m^2 \cdot g^{-1}$. In the same way the porewall volumes (P^{wall}) decrease from 0.14 $cm^3 \cdot g^{-1}$ (tms) to no porosity (aza) and 0.02 $cm^3 \cdot g^{-1}$ (mms). High mesopore volumes of 0.52-0.88 $cm^3 \cdot g^{-1}$ were observed for all samples, proving that the block copolymer template has been efficiently removed from the mesopore structure. All samples exhibit monomodal pore size distributions with pore diameters (D^{BJH}) of 8.7-11.4 nm (Figure 3.3.4). The differences in diameter cannot satisfactorily be explained by the size of the organo-silyl groups, as sample aza exhibits the largest pore size. As already mentioned, treatment of the monoliths with higher concentrations of aza/PE solutions leads to destruction of the mesoscopic- and also monolithic structure, as the basic aminopropyl functionality leads to dissolution of the silica backbone. At lower concentration silica is only dissolved superficially probably leading to a larger pore diameter and also broader pore size distribution of aza, the samples which also show the broadest Bragg reflections. The results obtained from nitrogen sorption analyses are in excellent agreement with the results obtained from SAXS measurements. Fitting to the ratio of the intensities of the Bragg reflections also confirms that for the aza modified samples, a drastic reduction of the pore wall thickness (2.8 nm compared to 4.5 nm) compared to the other functionalized monoliths is observed.

Samples modified with organotrialkoxy-silanes (phs, mps): Surface functionalization with these reagents does not only result in reaction with the surface, but the trialkoxysilanes are also prone to intermolecular reactions resulting in the formation of oligomeric species (which can be connected to the silica surface).

Again, the ad-/desorption isotherms of all samples can be classified as type IV with H1 hysteresis loops (Figure 3.3.4). In comparison to the samples modified with organodimethylsilyl groups, samples treated with organo-trialkoxysilanes exhibit significantly lower surface areas (S^{BET} 245-300 $m^2 \cdot g^{-1}$), and smaller mesopore sizes ($D^{BJH} \sim 8$ nm) and volumes ($P^{meso} \sim 0.25$ $cm^3 \cdot g^{-1}$) in the nitrogen sorption experiments (see also Table 3.3.1.), but similar repeating unit distances (~ 12 nm) in the SAXS experiments. These results suggest that the trialkoxysilanes have not only bound to the silica surface to form a monolayer, but have formed a polysiloxane network attached to the surface of the silica backbone with a thickness of about 2.5 nm (difference in the mesopore diameter D^{BJH} compared with sample tms) as anticipated.

No differences between the various samples could be observed by scanning and transmission electron microscopy. SEM images of the dried samples show cellular networks with open macroporosity and interconnected rod-shaped particles, suggesting that the organosilanes, particularly the organotrimethoxysilanes, have bonded specifically to the surface of the existing silica network and have not formed a second phase within the macropores. The particles itself exhibit periodically ordered, cylindrical mesopores arranged in a 2D hexagonal arrangement parallel to the particle length in the TEM. (Figure 3.3.5).
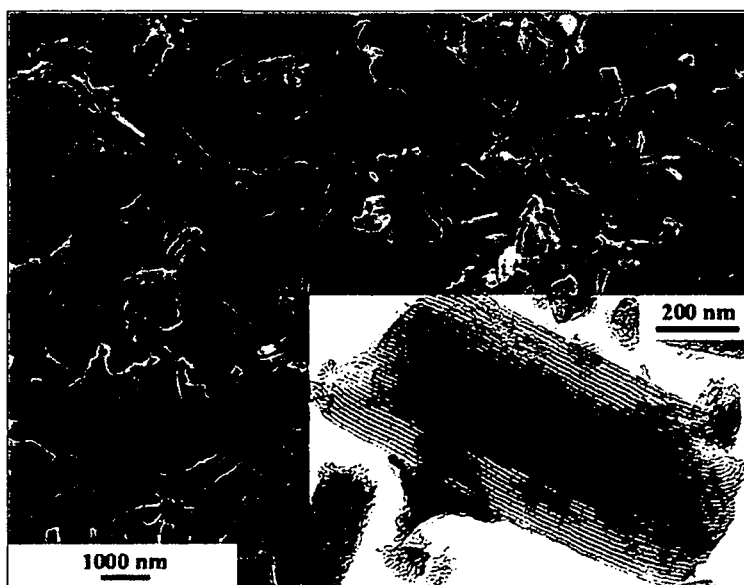
Figure 3.3.5. Representative SEM and TEM images of a (methylmethacryloyl)dimethyl- functionalized silica gel.

Chemical Composition. As no significant influence of the silanization prozess on the macro- and mesostructure of the gels was observed apart from different thicknesses of the organosilyl layer and the reduction of the pore wall thickness for aza, the chemical composition was investigated by means of thermo-gravimetric analyses and ^{29}Si- and ^{13}C solid-state NMR studies (Table 3.3.2). Furthermore, the amount of accessible double bonds of the methacrylate groups and also the amount of aminopropyl groups was quantified by reaction with bromine or acid-base titration, respectively.

Table 3.3.2 also gives the extraction efficiencies calculated from the TGA results in the temperature region around 200 °C which corresponds to the decomposition of the block

copolymer template. For all samples the extraction of the template is almost complete with efficiencies of 98-99 %.

Table 3.3.2. Chemical composition, surface loadings, and extraction efficiencies of the different functionalized hierarchically organized silica gel monoliths.

Sample	Extraction efficiency/%	Surface loadings /mmol·g(SiO$_2$)$^{-1}$	
		Si$_i^{NMR}$	Titration
tms	98	3.66	—
phs	98	4.18	—
aza	99	2.01	1.40
mps	98	10.9	—
mms	99	4.70	2.35

Distinct differences in the chemical composition of the samples from the treatment with different organosilanes were proven by means of ^{13}C CP-MAS NMR (Figure 3.3.6).
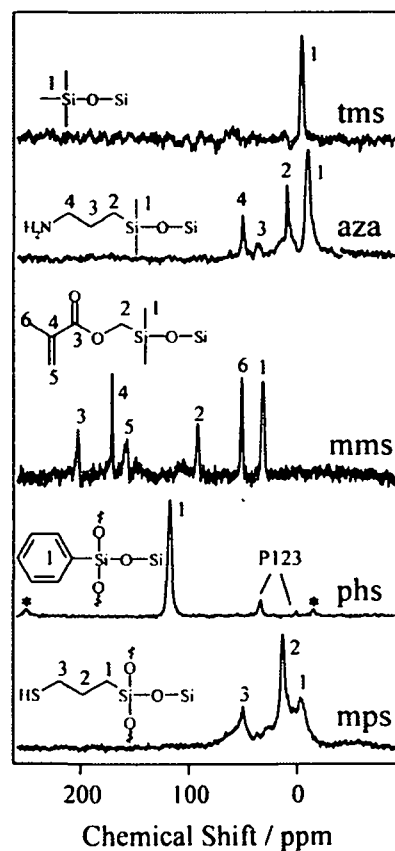
Figure 3.3.6. ^{13}C CP-MAS NMR spectra of the differently functionalized silica gels; peaks marked with an asterisk can be assigned to rotational side bands.

No sample shows strong resonances of the surfactant, which confirms the results from the TGA of an almost complete extraction of the surfactant from the gels. Only for *phs*, peaks that can be assigned to the block copolymer template are visible. The spectra of the surface modified samples all exhibit the expected signals of the organic groups that cover the silica surface, proving that the original organic functionalities remain intact during the extraction and drying process. Quantification of the surface bound groups was done by integration of the ^{29}Si SP-MAS NMR spectra. The extent of surface modification is dependent on the reactivity of the corresponding silane and on the size of the different organosilyl groups. It is known that a hydrated silica surface is covered with up to 5 silanol groups / nm^2 corresponding to a surface loading of 8 $mmol \cdot g^{-1}(SiO_2)$ (assuming a surface area of 904 $m^2 \cdot g^{-1}$, as found for sample *tms*).[34] These silanol groups can be (theoretically) used as anchors for the organosilyl moieties, but a surface coverage of 5 organosilyl groups / nm^2 is very unlikely due to the steric requirements. A reasonable value of 3.66 $mmol \cdot g^{-1}$ has been found for sample *tms*, which means that about every second silanol group has been silylated. The sample *mms*, modified with methylmethacryloyldimethylsilyl groups, revealed an unusually high coverage of 4.7 $mmol \cdot g^{-1}$. This can be explained by the high reactivity of this silane towards hydrolysis due to intermolecular interaction of the ester-group with the silicon atom and thereby autocatalysed hydrolysis.[132] It is very likely that the ester-group also increases the interaction between the silica surface and organosilane as an important intermediate step of the exchange of silica-surfactant hydrogen bonds to covalent siloxane bonds. The amount of accessible double bonds of the methacrylate group was determined by reacting them with bromine and subsequent iodometric titration of unreacted bromine.[134] The values obtained (2.35 $mmol \cdot g^{-1}$) are lower than those obtained by ^{29}Si SP-MAS NMR results, showing that only half of the groups bound to the surface are accessible for subsequent reactions.

Analogous to the double bond determination, the basicity and amount of accessible aminopropyl-groups was determined by acid-base titration with hydrochloric acid.[135] The curve (Figure 3.3.7) reveals two points of inflection, one at pH 7.0, corresponding to full protonation of the aminogroups, the second one at pH 4.7, corresponding to the protonation of free silanols. The amount of aminogroups can be calculated from the consumption of hydrochloric acid at the point of inflection at pH 7.0 to 1.4 $mmol \cdot g^{-1}$, which is lower than the value obtained by ^{29}Si SP MAS NMR (2.01 $mmol \cdot g^{-1}$). For the samples modified with organotrialkoxysilanes (phs, mps), high surface coverages of 4.18 (*phs*) and 10.9 (*mps*) $mmol \cdot g^{-1}$ have been observed by ^{29}Si SP-MAS NMR, suggesting in agreement with the results

from nitrogen sorption that the trialkoxysilanes do not result in the formation of a monolayer, but in oligosiloxanes attached to the surface of the silica backbone.
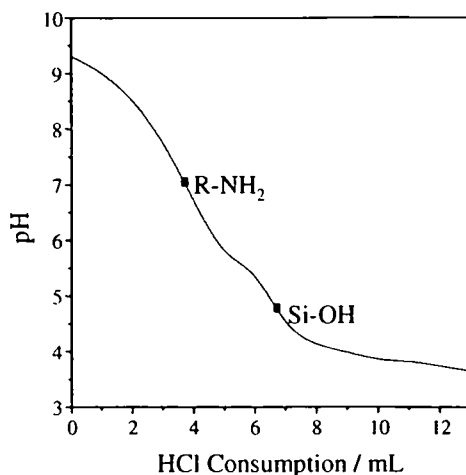
Figure 3.3.7. Titration curve obtained from aza with adding 10^{-2} M HCl at a speed of 0.03 mL·min^{-1}.

3.3.2. Conclusion

Functional hybrid organo-silica monoliths with a hierarchical organisation of the pore structure have been successfully prepared by a combination of a true-liquid crystal templating approach with ethylene glycol-modified silanes and drying via treatment with organosilanes. It was found that not only trimethylchlorosilanes can be used as silylation reagent for assistance of the drying procedure, but also functional organosilanes such as 3-mercaptopropyltrimethoxysilane, phenyltrimethoxysilane, 3-[(2,2-dimethyl-1-aza-2-silacyclopent-1-yl)dimethylsilyl]-1-propanamine, and (methylmethacryloyl)dimethyl-methoxysilane. The gel structure with its hierarchical built-up of macro- and mesopores as well as the periodic ordering of the mesopores is completely retained during the process of functionalization via grafting to the intrachannel hydroxyls. Only for the aminopropyl-modified sample (aza) a significant decrease of the pore wall thickness compared to the other samples is observed, probably due to the strongly basic properties of the organofunctional silane resulting in etching of the silica network. This post-synthesis modification procedure does not only reduce the number of synthetic steps in the synthesis of functional mesoscopically organized silica monoliths, since it combines three processing steps into one, such as surface functionalisation, extraction of the template and facilitation of drying, but also opens access to a wide range of ordered hybrid inorganic-organic monolithic frameworks. One additional benefit of this method is the high bonding density of functionalities of about 2-4 mmol·g(SiO$_2$)$^{-1}$.

3.4. Surface Silylation of Different Types of Porous Silica Materials with an Amino Acid-Functional Silane

Various representative porous silica materials such as Nucleosil® 100-10 (monomodal, spherical particles with a uniform mesoporosity used as packing material for HPLC columns[136]), a monolithic aerogel[106] and E17 monoliths (prepared at pH 1) with a hierarchical organisation of macro- and periodically arranged mesopores[21] (see Chapter 7.2.3.) were modified with an amino acid (alanine) functionality by a surface silylation reaction. A high degree of surface loading with amino acid moieties was achieved for all materials while preserving the porous, micro- and macroscopic structure. Furthermore, the surface silylation reaction allowed for a complete surfactant removal from the templated E17 monoliths in a simple one step process and subsequent drying of the E17 monoliths at ambient/reduced pressure. The modified aerogels were dried by supercritical extraction with carbon dioxide which preserved both the porous structure and chemical functionality. The materials were characterized with respect to their structure by small angle X-ray scattering, nitrogen sorption and electron microscopy, and with respect to their chemical composition by thermogravimetric analysis and solid state NMR studies.

Nucleosil® 100-10 (NUC, see Figure 3.4.1.) was chosen as a silica model material for several reasons. It is a very well defined material concerning its morphology – monomodal, spherical particles with a mean diameter of 10 μm, its porous structure – mesoporous with a mean pore size of 10 nm and a pore volume of 1 cm^3 g^{-1}, and its chemical composition – pure silica gel. Importantly, it has a high surface area (S^{BET} 350 m^2·g^{-1}), which is easily accessible for the investigated molecule due to the large mesopore size. This should allow for a high potential loading with the organic functionality, and therefore easier quantification of the extent of surface loading.
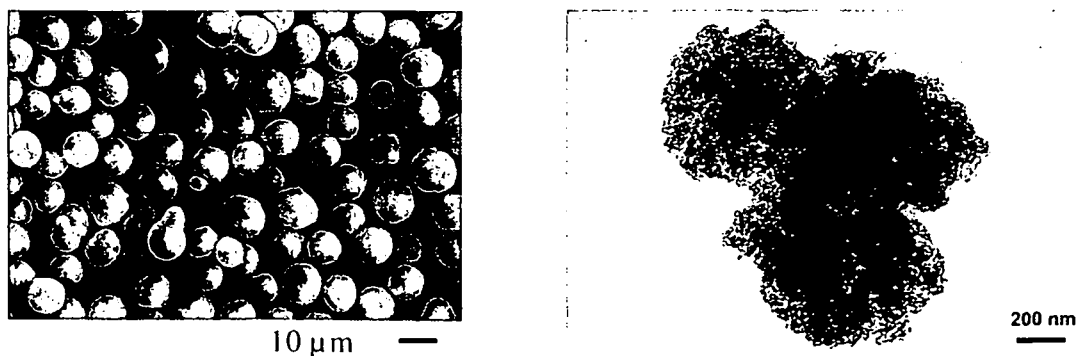
Figure 3.4.1. SEM (A) and TEM (B) images of Nucleosil® 100-10 (NUC) after modification with rac-34.

Furthermore, as the material contains exclusively (monomodal) mesopores, changes in the porous structure due to the surface modification process can be well detected by nitrogen sorption. Such materials are typically applied as stationary phase for HPLC columns, making the modified material also an immediate candidate as such a material with additional chemical selectivity.

Monolithic aerogels (*AER*, see Figure 3.4.2) are another interesting group of silica materials investigated in this work.[106] They are also (mainly) mesoporous materials, with even higher porosities and surface areas (S^{BET} 700 m^2·g^{-1}) compared to the nucleosil powder *NUC*. Furthermore, they are optically transparent which makes them suitable for sensing applications, for example UV-VIS detection of molecules that specifically bind to the organofunctional surface.
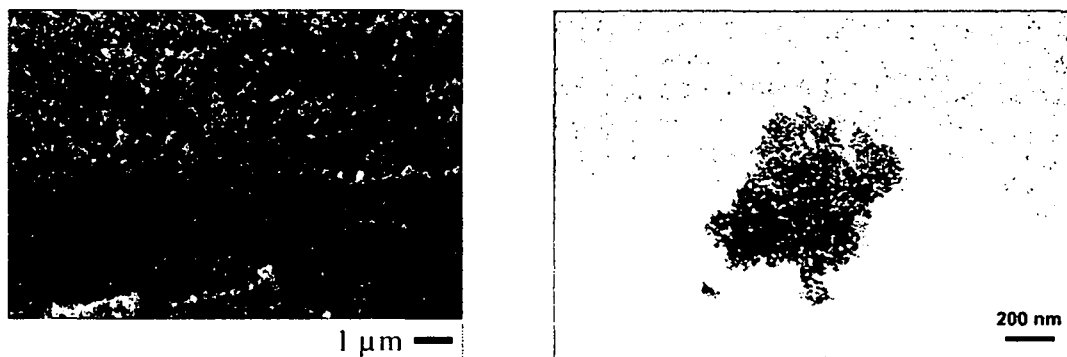
Figure 3.4.2. SEM (A) and TEM (B) images of a monolithic aerogel (*AER*) after modification with rac-34.

Monolithic silica gels with a hierarchical pore structure (*E17*, see figure 3.4.3) are the third type of material investigated.[21] This material has been developed in the course of this work (see Chapter 2) and has a very unique bimodal pore structure of interconnected macropores with 1 µm diameter and cylindrical mesopores with 10 nm diameter that are
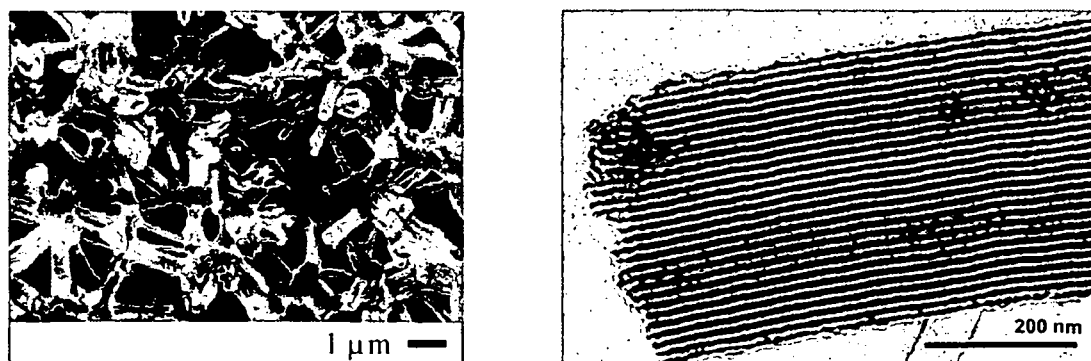
Figure 3.4.3. SEM (A) and TEM (B) images of a silica monolithic with bimodal pore structure (*E17*) after modification with rac-34.

arranged in a highly ordered 2D hexagonal pattern. Such a (highly porous) material provides large specific surface area and size-/shape selectivity due to the highly uniform mesopore system, and at the same time allows for a high mass transport through the macropores. Such features are required by a range of potential applications such as separation and immobilization (in particular of macromolecules, e.g. proteins), slow drug release, catalysis, and sensing.[27-29] Chemical functionalization of the surface increases the potential of such applications as it adds (chemical) selectivity to the material.[43,137]

In this work, full account to the degree of surface coverage with alanine moieties is given in comparison with a conventional surface modification agent (trimethylchlorosilane, see previous parts 3.2. and 3.3.) and a reference silane bearing a phenylsilyl moiety (trimethylphenylsilane), as well as a discussion of the influence on the structural features of the materials and the extraction efficiency with respect to removal of the block copolymer template from the E17 monolith.

3.4.1. Results and Discussion

Surface Modification Procedure. In order to hydrolyse the ester of the amino acid-functionality and the phenylsilyl-moiety, and at the same time covalently bind the molecule onto a silica surface *via* the silanol group formed by the hydrolysis (see Scheme 3.4.1.), rac-34 was refluxed in highly acidic aqueous medium in the presence of the different types of silica gels – *NUC* in form of the as-received, dry powder; *AER* in form of the as-synthesized, aged, wet alcogel; *E17* in form of the as synthesized, aged, wet gel (*E17as*) and in the same form, but after an additional surfactant extraction step with hydrochloric acid-ethanol solution (*E17ex*), see Chapter 7.2.4. To convert the amino-hydrochloride into the free amine, all samples were treated with propylene oxide under reflux and then washed with water, ethanol and finally diethyl ether.

Nucleosil powders were directly dried at 60 °C under vacuum, whereas for the *E17* monoliths the drying rate was decreased by heating the sample slowly up to 60 °C and pressure reduction. The alcogel samples cracked when immersed in the acidic modification solution. The pieces obtained after washing were supercritically dried with carbon dioxide after another solvent exchange step to methanol, resulting in transparent pieces with a size of ca. 0.5 cm.

rac-34

COOEt

NH$_3$Cl

+

SiO$_2$Si–OH

1. HCl reflux

HO–Si ⌒ COOH
NH$_3$Cl

2. propylene oxide reflux

HO–Si ⌒ COOH
NH$_2$

SiO$_2$Si–O–Si ⌒ COOH
NH$_2$
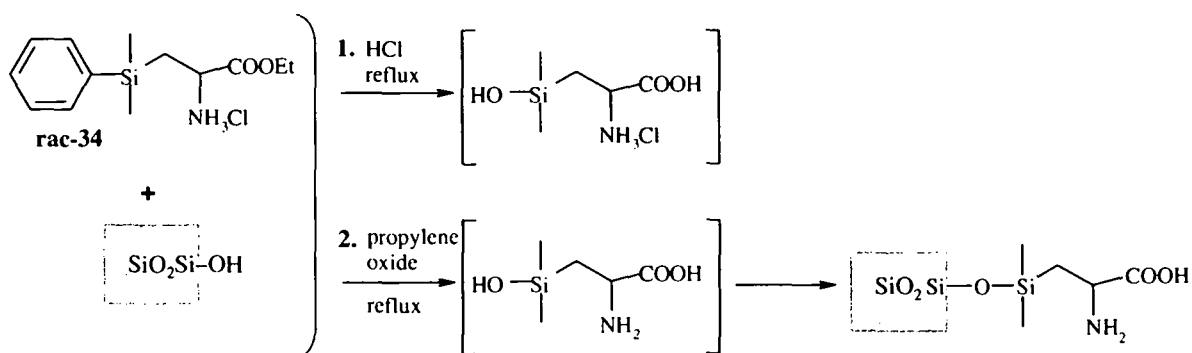
Scheme 3.4.1. Amino acid functionalization of silica by silylation of surface silanols with rac-34.

NUC was also treated by the procedure described above a) without the presence of rac-34, and b) for comparison of the reactivity of the phenylsilyl moiety in the presence of with trimethylphenylsilane. As reference for the structural and chemical composition of *AER*, a wet gel *AER* was supercritically dried with carbon dioxide as described above. As reference for the structural and chemical composition of *E17*, a sample treated with trimethylchlorosilane was chosen,[130,138] a process that has already been studied intensively for this material (see previous chapters). The surface silylation process leads to a spontaneous expulsion of pore fluid and surfactant due to the conversion of surface polarity from hydrophilic to hydrophobic, the surface modified material can then be dried by simple solvent evaporation. Furthermore, the surfactant can almost completely (98 %) be removed by this process. The trimethylsilyl group is the sterically least demanding trialkylsilyl group, therefore values for surface loading achieved with this group should give a clue for possible amounts of surface loading with other moieties.

Chemical Composition. As no significant influence of the silanization prozess on the macro- and mesostructure of the materials was observed apart from reduced surface areas and pore sizes due to the organosilyl layer (see Table 3.4.2.), the chemical composition was investigated by means of thermogravimetric analyses and ^{29}Si- and ^{13}C solid-state NMR studies (Table 3.4.1.).

Table 3.4.1. also gives the surfactant extraction efficiencies for *E17* monoliths calculated from the TGA results in the temperature region around 200 °C which corresponds to the decomposition of the block copolymer template.[60] For *E17ex*, which has been extracted before the silylation reaction, the extraction of the template is almost complete with an

efficiency of 99 % whereas for *E17as*, which has directly been silylated, the extraction efficiency is only 96 %.

Distinct differences in the chemical composition of the different materials before and after the treatment with rac-34, tmps and tmcs were proven by means of ^{13}C CP-MAS NMR (Figure 3.4.4.).

The as synthesized sample *E17* clearly exhibits the expected resonances for the poly(ethylene oxide)-poly(propylene oxide) triblock copolymer surfactant at 20 ppm and 70-80 ppm for the CH$_3$-atoms of the PPO units and the CH$_2$-groups of the block copolymer backbone, respectively. The unmodified aerogel sample *AER* showed the expected resonance at 50 ppm, which can be attributed to methoxy-units covering the surface (from the solvent exchange to methanol prior to supercritical drying). As expected, the spectrum of the reference sample *E17_tms* exhibits signals of the trimethylsilyl groups at 0 ppm.

All samples treated with rac-34 show the expected signals of the alaninedimethyl-silyl functionality proving that the original organic functionality remains intact during the modification, washing/extraction and drying processes, but in all samples additional peaks appear due to residual traces of the various solvents used: chemisorbed ethanol (Si-O-Et) and physisorbed diethyl ether resulting from the washing steps for samples *NUC* and *E17* (also in sample *NUC_tmps*), and chemisorbed methanol (Si-O-Me) resulting from the solvent exchange prior to supercritical drying with carbon dioxide for samples *AER*. In addition, sample *E17as_ala* shows signals that can be attributed to residual surfactant P123 which is in good agreement with the TGA results.

Compared with the other samples, *NUC_tmps* shows only a weak signal attributable to trimethylsilyl groups. It appears that hydrolysis of the phenylsilyl moiety in this molecule is not as high as in rac-34, although it must be mentioned that the intensity of the peaks in ^{13}C CP MAS NMR spectra depends highly on the mobility and the proton content of the sample. Considering the use of the same starting material, the same processing steps, and the same possible positioning of the organosilyl moieties, an approximate comparison is possible.

Table 3.4.1. Chemical composition, surface loadings, and extraction efficiencies of the different functionalized silica materials.

Sample	Functionality	Surface loading (^{29}Si NMR)		Surfactant Extraction / %
		/ N nm^{-2}	/ mmol g(SiO$_2$)$^{-1}$	
NUC	tmps	0	0	-
	ala	0.72	0.62	-
AER	ala	0.57	0.65	-
E17as	tms	2.1	3.7	98
	ala	0.66	1.2	96
E17ex	ala	-	-	99

Chemical shifts:

ala: 0 *(1)*, 20 *(2)*, 53 *(3)*, 175 *(4)* ppm

tms (OSi(CH$_3$)$_3$: 0 ppm

EtOH: 18, 57 ppm
Et$_2$O: 15, 67 ppm
MeO: 50 ppm
P123: 15, 70-80 ppm
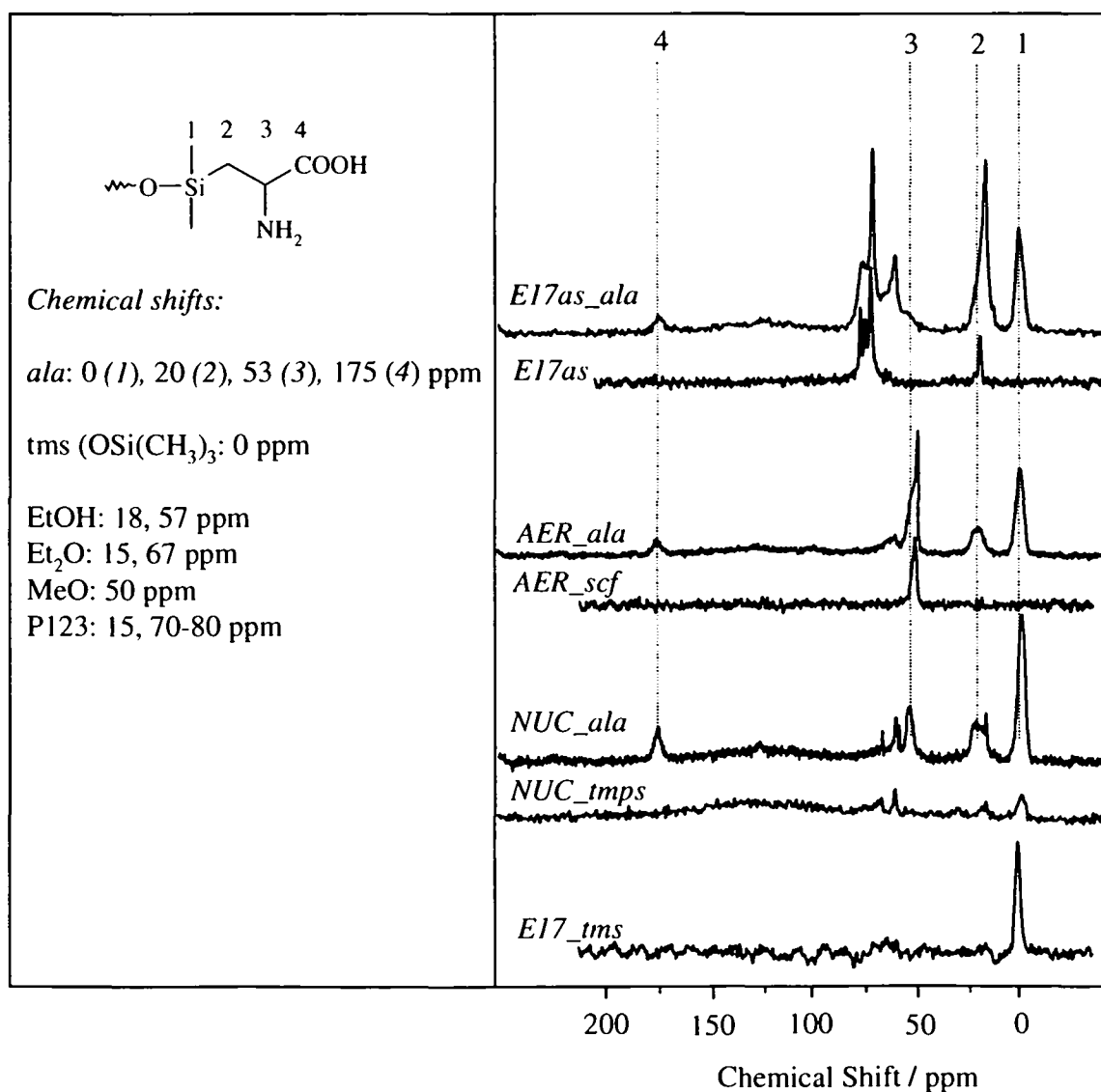
Figure 3.4.4. ^{13}C CP-MAS NMR spectra of the different functionalized silica materials.

Quantification of the surface bound groups was done by integration of the ^{29}Si SP-MAS NMR spectra. The values for the calculated surface loadings are listed in Table 3.4.1. The extent of surface modification is dependent on the reactivity of the corresponding silane and on the size of the different organosilyl groups. It is known that a hydrated silica surface is covered with up to 5 silanol groups / nm^2 corresponding to surface loadings of 3.1 (*NUC*), 6 (*AER*), 8 (*E17*) mmol·g^{-1}(SiO$_2$) (assuming the surface areas S^{BET} determined for the reference materials *NUC*, *AER_scf* and *E17_tms* (see table 3.3.2).[34] These silanol groups can be (theoretically) used as anchors for the organosilyl moieties, but a surface coverage of 5 organosilyl groups / nm^2 is very unlikely due to the steric requirements. A reasonable value of 3.66 mmol·g^{-1} (corresponding to 2.1 N·nm^{-2}) has been found for sample *E17_tms*, which means that about every second silanol group has been silylated. The surface loadings found for rac-34 do not differ significantly for the different silica model materials, even for the *E17* monolith still containing the surfactant template with high values around 0.65 N·nm^{-2}. This is about one third of the surface loading obtained for the trimethylsilyl group which can be explained by the higher steric requirements of the amino acid functional moiety. No significant surface loading was found for trimethylphenylsilane (*NUC_tmps*), proving the much lower reactivity of this phenylsilyl group towards hydrolysis compared with rac-34.
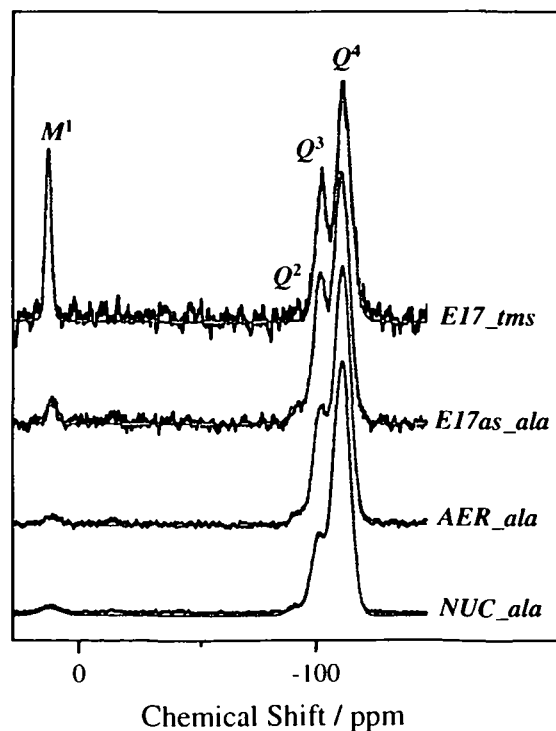
Figure 3.4.5. ^{29}Si SP-MAS NMR spectra of the different functionalized silica materials. The black curves correspond to the original spectra, the grey curves are the Gauss-fits to the spectra.

Structure. The microstructure of the final dried materials was investigated by means of nitrogen sorption, small angle X-ray scattering studies (for *E17*), and electron microscopy. The structural parameters of the final materials are summarized in Table 3.4.2.

The periodic arrangement of the pores of samples *E17* was confirmed by SAXS studies (figure 3.4.6). All patterns show up to four distinct Bragg diffraction peaks, which can be indexed to (10), (11), (20), and (21) associated with a 2D hexagonal symmetry (*p6mm*) with an interplanar d_{10} spacing of about 12 nm. The repeating unit distance itself, pore diameters (about 10 nm) and pore wall thicknesses (about 3.5 nm) calculated from fitting to the ratio of the intensities of the Bragg reflections do not show distinct influence of the functionality and extraction procedure applied (see Table 3.4.2).

Table 3.4.2. Structural parameters of the different functionalized materials.

Sample	SAXS			Nitrogen sorption						
	SAXS pore to pore distance / nm	SAXS pore wall /nm	D^{SAXS} /nm	C	S^{BET} /m²g⁻¹	D^{BJH} /nm	Pore wall /nm	V^{tot}	V^{meso}	V^{micro}
								/ cm³g⁻¹		
NUC	-	-	-	119	351	-	-	1.19		
NUC_blind	-	-	-	96	326	-	-	1.15		
NUC_ala	-	-	-	58	283	-	-	1.07		
NUC_tmps	-	-	-	100	338	-	-	1.19		
AER scf	-	-	-	89	676	-	-	3.13	1.46	0.066
AER ala	-	-	-	59	413	-	-	3.17	1.22	0.048
E17 tms	13.9±0.1	4.5±0.3	9.4±0.3	41	904	10.3	3.56	1.26	0.88	0.14
E17as_ala	13.6±0.1	3.7±0.3	9.9±0.3	43	544	*12.1*	*1.53*	1.28	0.98	0.039
E17ex ala	13.5±0.1	3.6±0.3	9.9±0.3	57	608	*12.3*	*1.21*	1.50	1.19	0.015
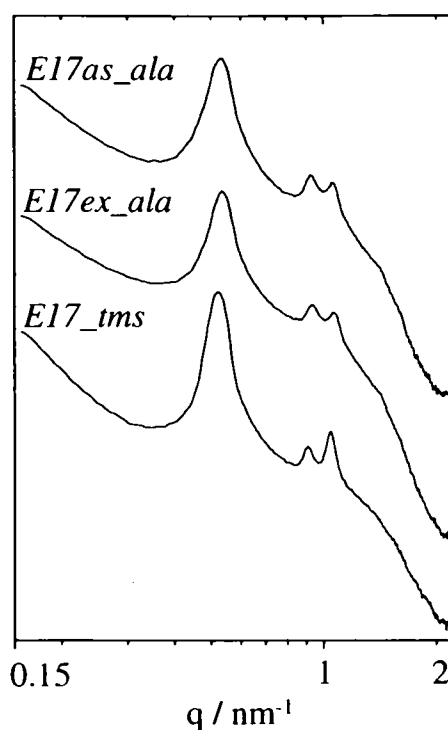
Figure 3.4.6. SAXS patterns of the modified *E17* monoliths.

Nitrogen adsorption/ desorption studies (Figure 3.4.7) were performed to get insight into the pore structure of the functionalized silica materials. Figure 3.4.7 shows representative nitrogen sorption isotherms for each type of sample. All samples show type IV isotherms with H1 hysteresis loops, indicative of materials with relatively uniform mesopore sizes. The narrowest pore size distribution is as expected being observed for sample *E17* with its almost perfectly cylindrical mesopores, as can be seen from the very steep slopes of the ad-/desorption branches. *AER* has the highest pore volume in the pore size range being observable by this method. The values for surface areas (S^{BET}), pore volumes (V^{micro}, V^{meso}, V^{tot}), the C-parameters (from the *BET* equation) as measure for the surface polarity, and pore diameters (D^{BJH}) are listed in Table 3.4.2.

NUC: The modification process leads to a decrease in the specific surface area from 351 m^2 g^{-1} for the native material (*NUC*) to 286 m^2 g^{-1} (*NUC_ala*) which can be attributed to a large extent to loading of the surface with the organosilyl moieties, as the same procedure performed without the presence of the alanine functional silane results in a lower decrease of surface area to 326 m^2 g^{-1} (*NUC_blind*). The pore volume is reduced in the same fashion by the modification process. The change in surface chemistry of sample *NUC_ala* from a polar silica surface to a more apolar surface loaded with organic moieties is also reflected by the
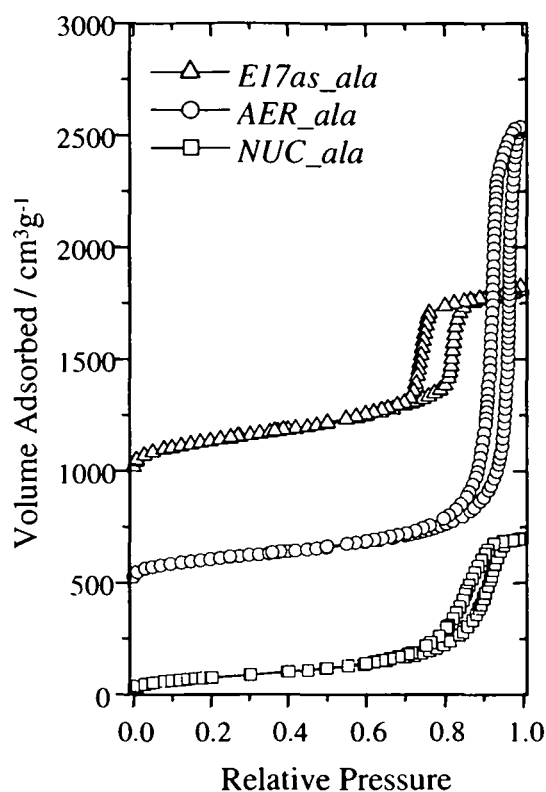
Figure 3.4.7. Representative N₂-sorption isotherms for the *ala* modified silica materials; y-offset 500 cm^3g^{-1}

lower C-parameter. No significant changes in surface area, pore volume, and C-parameter can be observed for the sample treated with trimethylphenylsilane (*NUC_tmps*), which is in good agreement with the NMR results showing that only a very low amount of trimethylsilyl groups has been attached to the surface.

AER and *E17*: Interpretation of the nitrogen results for the monolithic materials is not that straightforward, as in all cases not only the loading of the surface with organosilyl groups, but also the drying processes applied contribute to a reduction in surface area and porosity. On the other hand, surface modification processes can have a positive effect on the preservation of the porous structure as irreversible pore collapse due to the reduction of condensation of silanols on opposite porewall sides and the lower surface tension between pore fluid and porewall, resulting in lower capillary pressures and therefore mechanical stress during drying. For both sets of samples (*AER* and *E17*) the modified materials reveal slightly lower surface areas than the reference materials *AER_scf* and *E17_tms*, respectively. In case of the aerogel samples *AER*, this reduction can be attributed to the modification processing, especially when the as-synthesized alkaline gel is immersed in the highly acidic solution of

rac-34, which leads also to cracking of the monolithic gel body. If the process was to be optimized, cracking could possibly avoided by a stepwise reduction of the pH. For the surfactant templated gels $E17$, the reduction in surface area can be attributed to some extent to residual surfactant and to the loading of the surface with the organosilyl moieties as observed for the Nucleosil powder samples NUC. In contrast to the aerogel samples, the modification processing (refluxing under highly acidic conditions), increased the mechanical stability of the gels to such a high extent that they could be even dried directly from a highly volatile solvent like diethyl ether, which is not possible with samples treated with organochlorosilanes at room temperature like $E17\_tms$.[138] In this case, a less volatile solvent such as ethanol or hexane is necessary to achieve a low drying rate. Mesoporous silica materials templated with triblock copolymers such as SBA-15 are known to have not only large uniform and ordered channels which can easily be seen by nitrogen sorption but also complementary micro- and (small) mesopores located in the silica wall.[71] It has been evidenced for the $E17$ monolith in the previous chapter that the hydrophilic poly(ethylene oxide) chains of the template penetrate within the silica walls during the synthesis to result in micro- and (small) mesopores for $E17\_tms$ with a micropore volume V^{micro} of 0.14 cm^3·g^{-1}.[138] The micropore volumes calculated for samples treated with the alanine functional silane are very low around 0.03 cm^3·g^{-1} due to the larger size of the organosilyl moieties and some residual surfactant. Quite striking results were obtained for the BJH pore diameters D^{BJH} of amino acid modified $E17$ samples, which are almost 2 nm higher than the value obtained for the reference sample treated with tmcs, with no significant difference in the corresponding d-spacings, pore diameters and pore wall thicknesses obtained by SAXS. The pore wall thicknesses calculated using the BJH pore diameter are unrealistically low with values down to 1.2 nm. For this type of functionalized materials, nitrogen sorption does not allow for a reliable determination of pore diameters, which cannot be explained at the moment.

In summary, the values obtained allow for the positive conclusion that after the modification process and drying still high surface areas and porosities were found for both AER and $E17$ samples, showing that the unique porous structures have been preserved and no pore blockage has occurred. Only the microporosity is strongly affected, as can be seen from the strong decrease in micropore volumes, which is a first indication of the success of the surface modification. Secondly, the values of the C-parameters are in the same range as the one obtained for sample NUC_ala, suggesting a similarly modified surface.

3.4.2. Conclusions

Various porous silica model materials have been successfully modified with alanine-dimethyl silyl groups using a novel alanine-dimethylphenylsilane. The phenylsilyl moiety of this molecule shows a high reactivity towards acidic hydrolysis to form a silanol group which can then be used for covalent coupling to a silica surface yielding high surface coverages with amino acid functionality of about 0.65 $N \cdot nm^{-2}$. The different porous structures are completely retained during the process of functionalization via grafting to the intrachannel hydroxyls. This post-synthesis modification procedure does not only lead to surface functionalization, but also surfactant extraction from a templated material was achieved. Furthermore, it facilitates drying and increases the mechanical strength of monoliths with a bimodal pore structure.

4 Network Modification – Ethylene Glycol-Modified Organosilsesquioxane Precursors

4.1. Motivation

The use of organo(-bridged) silsesquioxane precursors [R–Si(OR')$_3$ and (R'O)$_3$Si–R–Si(OR')$_3$, R'= -CH$_3$ or -CH$_2$CH$_3$] to synthesize periodic mesoporous organo-silicas (PMO's) is an approach that has gained much attention in recent years.[15,17,18,22,26,50,51,75-84,137,139-147] The possibility to deliberately tailor framework and surface functionality at the molecular level of periodic mesoporous materials in addition to their unique features such as tunable pore size, narrow pore size distribution, high surface area, and controlled morphology, increases significantly their potential of application in e.g. catalysis, (bio-)immobilisation and separation, adsorption, sensing, and optoelectronics. The synthesis strategy consists of supramolecular templating with various surfactants (ionic and non-ionic) and the use of silsequioxane molecules with a wide variety of functional organic moieties R [R– Si(OR')$_3$ or (R'O)$_3$Si–R–Si(OR')$_3$, R'= -CH$_3$ or -CH$_2$CH$_3$] as sol-gel precursors under both alkaline and acidic conditions. Organosilanes of the type R– Si(OR')$_3$ can normally only be applied in a co-condensation process with tetraalkoxysilanes Si(OR')$_4$.[50,51] Silanes with bridging organic species (R'O)$_3$Si–R–Si(OR')$_3$ provide several advantages over the simple organosilanes, as the organic moieties contribute to the build-up of the network allowing for higher degrees of substitution up to 100 % and therefore completely homogeneous distribution of organic moieties within the framework. Phenylene-bridged materials synthesized with cationic surfactants revealed even molecular scale periodicity along the pore channels with a lamellar scaffold of hydrophobic phenylene layers and hydrophilic silica layers in addition to the periodic mesopore structure,[77] whereas the molecular scale ordering was very low when non-ionic surfactants were applied, and could only be observed by TEM.[141] However, all syntheses reported so far describe only the fabrication of powders or films[139,144,148], and not of monolithic materials, although the ability to mold porous materials into any desired shape and size increases their range of application significantly. In particular the synthesis of monolithic materials with hierarchical pore structures is an extensive field of investigation, as the combination of different pore size regimes within one material leads to multiple benefits arising from each regime, e.g. micro- and mesopores act size- or shape selective, and macropores reduce diffusion limitations to the active sites.[28] These features are of interest for

a wide range of application fields such as separation science, catalyst or biocatalyst supports, and sensing. The first reports on organo-silica materials in monolithic form with a bimodal pore-structure in the form of interconnected macropores and periodically ordered mesopores have been published by Nakanishi and co-workers.[26,137] They describe the synthesis of alkylene-bridged silica monoliths using a non-ionic block copolymer (P123) as template in combination with 1,3,5-trimethylbenzene as swelling agent, an additive that enhances the self-organization of structure-directing agents.

A different approach to synthesize silica monoliths with a hierarchical build-up of highly ordered mesopores and interconnected, uniform macropores has been presented in Chapter 2.[21,59] The key of this work has been the substitution of ethoxy-/methoxy groups of conventional tetraalkoxysilane precursors with short chain glycols as they show much better compatibilities with the self-assembly of silica/surfactant mesophases compared to ethanol or methanol.[105] Furthermore, the glycol-modified silanes, e.g. tetrakis-(2-hydroxyethyl)-orthosilicate (EGMS), are water-soluble and can be hydrolysed/condensed without addition of an acid or base catalyst at neutral conditions in purely aqueous medium. The synthetic process is therefore simplified, as no toxic and/or expensive additives like swelling-agents and co-solvents are required.

This chapter represents the extension of this approach towards the synthesis of organo-silica hybrid materials. Two approaches are presented for the modification of materials prepared from ethylene glycol-modified silanes with organic groups: a) co-condensation reactions of ethylene glycol-modified tetraalkoxysilanes with the corresponding ethylene glycol-modified trialkoxysilanes (phenyl- or methylsilanes), b) reaction of ethylene glycol-modified bridged silanes (ethylene- and phenylene-bridged silanes). Tris-(2-hydroxyethoxy)methylsilane, tris-(2-hydroxyethoxy)phenylsilane, 1,2-bis[tris-(2-hydroxyethoxy)silyl]ethane and 1,4-bis[tris-(2-hydroxyethoxy)silyl]benzene were obtained by transesterification reaction from the ethoxy-derivatives of the silanes and ethylene glycol. All ethylene glycol-modified derivatives are able to form gels in purely aqueous media under neutral pH conditions. Furthermore, monoliths with unique hierarchical structures with a bimodal pore size distribution were prepared by sol-gel processing using a block copolymeric surfactant (Pluronic P123) as structure directing and phase separation agent. Drying and surfactant extraction was performed by supercritical drying with carbon dioxide resulting in crack free monoliths with intact organic moieties. The macro- and mesoporous structure, in particular the periodic ordering of the mesostructure, strongly depend on the degree of

substitution of EGMS with organosilane but also on the pH of the sol-gel mixture and the Si/P123 ratio. Periodically ordered mesopores were obtained up to 25 mol% Si^{OrGMS} for MeGMS and PhGMS, respectively. For the phenylene-bridged silane a fully substituted network with a highly ordered mesoporous structure and even molecular scale periodicity within the pore walls embedded within a unique macroporous scaffold was obtained.

Small angle X-ray scattering, nitrogen sorption, electron microscopy, thermogravimetric analysis and solid state NMR studies were applied for a detailed structural and chemical characterization of samples from different organosilanes and synthesis conditions, thus allowing for a comprehensive comparison of the various gels.

4.2. Results and Discussion

4.2.1. Gel Synthesis

Figure 4.1. shows the synthesis scheme starting with the synthesis of the ethylene glycol modified precursors tris-(2-hydroxyethoxy)methylsilane (MeGMS), tris-(2-hydroxyethoxy)phenylsilane (PhGMS), 1,2-bis[tris-(2-hydroxyethoxy)silyl]ethane (bEtGMS) and 1,4-bis[tris-(2-hydroxyethoxy)silyl]benzene (bPhEGMS) by direct trans-esterification reaction of the ethoxy- (or methoxy) derivatives with ethylene glycol using one equivalent of ethylene glycol for each alkoxy group. No additional solvent or catalyst is required for this reaction from which MeGMS and PhGMS were obtained as colorless viscous liquids whereas bEtGMS and bPhGMS are colourless polymeric solids. The final products are characterized by a defined silicon content which was determined by thermogravimetric analysis to 8.4 wt% for MeGMS, 9.6 wt% for PhGMS, 12 wt% for bEtGMS and 11 wt% for bPhGMS. The weight loss profile also showed no traces of residual ethanol or methanol (no weight loss up to 170 °C) proving the complete alcohol exchange. A significant weight loss around 200 °C can be attributed to non-covalently bound ethylene glycol which is due to the ability of ethylene glycol to form bridged or chelated silane species (see Figure 4.1.) which in addition to hydrogen-bonding interactions lead to the high viscosity or even polymeric character of the precursors. Due to the poor solubility of the organo-bridged silanes in appropriate solvents, only solid state NMR experiments were carried out for the final, dried materials to prove the incorporation of the organic moieties.
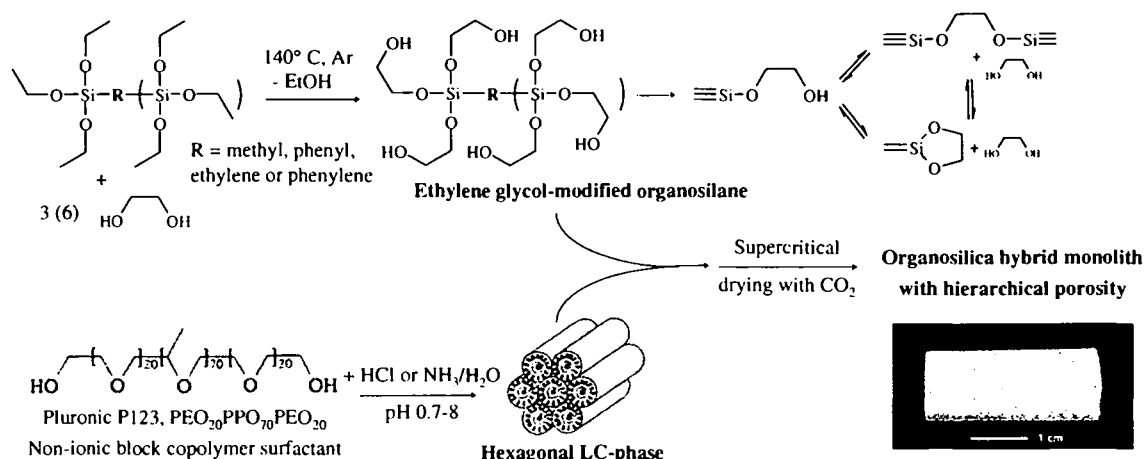
Figure 4.1. Synthesis from the ethylene glycol-modified precursor synthesis to the final, dried material.

In the second step, these novel, water-soluble (except PhGMS) precursors were applied in a facile, supramolecular templating process using P123 as structure directing agent in purely aqueous medium at different pH conditions. Monolithic silica gels were prepared by a) co-condensation reactions of an ethylene glycol-modified tetraalkoxysilane with the corresponding ethylene glycol-modified trialkoxysilanes (MeGMS and PhGMS), b) reaction of ethylene glycol-modified bridged silanes (bEtGMS and bPhGMS) in the presence of an aqueous liquid crystal (LC)-phase of 30 wt% P123 surfactant at 40° C. The pH was adjusted using hydrochloric acid or ammonium hydroxide. For a) the Si/P123 ratio was kept constant at 8/30 while varying the content of organosilane in the range of Si^{Or} = 10-100 mol% and varying the pH between 0.7 and 8. For b) only the pure organo-bridged silane was applied varying the Si/P123 ratio in the range from 5.8 to 8 at a pH of 2.5. The concentration of P123 in water was kept constant at a ratio of P123/water = 30/70 for all samples. All these parameters – type of organic moiety, degree of substitution with organic moieties Si^{Or}, pH and Si/P123 ratio – have a strong influence on the gelation times, the formation of the mesostructure and the morphology/macroporous structure. To avoid cracking and large shrinkage, template and pore fluid were removed by supercritical fluid extraction.[130] Soft calcination at 350 °C was tested as an alternative method,[26] but caused significant oxidative Si-C bond cleavage (see solid state NMR results, samples bEt and bPh).

4.2.2. Gelation Times

To obtain preliminary information about the sol-gel chemistry of the newly synthesized precursors, gelation experiments were performed without addition of surfactant using the final Si/H_2O concentration of 8/70 and variation of the pH between 0.7 and 8. Another set of gelation experiments was carried out at pH 2.5 with addition of surfactant using the final $Si/P123/H_2O$ ratio of 8/30/70 varying the degree of substitution Si^{Or}.

Without P123: Figure 4.2 shows the gelation times of the ethylene glycol-modified precursors in dependence of the pH. Upon mixing with the aqueous phase MeGMS immediately formed a homogeneous solution, whereas PhGMS formed an emulsion first, but turned into a homogeneous solution before the point of gelation. The polymeric precursors bEtGMS and bPhGMS could be dissolved by vigorous stirring so that homogeneous solutions were obtained before gelation occurred. All silanes were able to form gels in purely aqueous media in the pH range 0.7-8, even under neutral pH conditions. All organosilanes showed lower gelation times than pure EGMS, but similar trends with respect to pH dependency could be observed. The higher reaction rate can be explained by the inductive effect of the organic group (+I effect) in organo-substituted alkoxysilanes which increases the reaction rate. As for EGMS, unusually low gelation times between 13-300 min are found at neutral pH conditions which again can be explained by the much higher water solubility of the ethylene glycol-modified derivatives.
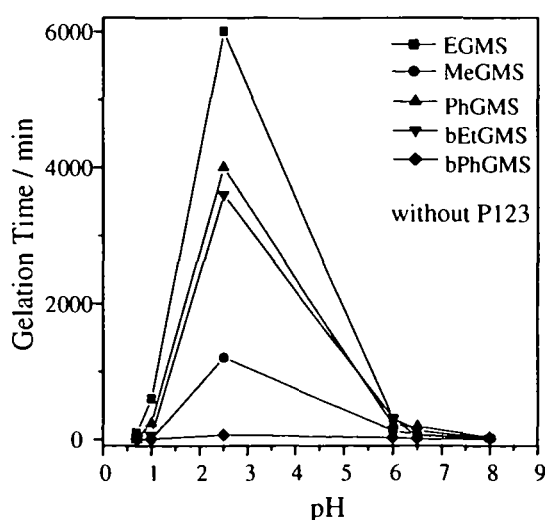
Figure 4.2. Gelation times of the various ethylene glycol-modified organosilanes at different pH in purely aqueous media without surfactant.

As expected, the maximum in gelation times for all precursors lies in the range of the isoelectric point around pH 2.5, where also the most pronounced differences in gelation times could be observed (60-6000 min). At this pH the reactivity increases in the following order: EGMS<<PhGMS~bEtGMS<< MeGMS<bPhGMS. The different reaction rates for the different organosilanes are mainly governed by two factors: the bulkier phenyl group decreases the reaction rate (for PhGMS) because of sterical reasons. For silanes with bridging organic groups, lower gelation times are found due to the higher connectivity of the formed network. The high reactivity of bPhGMS can be explained by intermolecular interactions of the phenylene moieties (hydrophobic- and π-π-stacking interactions) which facilitate the condensation and network formation reactions.

With P123: Figure 4.3. shows the gelation times of the ethylene glycol-modified precursors at pH 2.5 in dependence of the degree of substitution Si^{Or}. Gelation times increased for all precursors with increasing content of organic groups although the reactivity of the organosilanes without the presence of surfactant was higher in comparison with pure EGMS. Above 25 mol% Si^{Or} no gelation occurred for the non-bridged organosilanes. In the case of MeGMS precipitates were obtained instead, whereas for PhGMS no solid phase formed at all. For all organo-bridged silanes (bEtGMSand bPhGMS) gels were obtained up to Si^{Or} 100%. As in the gelation experiments without surfactant bPhGMS showed a particularly high reactivity, again very likely due to intermolecular interactions of the phenylene moieties.
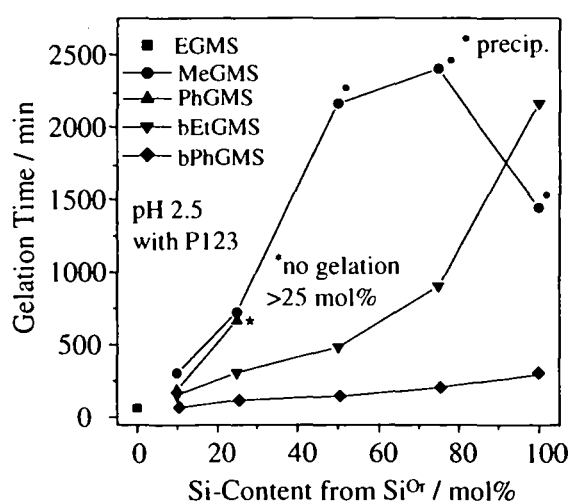
Figure 4.3. Gelation times of the various ethylene glycol-modified organosilanes at pH 2.5 in purely aqueous media with P123 (P123/H₂O = 30/70).

4.2.3. Structural Properties of the Resulting Gel Bodies

The materials discussed in this work are hierarchically structured organo-silica monoliths built up from different macroporous scaffolds which comprise in most cases mesopores which sometimes are periodically ordered cylindrical mesopores arranged in a 2D hexagonal pattern. A third pore size level can be found in the form of micropores in the mesopore walls. All discussed samples were obtained in the form of rather large, white, crack-free monoliths after supercritical drying, with dimensions of 1 cm in diameter and 3 cm in height. This hierarchical build-up is illustrated for sample bPh_a in Figure 4.4. showing a photograph of the monolith and electron micrographs of the underlying porous structure.
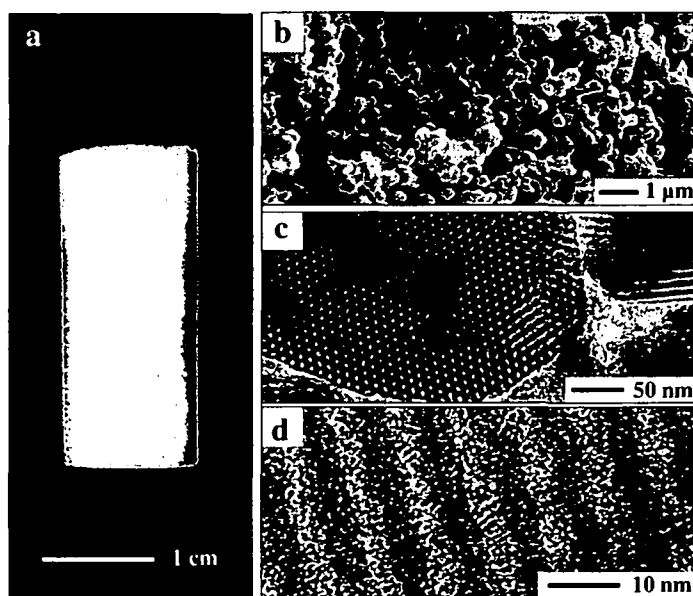
Figure 4.4. Hierarchy on four levels: Photograph (a), SEM image (b), and TEM images (c, d) of the dried phenylene-bridged silica monolith bPh_a, exhibiting its hierarchical build-up.

The structural parameters of the final materials after supercritical drying are summarized in Tables 4.1. and 4.2.

Table 4.1. Structural parameters of the methyl- (Me) and phenyl (Ph) silsesquioxane monoliths.

Samples	pH	Apparent density /g·cm^{-3}	SAXS d$_{10}$ (w) /nm (%)	Nitrogen sorption S^{BET} /m^2 g^{-1}	C	V^t /cm^3 g^{-1}	V^{meso} /cm^3 g^{-1}	V^{micro} /cm^3 g^{-1}	D^{BJH} (w) /nm (%)	t^{wall} /nm
Me10	6	0.35	9.8 (8.4)	580	190	0.55	0.35	0.13	5.2 (25)	6.10
	2.5	0.31	10.4 (12)	690	170	0.71	0.48	0.12	6.1 (12)	5.86
	1	0.26	10.4 (34)	930	70	2.05	0.39	0.04	6.5 (25)	5.58
	0.7	0.23	12.2 (33)	1060	50	2.27	0.56	0.08	9.7 (18)	4.43
Me25	6	0.32	-	970	55	1.70	0.33	0.03	6.2 (63)	-
	2.5	0.41	8.4 (11)	360	540	0.40	0.13	0.09	3.1 (65)	6.60
Me50	6	0.46	-	980	50	1.53	-	0.02	-	-
Me75	6	0.38	-	820	45	1.32	-	0.08	-	-
Me100	6	0.66	-	350	155	0.33	-	0.09	-	-
Ph10	2.5	0.26	10.3 (6.6)	780	110	0.76	0.61	0.14	6.3 (9.0)	5.6
Ph25	2.5	0.62	7.9 (8.2)	535	70	0.37	0.25	0.09	3.4 (71)	5.7
Ph25	6.0	0.32	9.3 (7.2)	604	70	0.57	0.45	0.05	4.9 (18)	5.8

Table 4.3. Structural parameters of the ethylene- (bEt) and phenylene-bridged (bPh) silsesquioxane monoliths.

Sample	pH	Apparent density /g·cm^{-3}	SAXS d$_{10}$ (w) /nm (%)	Nitrogen sorption S^{BET} /m^2·g^{-1}	C	V^t /cm^3·g^{-1}	V^{meso} /cm^3·g^{-1}	V^{micro} /cm^3·g^{-1}	D^{BJH} (w) /nm (%)	t^{wall} /nm
bEt_a	2.5	0.32	8.2 (20)	300	90	0.30	0.15	0.02	3.7 (51)	5.8
bEt_b	2.5	0.49	-	160	75	0.17	0.08	0.02	4.6 (52)	-
bEt_c	2.5	0.68	-	450	210	0.42	0.16	0.20	3.8 (63)	-
bPh_a	2.5	0.24	10.5 (9.0)	500	100	0.62	0.55	0.05	6.5 (8.2)	5.6
bPh_b	2.5	0.38	10.7 (17)	415	80	0.54	0.48	0.04	6.7 (9.1)	5.7
bPh_c	2.5	0.54	11.1 (40)	640	80	1.13	0.09	0.09	6.7 (25)	6.1

Small Angle X-ray Scattering. Small angle X-ray scattering patterns were collected for all solids after the drying step and are illustrated in Figures 4.5.-4.6. In general, samples with an ordered porous structure show up to four distinct Bragg diffraction peaks, which can be indexed to (10), (11), (20) and (21) associated with a *p6mm* hexagonal symmetry with a repeating unit distance of about 11 nm, indicating the formation of highly ordered 2D hexagonal mesostructures. In some samples, the (11) and (20) reflections could not be resolved well due to the broadness of the peaks. The corresponding unit cell parameters of the dried materials from the various glycol-modified silanes can be found in Tables 4.1.-4.2.

Methyl silsesquioxane gels (Me): substitution of EGMS with MeGMS results in a decrease of ordering in the mesoscopic regime. Periodically ordered structures could be found only up to a content of Si^{Me} of 25 mol% and for this content only at pH 2.5, which is the optimum pH to obtain ordered structures for this system, but for higher degrees of substitution, no gels could be obtained at this pH (see Figure 4.3.). For a lower degree of substitution of $Si^{Me} = 10$ mol%, very well hexagonally ordered mesostructures were found for both pH 6 and 2.5.

Phenyl silsesquioxane gels (Ph): A similar situation as for the methyl silsesquioxane gels was found with the only difference that for a substitution of $Si^{Ph} = 25$ mol%, the optimum pH for a high degree of mesostructural ordering was found to be pH 6 and not at pH 2.5.

It has already been shown (Chapter 2) that a high degree in structural ordering correlates with long gelation times which are normally found around pH 2.5. Substitution of EGMS with OrGMS increases the gelation times but decreases the tendency of the organosilica-surfactant self-assembly due to the more hydrophobic character of the organosilica network and therefore reduced interaction with the hydrophilic parts of the surfactant. Furthermore, for higher degrees of substitution with OrGMS the network formation is becoming more and more difficult due to the lower connectivity of the network resulting from trialkoxysilanes (OrGMS) in comparison to the tetraalkoxysilane (EGMS), and the steric requirements of the organic moieties.
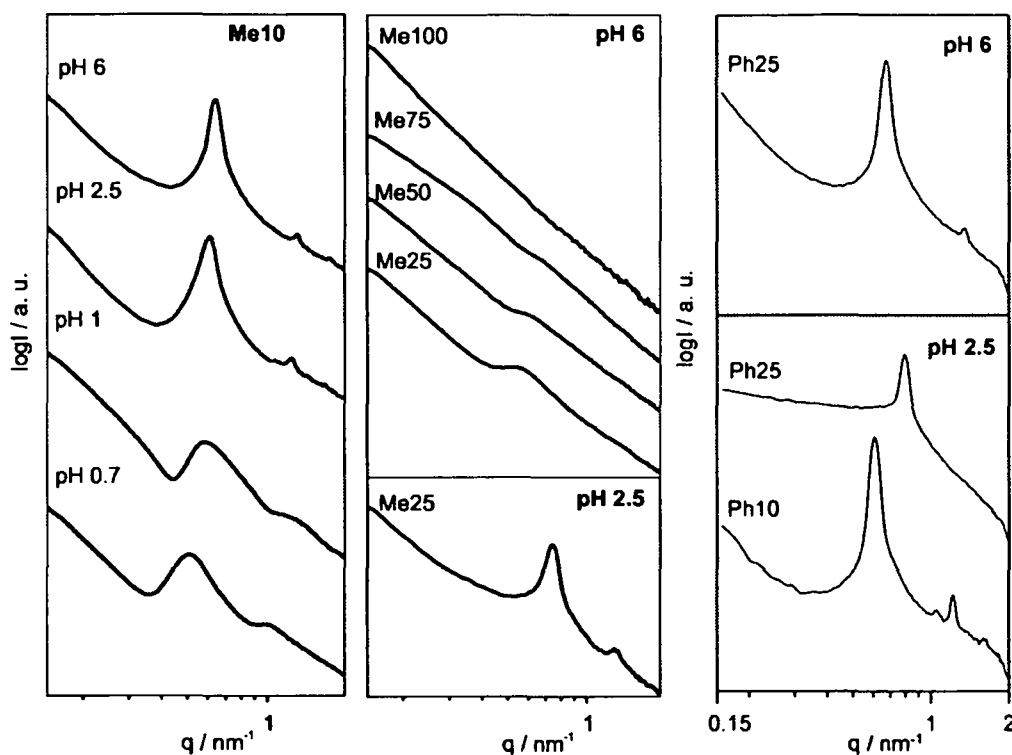
Figure 4.5. Small angle X-ray scattering patterns of the methyl (Me) and phenyl (Ph) silsesquioxane monoliths.

Ethylene-bridged silsesquioxane gels (bEt): Figure 4.5. shows the SAXS patterns of bEt gels prepared with different Si/P123 ratios. For no bEt sample, the characteristic pattern of a 2D hexagonal mesostructure was obtained. For samples bEt_a and bEt_c, a single peak with a corresponding characteristic length of ca. 10 nm could be observed, suggesting the existence of a short range order of pores but no periodic arrangement.

Phenylene-bridged silsesquioxane gels (bPh): Figure 4.5. shows the SAXS patterns of bPh gels prepared with same Si/P123 ratios as the bEt gels. Starting from the Si/P123 ratio applied for the Me and Ph gels (bPh_c), the reduction of the Si/P123 ratio leads to a strong increase in structural ordering. Sample bPh_a reveals the very well resolved pattern with a very narrow peak width corresponding to a high degree of periodicity and uniform pore structure. The pattern exhibits four well-resolved Bragg diffraction peaks, which can be indexed to (10), (11), (20), and (21) reflections associated with a 2D hexagonal symmetry (*p6mm*) with a repeating unit distance d_{10} of 10.5 nm.
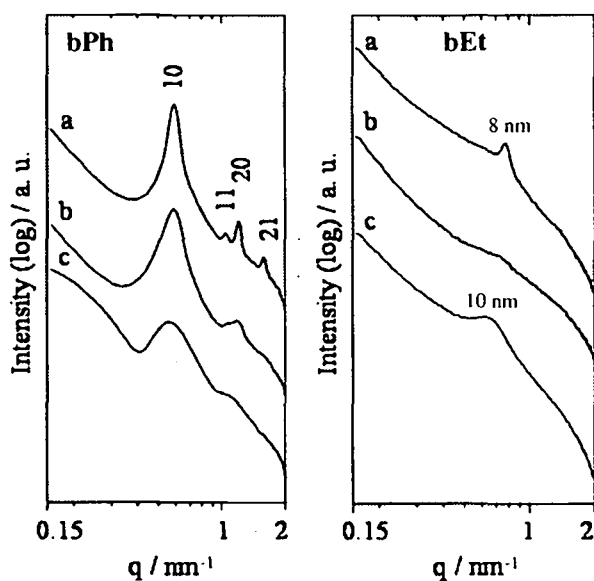
Figure 4.6. Small angle X-ray scattering patterns of the ethylene- and phenylene-bridged silsesquioxane monoliths prepared with different Si/P123 ratios: a) 0.19, b) 0.23 and c) 0.27.
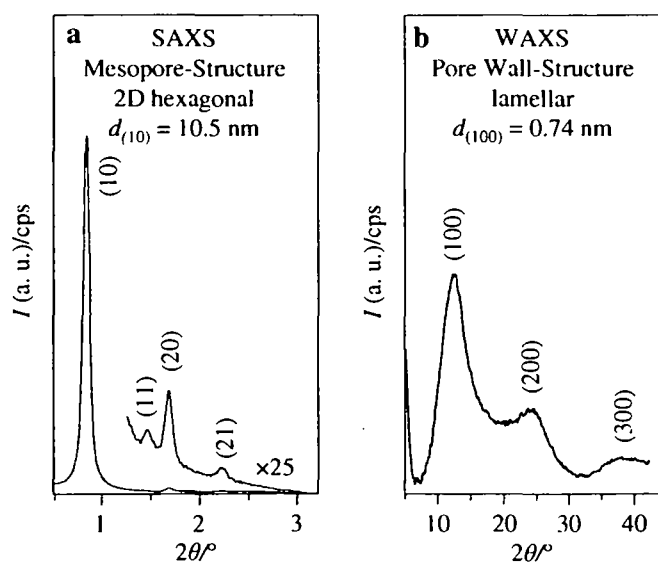
Figure 4.7. SAXS (a) and WAXS (after subtraction of the amorphous silica peak) (b) patterns of sample bPh_a showing the meso- and molecular scale periodicity of the dried hybrid material.

Wide Angle X-ray Scattering (WAXS). For sample bPh_a, also wide angle X-ray scattering experiments were performed in order to obtain information about the pore wall structure (see Figure 4.7.). As already mentioned in the introduction of this chapter (4.2.), phenylene-bridged materials synthesized with cationic surfactants reveal a molecular scale periodicity along the pore-channels with a lamellar scaffold of hydrophobic phenylene layers and hydrophilic silica layers in addition to the periodic mesopore structure,[77] whereas the

molecular scale ordering has been found to be very low when non-ionic surfactants were applied, and could only be observed by TEM.[141] For the investigated sample bPh_a, clear proof of molecular scale periodicity within the pore walls could be given by the WAXS experiments. Figure 4.6. shows the WAXS pattern of the dried sample after subtraction of the amorphous silica peak around $22° \ 2\theta^{77}$ which overlaps with the (200) reflection at $24.0° \ 2\theta$ of the lamellar structure. The silica peak has been determined using ethylene-bridged silica (bEt_a) without molecular scale periodicity as reference material and was normalized. The WAXS pattern after background subtraction shows three broad, but distinct Bragg diffraction peaks which can be indexed to (100), (200), and (300) reflections of a lamellar phase with a repeating unit distance d_{100} of 0.74 nm, the same value which has been observed for the highly ordered phenylene-bridged silica materials synthesized with cationic surfactants.[77]

The high degree of periodicity of the mesostructure and also the molecular ordering of the pore walls suggests that the hydrophilic character of ethylene glycol strongly enhances the phenylene-silica/surfactant self-assembly and also the hydrophobic/π-π stacking interactions of the phenylene moities.

Nitrogen Sorption. Nitrogen adsorption/desorption studies (Figures 4.8.-4.9.) were performed to get insight into the pore structure of the organo-silica gel monoliths. The values for surface area (S^{BET}), C-parameter, pore volumes (V', V^{meso}, V^{micro}) and pore diameters D^{BJH} are listed in Tables 4.1.-4.2. Mesoporous silica materials templated with triblock copolymers such as SBA-15 are known to have not only large uniform and ordered channels which can easily be seen by nitrogen sorption but also complementary micro- and (small) mesopores located in the silica wall. It has been evidenced that the hydrophilic poly(ethylene oxide) chains of the template penetrate within the silica walls during the synthesis to result in micro- and (small) mesopores upon calcination.[71] All samples presented in this chapter reveal a certain extent of microporosity with the corresponding pore volume V^{micro}. All samples also reveal primary mesopores as a result from the supramolecular templating with P123, in most cases with a uniform pore size distribution, with the corresponding pore volume V^{meso}. Some samples also reveal secondary mesoporosity and macroporosity (the full range is not accessible by nitrogen sorption), which is related to textural porosity (e.g. samples Me10 prepared at pH 1 and 0.7, and bPh_c). The total pore volume V' comprises all of the three regimes.

Methyl silsesquioxane gels (Me): The nitrogen sorption isotherms reflect the findings from the SAXS experiments such that for all samples that revealed mesoscopic periodicity, type IV

isotherms with H1 hysteresis loops were found which is indicative of a mesoporous material with a uniform pore size (see Figure 4.8., samples Me10 prepared at pH 6 and 2.5). The isotherms obtained for samples Me10 prepared at pH 1 and 0.7, and sample Me25 prepared at pH 6 reveal the presence of a bimodal pore structure with relatively uniform primary mesopores resulting from the templating with P123 and a second regime of larger meso- and small macropores resulting from the phase separation process. These samples also reveal the largest pore volumes V^t as the size of their macropores is accessible by nitrogen sorption in contrast to samples with larger macropores (>200 nm). Samples revealing primary mesopores also show a corresponding peak in the SAXS pattern. The decrease of mesoscopic ordering with increasing content of Si^{Mc} found in the SAXS experiments is also reflected in the nitrogen sorption isotherms (see Figure 4.8., samples Me10-Me100 prepared at pH 6). Specific surface areas S^{BET} are high with values of 350 up to 1060 $m^2 \cdot g^{-1}$ and can be correlated well with the amount of total pore volumes V^t observed which lie in the range from 0.24-2.27 $cm^3 \cdot g^{-1}$. High primary mesopore volumes V^{meso} of up to 0.56 $cm^3 \cdot g^{-1}$ were observed for all samples with uniform pore structures, proving that the block copolymer template has been efficiently removed from the mesopore structure. Samples Me10 and Me25 exhibit monomodal mesopore size distributions with pore diameters (D^{BJH}) ranging from 3.10-9.68 nm. The precise numerical values and the peak width are listed in Table 4.1. The peak width is a good measure for the relative uniformity of the pores and is in good agreement with the findings from the SAXS experiments.
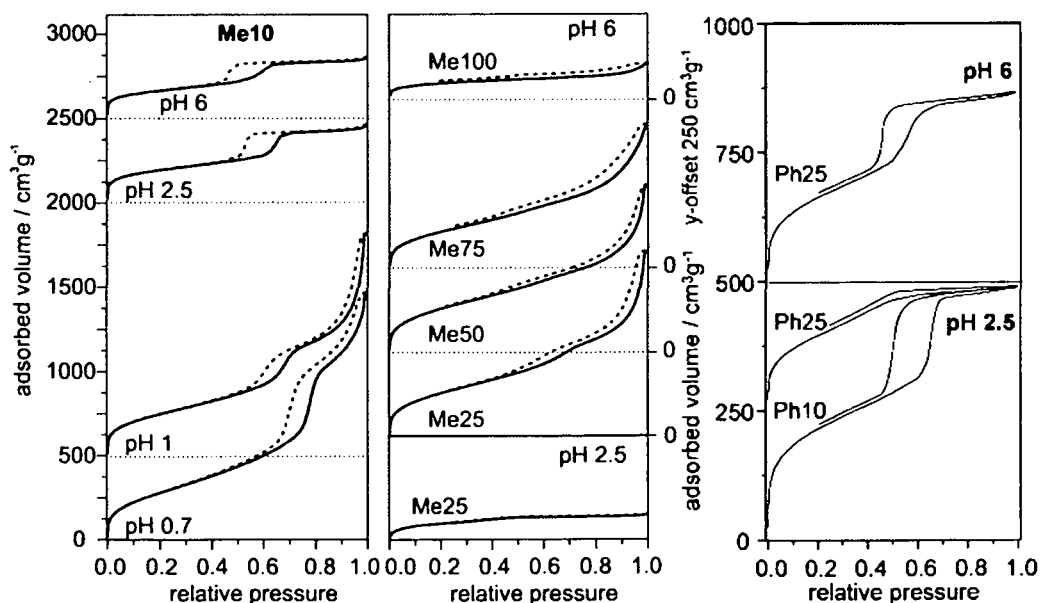
Figure 4.8. Nitrogen sorption isotherms of the methyl- (Me) and phenyl (Ph) silsesquioxane gels.

Phenyl silsesquioxane gels (Ph): The nitrogen sorption isotherms again reflect the findings from the SAXS experiments of a uniform periodically ordered (2D hexagonal) mesostructure such that type IV with H1 hysteresis loops were found which are indicative of a mesoporous material with a uniform pore size (see Figure 4.8.). Sample Ph25 prepared at pH 2.5 does only reveal a very small hysteresis which is due to the smaller mesopore size. Specific surface areas S^{BET} are high with values between 535 and 780 $m^2 \cdot g^{-1}$ and can be correlated well with the amount of total pore volumes V^t observed which lie in the range from 0.37-0.76 $cm^3 \cdot g^{-1}$. High primary mesopore volumes V^{meso} of up to 0.61 $cm^3 \cdot g^{-1}$ were observed for all samples, proving that the block copolymer template has been efficiently removed from the mesopore structure. All presented samples exhibit monomodal mesopore size distributions with pore diameters (D^{BJH}) ranging from 3.4 to 6.3 nm. The precise numerical values and the peak width are listed in Table 4.1. The peak width is a good measure for the relative uniformity of the pores and is in good agreement with the results from the SAXS experiments.

Ethylene-bridged silsesquioxane gels (bEt): The nitrogen sorption isotherms again reflect the findings from the SAXS experiments of not particularly uniform mesostructures as such that type IV isotherms with H2 hysteresis loops were found which are indicative of a mesoporous material with a non uniform pore system (see Figure 4.9.). Specific surface areas (S^{BET}, see also Table 4.2.) are comparably low with values between 160 and 450 $m^2 \cdot g^{-1}$ and can be correlated well with the amount of total pore volumes V^t observed which lie in the range from 0.17-0.42 $cm^3 \cdot g^{-1}$. Relatively low primary mesopore volumes V^{meso} of 0.10-0.20 $cm^3 \cdot g^{-1}$ were observed for all samples. All presented samples exhibit broad mesopore size distributions with mean pore diameters (D^{BJH}) ranging from 3.8 to 4.6 nm. The precise numerical values and the peak width are listed in Table 4.2.

Phenylene-bridged silsesquioxane gels (bPh): The nitrogen sorption isotherms reflect the findings from the SAXS experiments such that for all samples type IV isotherms with H1 hysteresis loops were found which is indicative of a mesoporous material with a uniform pore size (see Figure 4.9.). The isotherm obtained for sample bPh_c reveals the presence of a bimodal pore structure with uniform primary mesopores resulting from the templating with P123 and a second regime of larger meso- and small macropores resulting from the phase separation process. This sample also reveals the largest pore volume V^t for this set of samples as the size of its macropores is accessible by nitrogen sorption in contrast to samples with larger macropores (>200 nm). The decrease of mesoscopic ordering with increasing Si/P123 ratio found in the SAXS experiments is also reflected in the pore size distributions (see Table

4.2. for the relative peak width). Specific surface areas S^{BET} are high with values of 415 up to 635 $m^2 \cdot g^{-1}$ and can be correlated well with the amount of total pore volumes V^t observed which lie in the range from 0.54 to 1.13 $cm^3 \cdot g^{-1}$. High primary mesopore volumes V^{meso} of around 0.5 $cm^3 \cdot g^{-1}$ were observed for bPh_a and bPh_b, whereas bPh_c which reveals the highest total pore volume and the highest micropore volume has a primary mesopore volume of only 0.18 $cm^3 \cdot g^{-1}$. However, for all samples it can be concluded that the block copolymer template has been efficiently removed from the meso- and micropore structure. All samples exhibit monomodal primary mesopore size distributions with pore diameters (D^{BJH}) ranging from 6.5-6.7 nm.
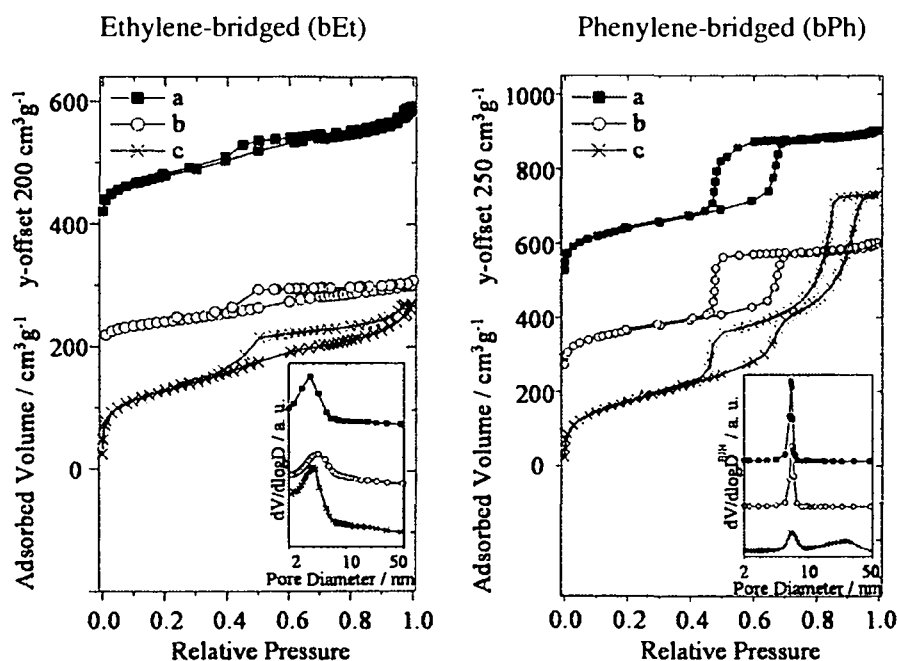
Figure 4.9. Nitrogen sorption isotherms of the ethylene-bridged (bEt) and phenylene-bridged (bPh) silsesquioxane monoliths.

Electron Microscopy. Scanning- (SEM) and transmission (TEM, only shown for sample bPh_a) electron micrographs (Figures 4.4., 4.10.-4.11.) of the dried samples show the hierarchical structural build-up of the monolithic hybrid materials. The macro-domains observed for most materials form due to a phase separation process into an organosilica/surfactant rich phase and a solvent rich phase (water and ethylene glycol) during the self-assembly and sol-gel processes. This phase separation can proceed either via spinodal decomposition or a nucleation and particle growth mechanism. In the case of spinodal decomposition, phase separation is induced by the presence of surfactant which

adsorbs onto the growing silica oligomers and occurs relatively fast compared to the process of gelation. It is therefore observed mostly for relatively high surfactant concentrations and/or long gelation times. The resulting morphology is a bicontinuous, cellular, macroporous scaffold with the dimensions being dependent on the relative rates of phase separation and gelation. For a constant gelation time, faster phase separation leads to larger dimensions, hence larger macropores. A nucleation and growth mechanism on the other hand, is the result of a relatively slow, but pronounced (organo)silica/surfactant self-assembly process, which can be only observed for long gelation times and optimum Si/P123 ratios. The resulting morphology of the solid phase is formed after the phase separation and is mainly governed by the competition of two factors – colloidal surface free energy (F) and the free energy of mesostructure formation (ΔG) – leading to spherical particles if F is dominant, and to rod-like single crystals (for a 2D hexagonal mesostructure) if ΔG is dominant as observed for sample E17 prepared from pure EGMS at pH 2.5 and 1 (see Chapters 2 and 3). The longer the gelation times and the more pronounced the self-assembly process (high free energy of mesostructure formation), the larger the resulting dimensions of the particles and macropores. In some cases, no macroscopic phase separation occurs, mostly for high Si/P123 ratios and/or at very low pH due to the low gelation times at low pH and probably also due to electrostatic repulsion of the highly charged silica particles.

Methyl silsesquioxane gels (Me). The SEM images reveal interconnected (open) macroporosity, but various morphologies for the different samples (Figure 4.10.). Both pH and degree of substitution Si^{Me} show a strong influence on the phase separation process and the resulting morphologies. A cellular network built up from rod-shaped aggregates of 2-3 µm in length and about 0.5 µm in diameter very similar to the E17 gel prepared from pure EGMS at pH 2.5 (see chapter 1) is observed for Me10 prepared at pH 6. The same morphology but with a smaller feature size (approximately half the value) is observed for sample Me10 prepared at pH 2.5. In good agreement with the observations from nitrogen sorption (small macropores), samples Me10 prepared at pH 1 and 0.7 as well as sample Me25 prepared at pH 6 show very small, aerogel like structural features in the nanometer regime. A quite remarkable sponge-like structure is observed for sample Me25 prepared at pH 2.5, a sample that also reveals quite well ordered mesopores.
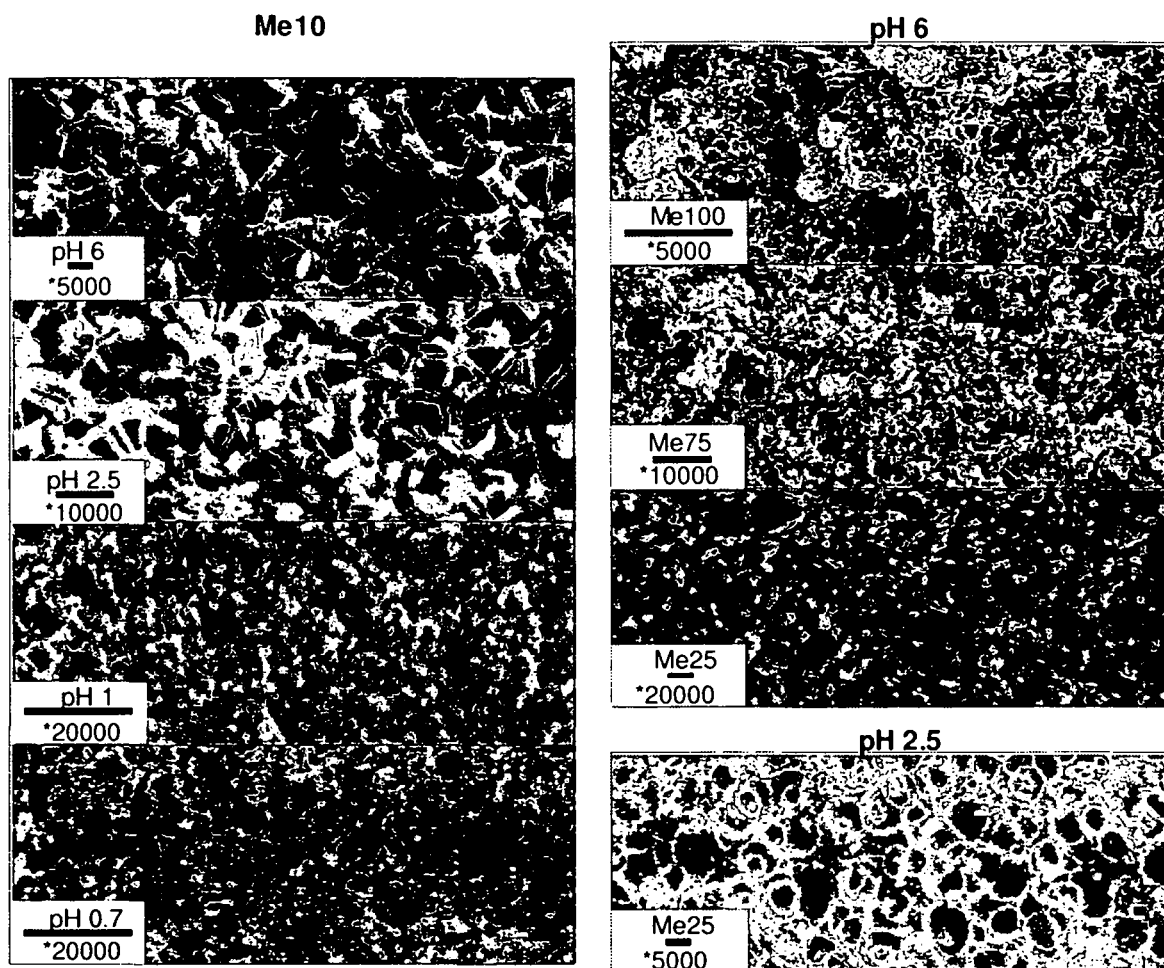
Figure 4.10. SEM images of the methyl silsesqioxane monoliths (Me). Scale bars 1 μm.

Even more striking are the results for the organo-bridged materials. For these materials, only the Si/P123 ratio was varied at a given pH of 2.5 which lead to very strong variations of the morphologies. Furthermore, for the two different organic moieties, totally different morphologies were obtained.

Ethylene-bridged silsesquioxane gels (bEt): The scanning electron micrographs are shown in Figures 4.11. left, a-c. Sample bEt_a is built up from relatively small, elongated, mesoporous particles with dimensions of 0.2 and 0.75 μm, the macropores are approximately 1 μm. This morphology can be explained by a particle growth mechanism with slow formation of mesostructure, gelation, and macroscopic phase separation. Increasing the Si/P123 ratio leads to the formation of a sponge-like, cellular morphology (bEt_b) with larger macropores of ca. 2 μm. The macroporous scaffold also comprises mesopores, but no structural ordering could be observed for this sample. The formation of this structure can be explained by a spinodal

85

Ethylene-bridged (bEt)   Phenylene-bridged (bPh)

— 1 µm   — 1 µm
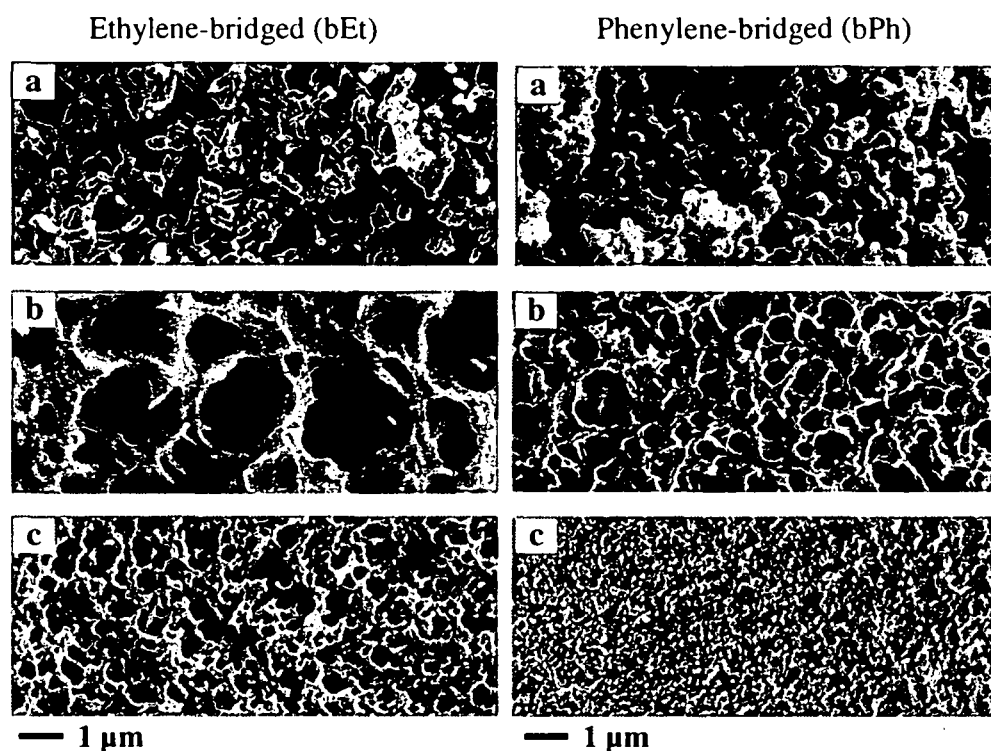
Figure 4.11. SEM images of the ethylene- (bEt, left) and phenylene-bridged (bPh, right) silsesqioxane monoliths.

decomposition with the same long gelation time as sample bEt_a, but faster macroscopic phase separation and no distinct mesostructure formation. Further increase of the Si/P123 ratio leads to an even faster spinodal decomposition resulting in a similar sponge-like, cellular morphology with smaller macropores of 0.75 µm. Interestingly, some mesostructure formation could be observed for this sample.

Phenylene-bridged silsesquioxane gels (bPh): Scanning- (SEM) and transmission (TEM) electron micrographs of sample bPh_a (Figures 4.11 right, -a, and 4.4-b, -c and -d) show the structural build-up of the monolithic hybrid material from interconnected, hexagon shaped particles (~400 nm), which are 'single crystals' of a highly ordered 2D hexagonal mesophase with a repeating unit distance of 10 nm and a pore size of 7 nm. The particles build up a macroporous framework with a pore size of ~400 nm. The formation of hexagon shaped particles can be explained by a particularly quick phase separation due to the high hydrolysis rate of the (water-soluble) ethylene glycol-modified precursor and its high compatibility with the phenylene-bridged silica/surfactant self-assembly. TEM images at high magnification (Figure 4.4.-d) revealed also structural ordering of the pore-walls in form of a distorted

lamellar pattern along the cylindrical pore channel, with the lamellar layers running not perfectly perpendicular to the cylinder axis, but tilted by a small angle.

Increasing the Si/P123 ratio leads to less pronounced mesostructure formation and the observed morphology of sample bPh_b resembles more the features of a spinodal decomposition with a sponge-like, cellular scaffold with macropores of ca. 1 μm. Upon further increase of the Si/P123 ratio (sample bPh_c) no macroscopic phase separation can be observed due to the lower gelation times and higher Si/P123 ratio. The resulting morphology is a colloidal network with very small, mesoporous particles (0.05 μm), with an ordered mesostructure.

Hg-Porosimetry. Due to the overall interesting features of sample bPh_a, the macroporosity was further investigated by Hg-porosimetry (Figure 4.12.) revealing open, uniform macropores with a pore diameter of 260 nm and a high corresponding macropore volume of $0.85\ cm^3 g^{-1}$.
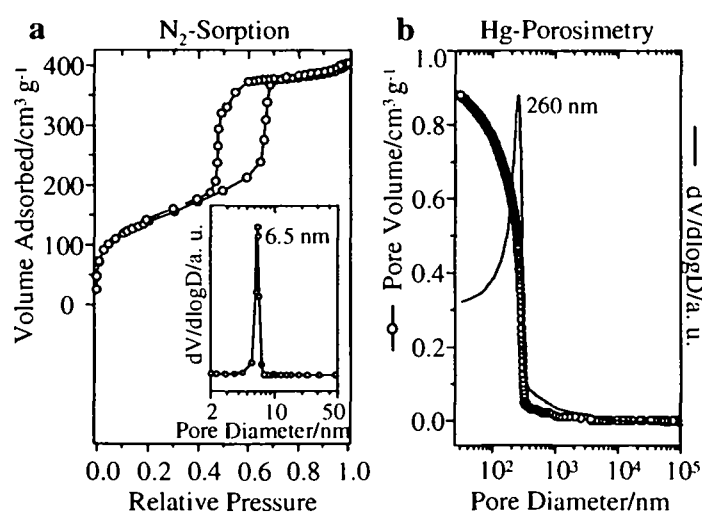
Figure 4.12. N_2-Sorption isotherm and BJH mesopore size distribution (a), and Hg-Porosimetry intrusion curve and macropore size distribution (b) revealing the bimodal pore-structure of the phenylene-bridged silsesquioxane gel bPh_a.

4.2.4. Chemical Composition of the Resulting Gel Bodies

After supercritical drying and soft calcination at 350 °C, respectively, the hybrid materials were investigated with respect to incorporation and preservation of the organic moieties, surfactant extraction, and degree of condensation of the organo silica network by means of solid state NMR and thermogravimetric analyses.

Solid State NMR Studies. The chemical composition of the organosilica hybrid materials was investigated by means of ^{13}C and ^{29}Si solid state NMR studies (Figures 4.13.-4.16.). The ^{13}C CP NMR spectra of the supercritically dried samples revealed the expected signals (shifted by ca. -10 ppm due to inaccurate calibration of the instrument), for the various organic moieties (methyl functionality (Me) at -10 ppm, phenyl functionality (Ph) at 116, 118 and 122 ppm, ethylene-bridged functionality at 6 ppm, and phenylene-bridged functionality at 122 ppm. Some spectra reveal a signal at 37 ppm corresponding to surface methoxy-groups, which are a result of the solvent exchange to methanol prior to supercritical drying. Very small signals around 5 and 50 ppm due to residual surfactant prove the high surfactant extraction efficiency of the supercritical drying process. In the spectrum recorded of a bPh sample calcined at 350 °C, additional signals in the aromatic region appear (δ 143, 112, and 107 ppm), indicating partial oxidative cleavage of Si-C bonds.
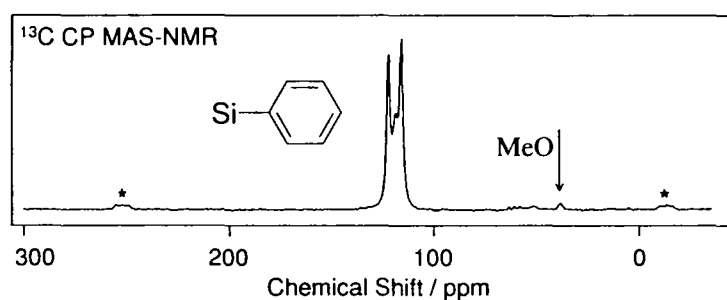
Figure 4.13. ^{13}C CP NMR spectrum of the phenyl silsesquioxane gel Ph75 prepared at pH 6 after supercritical drying.

Methyl silsesquioxane gels (Me). In order to investigate the completeness of the co-condensation reaction (full incorporation of the organo silsesquioxane species) a quantitative ^{29}Si SP NMR spectrum was recorded for sample Me75 prepared at pH 6 (see Figure 4.14.). The spectrum reveals as expected *T*- and *Q*-signals – T^2, T^3, Q^3 and Q^4 with chemical shifts of -65.4, -73.8, -108.9 ppm and -119.0 ppm, with relative peak intensities of $Q^4/Q^3/T^3/T^2$ = 22/3/57/18. The ratio of Q/T units of 25/75 corresponds exactly to the ratio of Si^{EGMS}/Si^{MeGMS} of the synthesis composition proving a full incorporation of organic units into the final material. Furthermore, it can be assumed that no Si-C bond cleavage occurred during the supercritical drying process. Quantification of the incorporation of phenyl moieties could be easily determined by thermogravimetric analysis (which is not possible for the methyl groups due the lower decomposition temperature which overlaps with the weight loss due to network condensation), therefore no ^{29}Si NMR spectra were recorded.
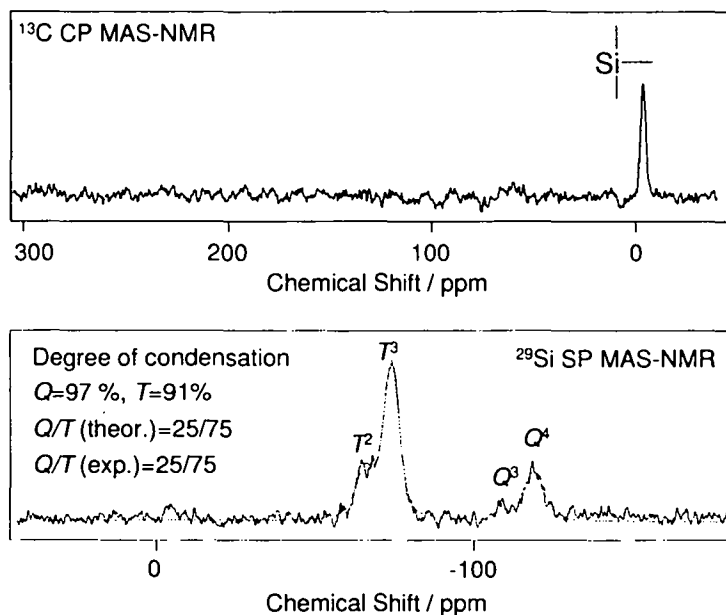
Figure 4.14. Solid state NMR spectra of the methyl silsesquioxane gel Me75 prepared at pH 6 after supercritical drying (^{13}C CP and ^{29}Si SP spectra).

Ethylene-bridged silsesquioxane gels (bEt_a): In order to investigate the impact of supercritical drying and as an alternative method soft calcination at 350 °C on the chemical composition of the hybrid material, ^{29}Si NMR spectra were recorded (see Figure 4.15.). For the sample treated with supercritical drying, a quantitative (SP) spectrum was recorded in order to calculate also the degree of condensation. In this spectrum, only T-signals – T^1 and T^2 with chemical shifts of -59.2 and -63.1 ppm, and relative peak intensities of T^2/T^1 = 93.3/6.7 – were detected, proving that no Si-C bond cleavage occurred throughout the whole synthesis. The rather large amount of T^2-units is not indicating a low degree of condensation, but can be explained by the contribution of the bridging ethylene units to the network crosslinking. The degree of condensation has been calculated to 66.7 %. In the ^{29}Si CP NMR spectrum after soft calcination at 350° C, additional signals (Q^{2-4}) appear due to oxidative cleavage of Si-C bonds during calcination.
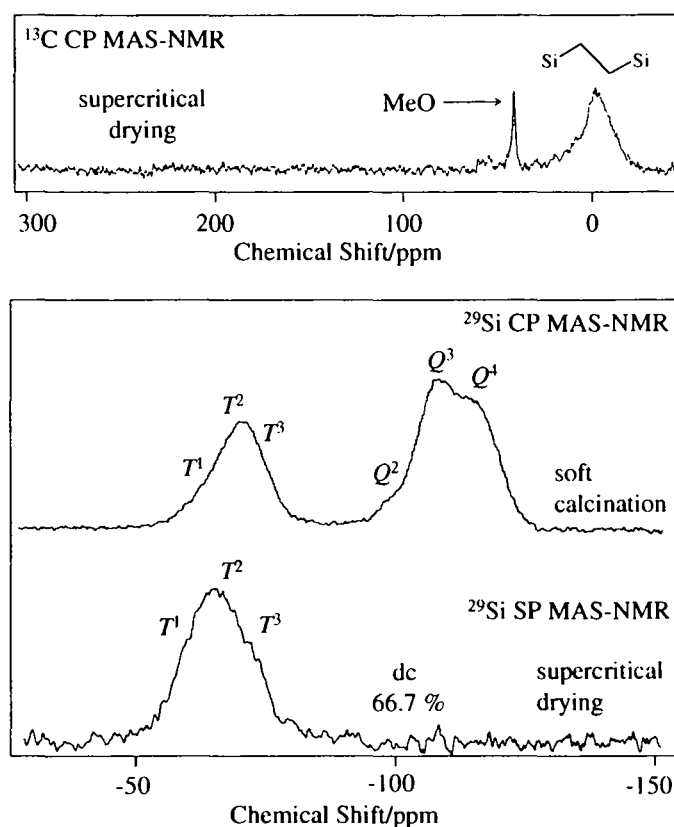
Figure 4.15. Solid state NMR spectra of the ethylene-bridged silsesquioxane gel bEt_a after supercritical drying (^{13}C CP and ^{29}Si SP spectra) and soft calcination (^{29}Si CP spectrum).

Phenylene-bridged silsesquioxane gels (bPh_a): In order to investigate the impact of supercritical drying and as an alternative method soft calcination at 350 °C on the chemical composition of the hybrid material, ^{29}Si NMR spectra were recorded (see Figure 4.16.). In the quantitative ^{29}Si SP NMR spectrum only T-signals – T^1, T^2, and T^3 with chemical shifts of - 66.5, -74.6, and -83.0 ppm, and relative peak intensities of $T^3/T^2/T^1$ = 0.26/0.59/0.15 – were detected after supercritical drying, proving that no Si-C bond cleavage occurred throughout the whole synthesis. The rather large amount of T^2-units is not indicating a low degree of condensation but can be explained by the contribution of the bridging phenylene units to the network crosslinking. A higher degree of condensation than for sample bEt_a can be calculated for sample bPh_a (70.4 %), which is consistent with the much higher gelation times of observed for all bEt samples. Cleavage of Si-C bonds during soft calcination as indicated by the ^{13}C NMR spectrum is confirmed by ^{29}Si CP experiments (appearance of Q^{2-4} signals).
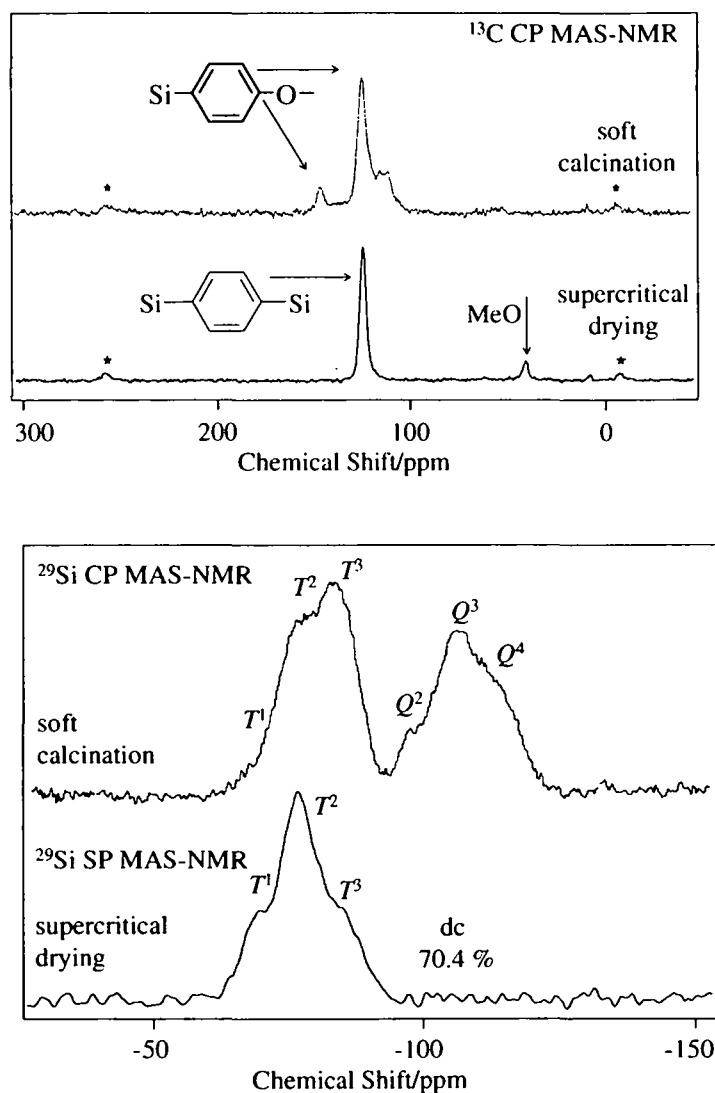
Figure 4.16. Solid state NMR spectra of the phenylene-bridged silsesquioxane gel bPh_a after supercritical drying (^{13}C CP and ^{29}Si SP spectra) and soft calcination (^{13}C CP and ^{29}Si CP spectra).

Thermogravimetric Analysis (TGA). As already mentioned in the chapter above, for the phenyl silsesquioxane gels, completeness of incorporation was determined by TGA. In the weight loss profile, a distinct step at 600 °C can be observed, which can be attributed to the phenyl moieties. From the corresponding weight loss and the residual weight at 1000 °C, which is attributable to SiO_2 the Si^{EGMS}/Si^{PhGMS} ratio has been calculated for the samples P10-P75 prepared at pH 6 and is in perfect agreement with the ratio of Si^{EGMS}/Si^{MeGMS} of the synthesis composition proving a full incorporation of organic units into the final material.

4.3. Conclusion

Different ethylene glycol-modified derivatives of organoalkoxysilanes such as methyl-, phenyl-, ethylene-bridged and phenylene-bridged alkoxysilane have been synthesized and applied in a TLCT approach with the non-ionic poly(ethylene oxide)-based block copolymeric surfactant P123 in aqueous (neutral) and acidic conditions. In summary, this chapter presents a simple, versatile method to fabricate a range of organosilica hybrid monoliths with a hierarchical build-up on three to four levels – a) deliberate macroscopic shape, b) uniform macropores, c) (in many cases highly ordered) mesopores plus micropores, and d) molecular periodicity of the phenylene moieties within the pore walls (only for phenylene-bridged silsesquioxane materials). The macroscopic gel morphology and periodic ordering of the mesopore structure can be significantly influenced by the choice of pH, type of and degree of substitution with organic functionality and the Si/P123 ratio. For each system, the optimal synthesis parameters have to be fine-tuned to get optimal results with respect to long-range periodicity of the mesostructure. The underlying notion of substituting the alkoxygroups of conventional (organo-)-alkoxysilane precursors with ethylene glycol can be readily extended to other organic functionalities. This method represents a versatile tool to tailor the chemical functionality of monolithic materials with well-defined, multi-modal pore structures, thus increasing their potential of application significantly.

5 Time Resolved Synchotron-SAXS Measurements

5.1. Motivation

Time-resolved SAXS measurements were carried out using the high intensity of the X-ray beam from the synchrotron radiation sources Elettra in Triest (Italy) and also Hasylab in Hamburg (Germany) with the aim to investigate the formation of ordered mesostructures as well as the sensitivity of the formed structures towards the different processing steps especially solvent exchange first to methanol and then to liquid carbon dioxide and finally even supercritical drying in carbon dioxide at a temperature of 45 °C and a pressure of 120 bar. Different experimental set-ups were used such as a home-made flow through cell in which the processes beginning with mixing of the components and the methanol exchange was monitored, whereas for supercritical drying, a high-pressure cell (Figure 5.1. right) was used. It is equipped with diamond windows, which allow in-situ measurements during exchange of methanol to carbon dioxide, (de-)pressurizing in the required pressure range of 0-100 bar, carbon dioxide flow and temperature regulation.
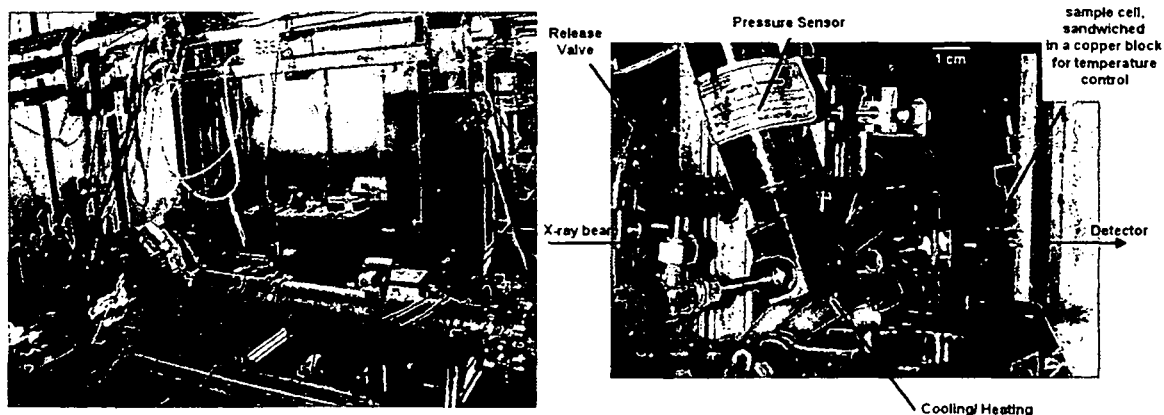
Figure 5.1. SAXS beamline at Elettra synchtron, Triest, Italy (left); High pressure sample cell for *in-situ* SAXS measurements during supercritical drying with carbon dioxide (right).

5.2. Results and Discussion

Figure 5.2. shows representative SAXS patterns (top part) of (A) the surfactant/water mixture (P123/H_2O in a ratio of 30/70 by weight), (B) during the formation of the gel network after addition of the ethylene glycol-modified silane (with a resulting composition of Si/P123/H_2O

93

= 4.7/30/70 by weight, which corresponds to sample E10, see Chapter 7.2.3.), and (C) a dried sample. The scattering curves show at least one distinct reflection due to the periodic arrangement of the surfactant/ water liquid crystal as well as of the evolving mesostructured silica phase. The changes in the repeating unit distance (d-spacing) calculated from this reflection represent best the formation and evolution of the mesostructures during the whole synthesis.

The addition of the silane to the surfactant/water mixture significantly disturbs the long range order of the supramolecular arrangments, (three well resolved reflections change to one broad maximum of low intensity). Even after the formation of a three-dimensional inorganic network (gelation) in the surfactant/ water mixture the evolution of the silica-surfactant mesophase continues which can be seen by the significant decrease of the repeating unit distance. To complete the cooperative self-assembly process and network condensation the gels were subjected to an aging procedure in the mother liquid (water/ ethylene glycol) for seven days at 30 °C. Preformed gels were measured repeatedly during the aging procedure. Prior to drying of the wet gels a solvent exchange process of aqueous ethylene glycol to methanol was performed. During all these processes, the long-range order in the material is becoming more pronounced and a significant decrease in the repeating unit distance is observed, which corresponds well to a higher degree of crosslinking in the inorganic network and loss of surfactant during solvent exchange.

The most crucial step in the preparation of large porous monoliths is drying, since evaporation of the pore liquid leads to large shrinkage or even collapse of the whole gel body. One typical procedure to prevent cracking is drying with supercritical fluids. Here, the building-up of a gas/liquid interface is avoided during drying, hence no capillary pressures evolve. In this report, an *in-situ* SAXS study of a supercritical drying process with carbon dioxide was performed, comprising an extraction step with liquid carbon dioxide to exchange methanol, an increase in temperature to 45 °C while simultaneously increasing the pressure (100 bar), thus transfering carbon dioxide into the supercritical state, and finally a venting step to ambient pressure. These experiments were performed on pre-prepared and aged, wet gel samples in the high pressure cell, which is displayed in Figure 5.1.

A

B

C

I (A.U.)

q / nm -1

q / nm -1

q / nm -1

14.0

13.5

13.0

12.5

12.0

11.5

d spacing / nm

Aging

Gelation

Solvent Exchange

H₂O → Methanol → Liquid CO₂
70 bar 15 °C

Supercritical Drying

0   200   2000

0   5   10   0   10   20

20   40   60   30   0

Time / min

Time / min   Time / min

Temperature / °C   Pressure / bar
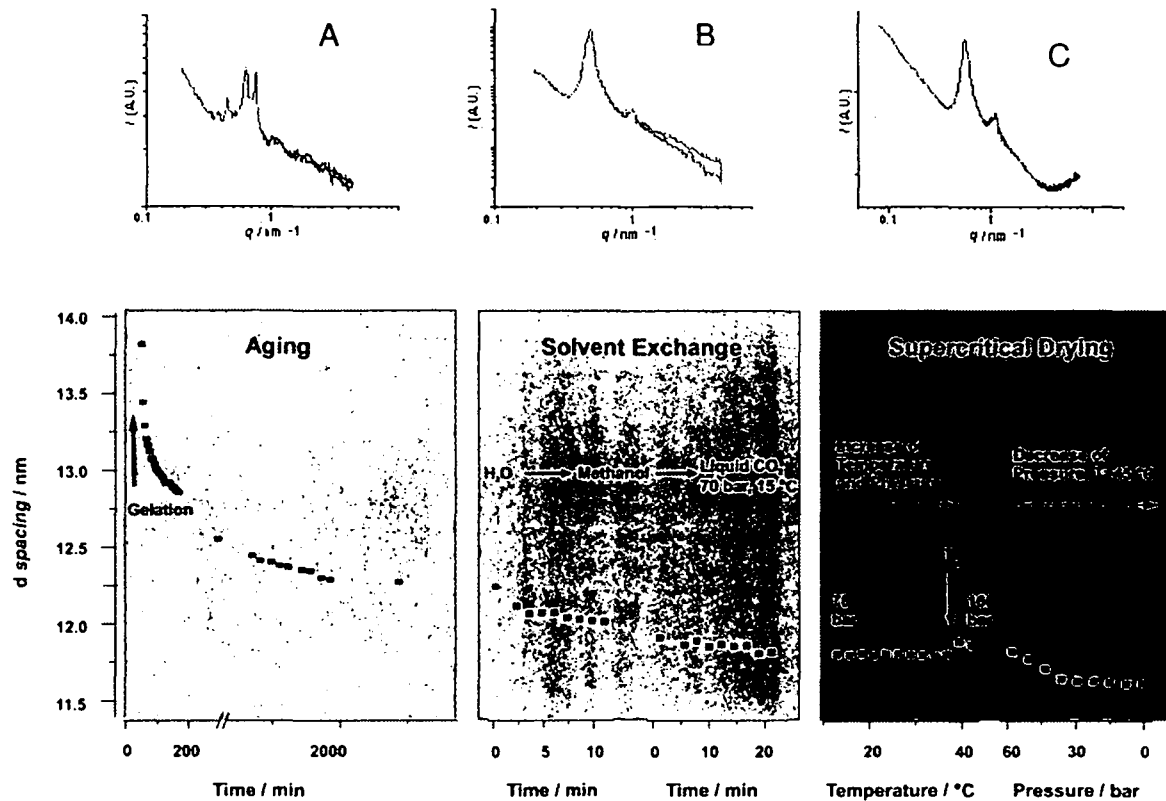
Figure 5.2. SAXS pattern of the water/surfactant mixture (A), shortly after gelation (B) and after supercritical drying (C), (top) and the evolution of the corresponding d-spacing during gel formation (30 sec/ measurement), solvent exchange from ethylene glycol/water mixture to methanol (in the liquid cell) to liquid carbon dioxide (in the high pressure cell) with preformed gels (30sec/ measurement) and supercritical drying with carbon dioxide (10sec/ measurement, bottom).

None of the solvent exchange and drying steps is detrimental to the mesostructure of the silica monoliths. Interestingly, the transition from liquid to supercritical CO_2 at 31 °C and ca. 80 bar leads to a small increase in the repeating unit distance, which cannot be explained at the moment. Venting the system to ambient pressure again results in a contraction of the gel network and a final d-spacing of 11.6 nm.

6 Application of Hierarchically Organized Monoliths as Stationary Phase for HPLC

6.1. Motivation

Chromatographic separation has been significantly brought forward by the invention of monolithic silica rods (Chromolith™) by Merck.[149] This innovative technology offers dramatic reductions in separation time, new dimensions to chromatographic techniques, the reduction of column backpressure to minimum and significantly increased sample throughput.

Based on an induced phase separation process during sol-gel reaction of tetraalkoxysilanes, highly porous monolithic rods of silica with a bimodal pore structure can be formed.[29,30,101,103] Each column consists of both a macroporous and mesoporous structure. Each macropore is on average 2 μm in diameter and together form a dense network of pores through which the eluent can rapidly flow, thus separation time is dramatically reduced. The mesopores form the further fine porous structure (13 nm) of the column interior and create a very large surface area on which adsorption of the target compounds can occur. This unique combination of macropores to allow rapid transit of the eluent and mesopores to create a large surface area means that Chromolith™ columns provide excellent separations in a fraction of the time that a standard particulate column does.
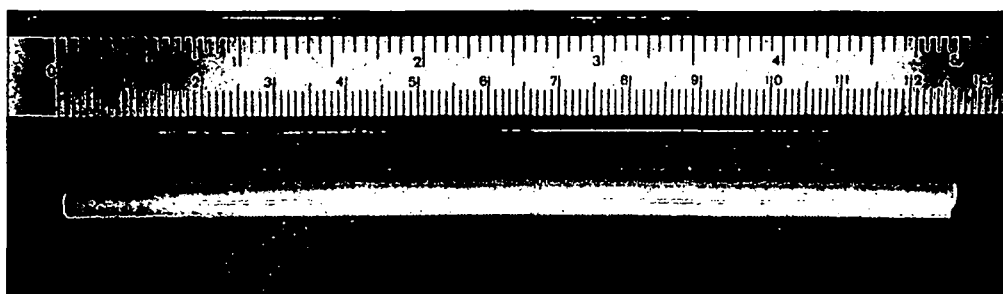
Figure 6.1. Photograph of the tested E17_tms monolith with dimensions 125-50 mm.

The structural properties of the Chromolith materials and the E17_tms monoliths prepared at pH 1 (see Chapter 3)[138] are listed in table 6.1. Our materials resemble similar features with the additional properties of a highly uniform, periodically ordered mesopore system, microporosity and higher total porosity and surface areas. In order to investigate the principal

suitability of our materials for application as HPLC columns e.g. with regard to the mechanical stability, and to test performance in standard tests for HPLC columns, E17 monoliths (prepared at pH 1) with dimensions of 100 mm length and 5 mm diameter were tested in collaboration with an industrial partner.

Table 6.1. Structural properties of the commercial chromolith column from Merck and the E17_tms monolith.

	Macropore size	Mesopore size	Pore volume	Total porosity	Surface area	Surface modification	Surface coverage
Chromolith	2 μm	13 nm	1 cm³/g	80 %	300 m²/g	none (Si) C18 (RP)	3.6 μmol/m²
E17_tms	2 μm	10 nm	V^{tot} 4 V^{meso} 1 cm³/g	90 %	880 m²/g	tms	4.1 μmol/m²

6.2. Sample Preparation and Testing Parameters

To increase the mechanical stability of the monoliths and pre-extract the surfactant before the surface modification (also to avoid cracking) they were refluxed in a mixture of concentrated HCl and ethanol (see Chapter 3.4.). Then, after solvent exchange to ethanol and then to petroleum ether, the monoliths were surface modified using trimethylchlorosilane-petroleum ether solutions and dried at ambient pressure (up to 200 °C) as described in Chapter 3.[130] By this procedure crack free monoliths (see figure 6.1) with a density of 0.2 g·cm⁻³ were obtained. SAXS measurements confirmed the presence of a 2D hexagonal mesostructure with a repeating unit distance d_{10} of 11.9 nm (see figure 6.2, left). Nitrogen sorption experiments showed the expected type IV isotherm with a H1 hysteresis loop (figure 6.2, right) which proves the presence of an open, uniform mesoporosity with a mean pore diameter of 10.1 nm, high surface area of 880 m²·g⁻¹, high mesopore volume of 1 cm³·g⁻¹ and some pore wall micro- and mesoporosity with a volume of 0.2 cm³·g⁻¹. All of these values are in very good agreement with the data presented in chapter 2 for sample E17_tms. These monoliths were then tested as columns for HPLC. The tests performed are based on standard tests for two different types of columns: Chromolith® RP is a reversed phase (hydrophobic) material.
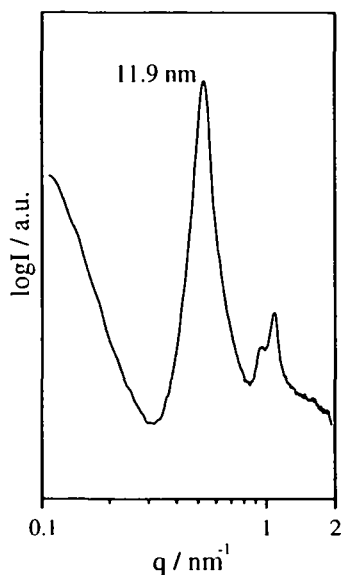
Figure 6.2. SAXS pattern of the E17_tms monolith.
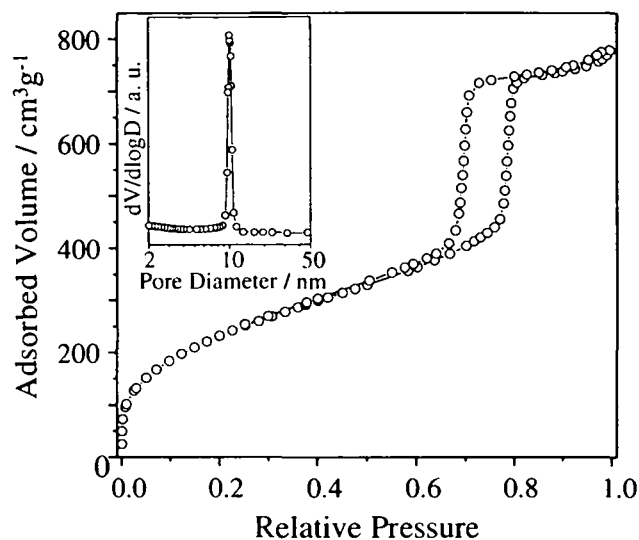
Figure 6.3. Nitrogen sorption isotherm and BJH mesopore size distribution (inset) of the E17_tms monolith.

The reversed-phase chromatography is the most popular mode of chromatography. Typically silylated silica is used where the surface of the silica material is chemically modified with n-alkyl chains. Most commonly, n-octadecyl bonded stationary phases are used followed by n-octyl and others. Chromolith® Si on the other hand is a high-purity silica and has been developed as a monolithic normal-phase material suitable for separating polar non-ionic organic compounds. The two sets of test parameters, which are normally applied for these different types of columns, were both applied to the same E17_tms monolith as listed in Table 6.2.

Table 6.2. Parameters of the RP- and Si-test

	RP-test	**Si-test**
eluent	acetonitrile/water 60/40	heptane/dioxane 95/5
flux	0.5 mL/min	1 mL/min
detection	UV 254 nm response fast	UV 254 nm response fast
temperature	RT	RT
injection	10 µL	5 µL
sample	1.3 mg thiourea	26.7 mg toluene
	10.3 mg progesterone	3.0 mg nitrobenzene
	1.0 mg anthracene	17.6 mg 2-nitroanisole
	solubilized in 100 mL eluent	solubilized in 100 mL eluent

6.3. Results and Discussion

Before the monoliths can be applied as stationary phase for HPLC, they have to be clad with a polymer coating. The details of the exact process are not provided by the industrial partner, only that the process could be easily adapted for the E17_tms monolith. The results of the following RP- and Si-tests are listed in tables 6.3 and 6.4 and the retention time profiles are shown in figures 6.3 and 6.4.

Table 6.3. Results of the RP-test.

RP-test							
	N/m	T USP Anthr.	k'-	alpha An/Pr	R An/Pr	pressure in bar	dimensions
	0.5					netto	
RP_01	11508	---	1.18	1.24	0.87	51	65-5mm
RP_02	50310	1.59	1.27	1.38	2.92	115	100-5mm
RP_03	32160	1.60	1.38	1.39	2.48	113	100-5mm
MW	31326	1.60	1.28	1.34	2.09		

Table 6.4. Results of the Si-test.

Si-test						
	N/m	T USP 2-Nitroa.	k'-	R Nbe/Nan	pressure in bar	dimensions
	1 mL/min				netto	
Si_01	7092	2.13	1.07	2.56	65	65-5 mm
Si_02	45690	2.04	1.36	9.57	125	100-5 mm
Si_03	53720	2.56	1.28	10.01	124	100-5 mm
MW	35501	2.24	1.24	7.38		

The results obtained are quite astonishing as in both tests the E17_tms monoliths showed a good separation. Normally, for a certain surface property (hydrophilic or hydrophobic) good separation can only be obtained for one or the other test. Another remarkable finding in a negative sense was the high backpressure which is normally only the case for small or blocked macropores.
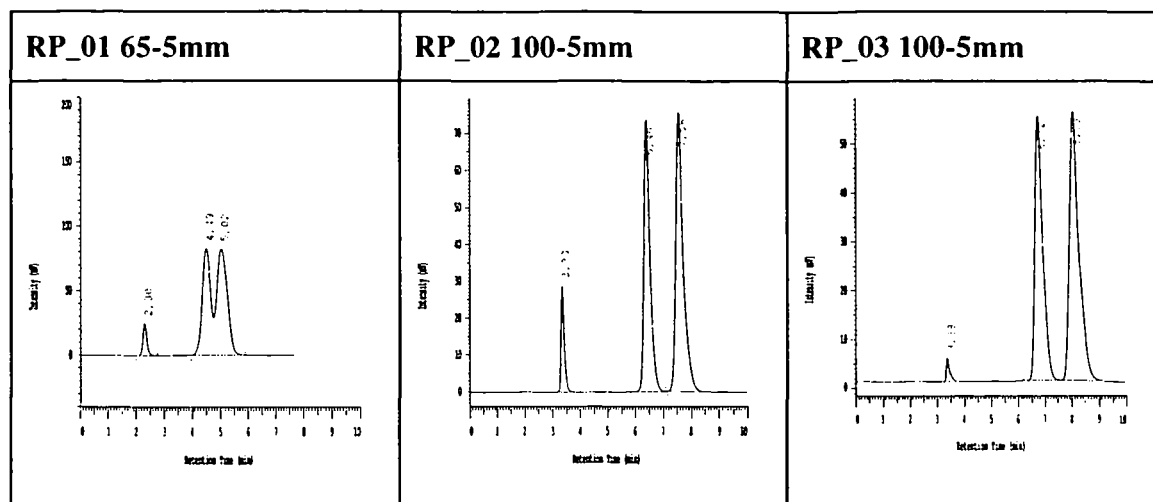
Figure 6.3. Retention time profiles obtained for the E17_tms monolith in the RP-test.
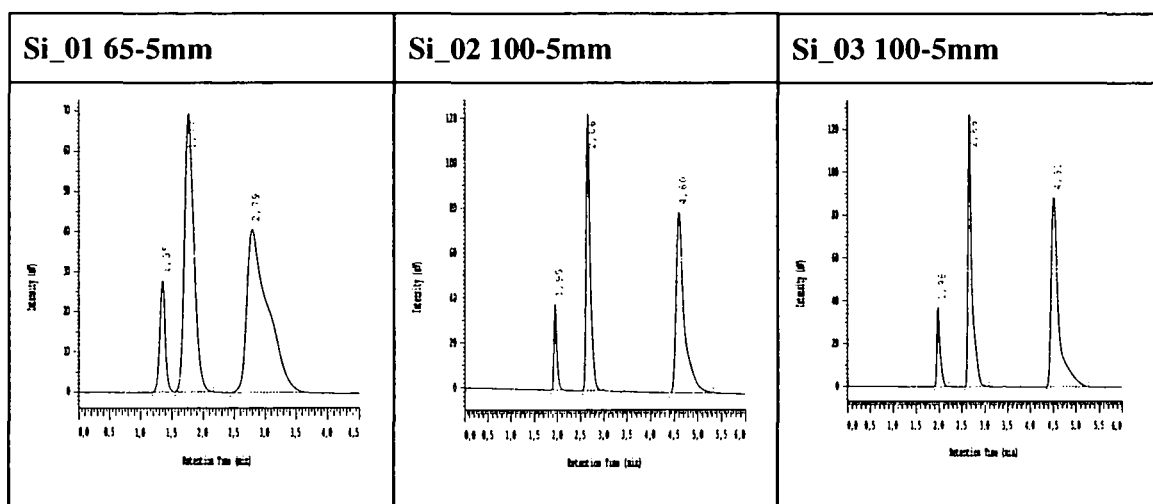
Figure 6.4. Retention time profiles obtained for the E17_tms monolith in the Si-test.

6.4. Conclusion

Work on the application for HPLC will continue, as the first results revealed novel properties with regard to the possibility to separate compounds of very different polarity and chemical character on a material with the same chemical properties. Other sets of E17_tms monoliths will be prepared and tested with a focus on reproducible synthesis of the macropore structure and on optimizing the macroporous structure in order to achieve better flow rates at lower pressures.

7 Experimental

7.1. Analytical Methods

7.1.1. Small and Wide Angle X-Ray Scattering (SAXS, WAXS)

Small and wide angle X-ray scattering (SAXS) investigations were undertaken in order to obtain information porous structure in the nanometer regime, in particular about periodical ordering of the porous and also the molecular structure. X-ray scattering techniques provide information on structures in the size range between 0.15 and 50 nm (with the equipment used). The scattering of X-rays results from fluctuations in the electron density. The larger the structures, the smaller are values for the scattered angles. Every change in slope or every maximum in the SAXS curves correlates with a characteristic length (particle size, particle spacing) in the material. For materials with periodically arranged structures, diffraction peaks are observed if the conditions of Bragg's law (Eq. 7.1.) are fulfilled:

Bragg's Law:

$$n \cdot \lambda = 2 \cdot d \cdot \sin\theta \qquad\qquad \text{Eq. 7.1.}$$

n...integer

λ...wavelength of the incident beam, for Cu-Kα radiation 0.154 nm

d...repeating unit distance

θ...angle of incidence
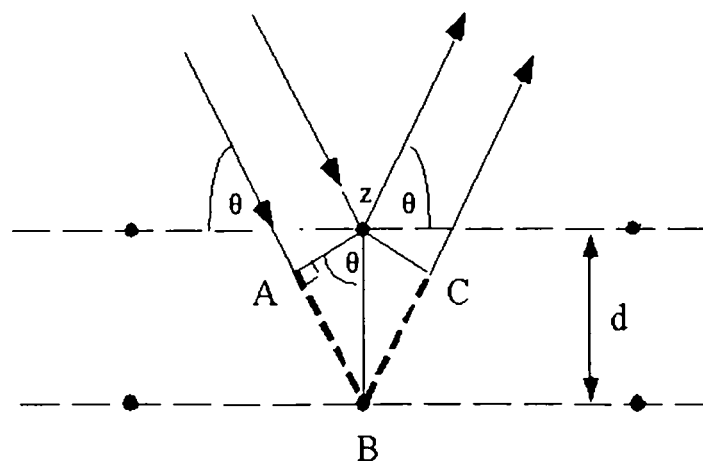
Figure 7.1. Schematic illustrating Bragg's Law of the diffraction of X-rays from periodic structures (i.e. lattice points, pores) with the repeating unit distance d.

The d-spacings with the index hkl for structures relevant to this work can be calculated by the formulas below:

Lamellar	$1/d^2 = (h^2 + k^2 + l^2)/a^2$	Eq. 7.2.
Hexagonal	$1/d^2 = 4/3(h^2 + hk + k^2)/a^2 + l^2/c^2$	Eq. 7.3.

With a, c being the dimensions of the unit cell.

Reflections observed for the structures relevant in this work:

lamellar: $h00$

$p6mm$ hexagonal (2D hexagonal): $hk0$

The d-spacings can be calculated from the SAXS curves by $2=2\pi/q$ wherein q is the scattering vector.

The diameter of pores and pore walls (the thickness of the silica backbone) for 2D hexagonal mesostructures (infinite cylinders packed in a hexagonal array) were determined from fits to the ratio of the intensities of the Bragg reflections. The sensitivity of the peak intensities to the form factor was used previously to determine the filling factor in C_{60} filled carbon nanotubes.[150] In our case, the position and the ratio of the peak intensities enable the determination of the pore diameter, the pore wall diameter and the pore-to-pore distance with the use of the form factor for infinite cylinders and a Gaussian intensity distribution for the Bragg reflections.[151]

Small and wide angle X-ray scattering (SAXS and WAXS) measurements were performed using a pinhole camera with a rotating anode generator (Ni-monochromated Cu-K_α radiation) and an area detector (Bruker AXS, Karlsruhe). The sample to detector distance was varied from 4 (WAXS) to 98 (SAXS) cm from which scattering curves in the q-range 0.1-37 nm^{-1} were obtained. All SAXS patterns were first radially averaged to obtain the function I(q), wherein $q = (4\pi/\lambda)\sin\theta$ is the scattering vector (2θ = diffraction angle; $\lambda = 0.154$ nm), and then corrected for background scattering from the experimental setup. SAXS measurements were carried out on dried as well as calcined gel samples.

The time-dependent high-pressure measurements were performed at the Austrian high-flux SAXS beamline at Elettra using a fixed wavelength $\lambda = 0.077$ nm, with a camera length of 204 cm, equipped with a 150 mm linear wire PSD (Gabriel-type gas detector), which provided an effective q-range 0.08-4 nm^{-1}.[152,153] Here q is the magnitude of the momentum

transfer ($q=4\pi\sin(\theta)/\lambda$ with 2θ being the scattering angle). The high-pressure X-ray cell was made of stainless-steel with diamond windows (0.5 mm thick) and a sample volume of approximately 30 mm^3 and flow-through capability (Figure 5.1). In the sample stage the cell was sandwiched between two copper blocks through which thermostated water circulated. Both temperature and pressure was computer-controlled.[154] CO_2 was used both as solvent and pressurizing agent. The cylinder containing CO_2 in the liquid-state was connected via a valve to a high-pressure network, which allowed both, to increase and decrease the pressure in the sample cell.

The SAXS measurements were carried out during the gelation process, thus continuously following network and mesophase formation. Preformed gels were investigated at different times during aging (1 to 7 days), followed by in-situ measurements of the solvent exchange process to methanol (of gels that have been aged for seven days). For these measurements, liquid samples and also preformed gel samples were placed in a home-made flow-through cell with a sample volume of about 1 cm^3. For supercritical extraction with liquid carbon dioxide, the wet gels were placed in the high-pressure cell. After solvent exchange from methanol to liquid carbon dioxide at 20 °C and 70 bar, the temperature and pressure were raised computer-controlled to 45 °C and 100 bar.

7.1.2. Nitrogen Sorption

The measurement of nitrogen adsorption and desorption at 77 K provides information about the surface area, surface energy, pore shape and volume as well as pore size distribution in the micro-, meso- and lower macropore size range between 0.5-100 nm.[47] Adsorption/ desorption isotherms are obtained by plotting the adsorbed volume as a function of the relative pressure p/p_0 wherein p is the gas pressure above the sample and p_0 the saturation pressure of the adsorbent. In the present context, adsorption is the increase in concentration of a gaseous component (nitrogen in our case) in the vicinity of a gas-solid interface. Physisorption occurs whenever a clean solid (the adsorbent) is exposed to a gas (the adsorptive). By general convention, the adsorbed material is known as the adsorbate. The forces involved in physisorption are the same as those responsible for the condensation of vapors and the deviations from the ideal gas behavior. Although there is no chemical bonding to the surface (unlike in chemisorption), if they are polar the physisorbed molecules undergo specific interactions with particular functional groups (e.g. surface hydroxyls). The adsorption energy

is also enhanced when molecules enter pores of molecular dimensions. The following groups of pores are designated by IUPAC according to their width:[155]

Ultramicropores   < 0.7 nm

Supermicropores   0.7-2 nm

Mesopores   2-50 nm

Macropores   > 50 nm

Although other factors are also important (e.g. pore shape and molecular structure), the adsorption mechanism is to a large extent controlled by the pore size. Thus, it is possible to identify three distinctive processes: monolayer-multilayer adsorption, micropore filling and capillary condensation. The division in pore classes is based mainly on the adsorption behavior of nitrogen and its mean molecule diameter of ca. 0.4 nm. Primary micropore filling occurs in ultramicropores below 0.7 nm at relative pressures p/p_0 between 10^{-3} and 10^{-4} and results in a close packing of molecules. Supermicropores are being filled over a wider p/p_0 range reaching into the range of multilayer adsorption. The mechanism is a cooperative process called secondary cooperative filling. Due to the larger space available in the pore, a closer packing of nitrogen molecules is achieved.

The mesopore range is limited by the validity of the Kelvin equation which correlates the vapor pressure of liquids with surface curvature. On the upper end of the scale (50 nm) no curved meniscus for the adsorbate filling the pore capillary exists, whereas on the lower limit (2 nm) only five nitrogen molecules lie next to each other which cannot be considered a liquid but an accumulation of molecules. For nitrogen, the pore radius can be calculated to:

Kelvin Equation:

$$r_K \, / \, nm = - \, 0.415/\log(p/p_0)$$ Eq. 7.4.

r_K...Kelvin radius

The Kelvin radius does not contain the t-layer, which is relatively strongly bound to the pore surface and has to be considered in addition for determination of the pore size.

$$r_P = r_K + t$$ Eq. 7.5.

r_P...pore radius

t...standard multilayer thickness

Isotherms. Six characteristic shapes of physisorption isotherms are identified in the IUPAC classification shown in Figure 7.2.[155] The Type I isotherm, which shows a long saturation plateau, is still sometimes referred to as the 'Langmuir isotherm', but this is misleading because generally the physisorption process involves micropore filling rather than surface coverage. In contrast, the Type II isotherm has no plateau and is usually the result of monolayer-multilayer adsorption on the open surface of a nonporous or macroporous adsorbent. However, a Type III isotherm is obtained if the adsorbent-adsorbate interaction is weak, while a stepwise Type VI isotherm is a special case of layer-by-layer adsorption on a uniform surface such as graphite. Characteristic features of Type IV isotherms are the final saturation plateau and, in many cases, a hysteresis loop, which is associated with capillary condensation in mesopores. True Type V isotherms are rare, the best examples being given by the adsorption of water vapour by porous carbons.
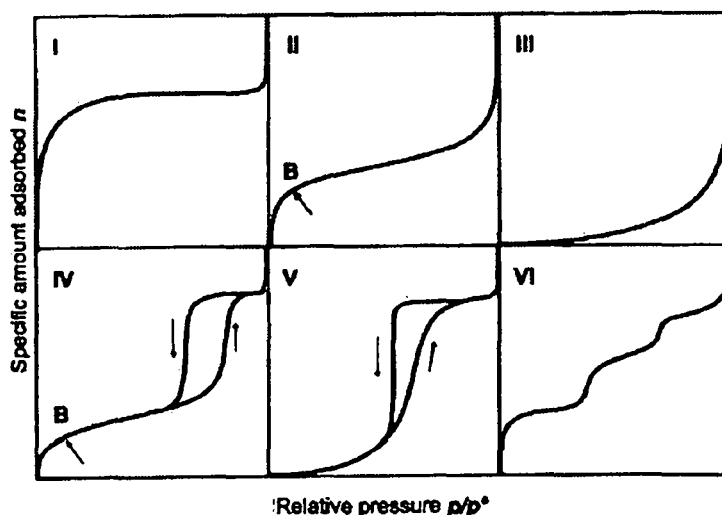
Figure 7.2. The IUPAC classification of physisorption isotherms.[155]

Hysteresis Loops. Physisorption is often associated with hysteresis, which is manifested when the amount adsorbed is not brought to the same level by an increase or decrease in pressure to a given set of 'equilibrium' conditions. Hysteresis loops, which appear in the middle, multilayer range of Type IV isotherms, are associated with capillary condensation. Most mesoporous adsorbents give distinctive and reproducible hysteresis loops. The major types are represented in the IUPAC classification given in Figure 7.3.[155] The characteristic features of some types of loop are associated with certain well-defined pore structures. For example, Type H1 is a fairly narrow loop with very steep and nearly parallel adsorption and desorption

branches. The Type H1 loop is given by an adsorbent with a narrow distribution of uniform pores (e.g. open-ended tubular pores as in MCM-41 and SBA-15). In contrast, the Type H2 loop is broad with a long and almost flat plateau and a steep desorption branch. Many inorganic oxide gels give the more common Type H2 loops. The pore structures in these materials are generally complex and tend to be made up of interconnected networks of pores of different size and shape. Type H3 and H4 loops do not terminate in a plateau at high relative pressures p/p_0. They do not close at $p/p_0 < 1$ and their limiting desorption boundary curves are dependent on the experimental conditions. These hysteresis loops are often given by the aggregates of platy particles or adsorbents containing slit-shaped pores.
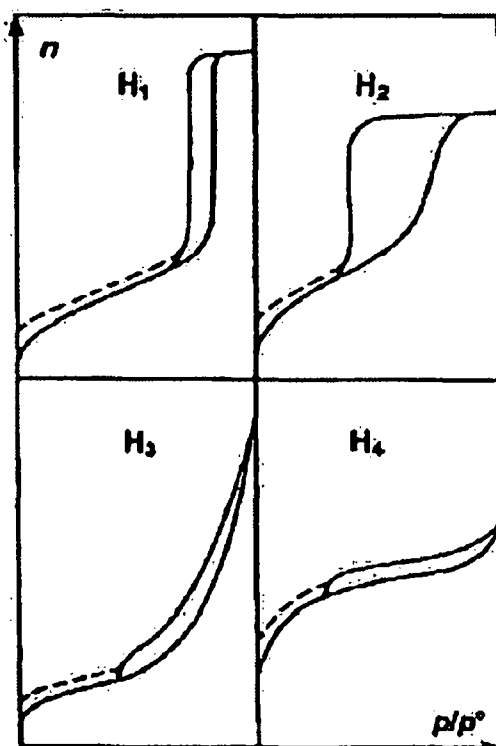
Figure 7.3. The IUPAC classification of hysteresis loops.[155]

A feature common to many loops is that for a given adsorptive at a particular temperature, the hysteresis loop does not extend below a certain p/p_0. This lower limit of hysteresis is dependent on the adsorptive and the operational temperature, but not the adsorbent. In the case of nitrogen adsorption at 77 K, the lower closure point is at $p/p_0 = 0.42$.

Surface Area Calculation by the BET Method[156]. The original BET treatment by Brunauer, Emmett and Teller was essentially a multilayer extension of the Langmuir kinetic model of monolayer adsorption on an array of identical sites. The Langmuir concept of ideal localized monolayer adsorption was thereby extended to include the formation of an infinite or finite number of adsorbed layers. According to the BET model, the molecules in one layer can act as possible sites for the adsorption of molecules of the next layer. The success of kinetic theories directed toward the measurements of surface areas depends upon their ability to predict the number of adsorbate molecules required to exactly cover the solid with a single molecular layer. Equally important is the cross-sectional area of each molecule or the effective area covered by each adsorbed molecule on the surface. The surface area then is the product of the number of molecules in a completed monolayer and the effective cross-sectional area of an adsorbate molecule. The effectiveness of the BET theory is that it enables an experimental determination of the number of molecules required to form a monolayer despite the fact that exactly one monomolecular layer is never actually formed.

The BET Equation (linear form):

$$\frac{p/p_0}{n(1-p/p_0)} = \frac{1}{n_m C} + \frac{C-1}{n_m C}(p/p_0)$$

Eq. 7.6.

n...amount of nitrogen molecules adsorbed

n_m...monolayer capacity

C...empirical constant

According to the BET theory, the constant C is related exponentially to the net molar energy of adsorption ($E_1 - E_L$) by the simplified equation:

$$C \approx \exp[(E_1 - E_L)/RT]$$

Eq. 7.7.

R...molar gas constant (8.314 $J \cdot K^{-1} \cdot mol^{-1}$)

T...temperature / K

E_1...energy of adsorption of the first layer / J

E_L...energy of liquefaction / J

The C value is a measure for surface-adsorbate interactions and therefore polarity of the surface, with a high C value correlating with relatively strong interactions. In the important case of nitrogen sorption at 77 K on many amorphous and non microporous solids, C is in the range of 100.

Two stages are involved in the evaluation of the BET surface area S^{BET}. First, it is necessary to construct the BET plot and from it to derive the value of n_m. The next stage is the calculation of the specific surface area S^{BET}, which requires knowledge of the average area σ occupied by each molecule in the completed monolayer (the molecular cross-sectional area). In accordance with Eq. 7.6., the BET plot of $[p/n(p_0 - p)]$ against p/p_0 should be a straight line with slope $s = [(C - 1)/n_mC]$ and intercept $i = 1/n_m$. This is usually the case for a limited part of the adsorption isotherm. Within this limited range of validity of the BET equation, n_m and C can be obtained. For Type II or IV isotherms on such adsorbents as silicas, porous glass, aluminas, and nonporous amorphous carbons the usual range of linearity of the BET plot is $p/p_0 \approx 0.04$-0.25. The BET area S^{BET} can be calculated from the BET monlayer capacity n_m by:

$$S^{BET} = n_m \cdot N_A \cdot \sigma \qquad \text{Eq. 7.8.}$$

N_A...Avogadro constant ($6.022 \cdot 10^{23}$ mol^{-1})

σ...molecular cross-sectional area (0.162 nm^2 for nitrogen)

The Standard Isotherm Concept (t-Plots)[47]. Every adsorbate-adsorbent system yields a unique adsorption isotherm. Yet, a variety of materials of different total surface area but otherwise alike have isotherm curves of similar shape when analyzed with the same adsorptive at the same temperature. These isotherms can very nearly be superimposed simply by normalizing the vertical scale. This has led to the concept of 'standard' isotherms individually applicable to a specific group of materials in such categories a metal oxides, metals, graphite, metal halides, silicas and organosilicas. The standard isotherm concept led to a means for detecting the presence and determining the volume of micropores and mesopores, and quantifying the thickness of the adsorbed gas layer t on external surfaces and the walls of mesopores and macropores. It is recommended that the standard isotherm for a group of materials be established from data pertinent to a nonporous specimen from the group. Several methods have been introduced by which to normalize the adsorbed quantities of the reference and sample data sets. One is to convert each quantity adsorbed V to its equivalent fraction of monolayer capacity V_m, i.e. V/V_m, or, expressed in molar quantities, n/n_m. The value of n_m is obtained from relationships such as that of Eq. 7.8. (BET theory). For the t-plot of Lippins, Linsen and de Boer, the vertical axes of the standard and experimental isotherms are normalized in relation to the average thickness of the adsorbed layer. Thickness t is determined at any point on the isotherm by multiplying the fraction of monolayer capacity

V/V_m at that point by the thickness of the monolayer. If the thickness of a nitrogen monolayer t_m is taken to be 0.354 nm, the thickness of any adsorbed layer is:

$$t/nm = 0.354 \cdot (V/V_m)$$

Eq. 7.9.

For any value of thickness there is some value of V for both the standard and test materials. A plot of V vs. t is the t-plot and an idealized example is shown in Figure 7.4. Adsorption data for a nonporous material when plotted a V vs. t yields a straight line going through the origin. Figure 7.4. shows the t-plot of a typical SBA-15 material (templated with P123) containing micro- and mesopores which is exemplary for the materials synthesized in the course of this work. Extrapolation of the linear portion in Reg-2 to the adsorption axis gives a positive intercept equivalent to the micropore volume. The point at which capillary condensation in mesopores begins is revealed by the upward shift of the plot. As the mesopores are restricted to a narrow size range, linearity returns as adsorption continues with the (primary) mesopore volume being equivalent to the offset from the line extrapolated for the micropore volume determination.
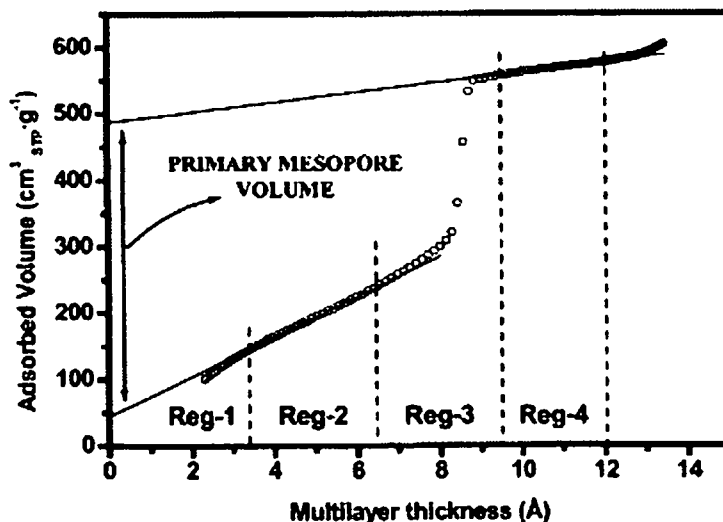
Figure 7.4. t-plot in the ranges of micro- and mesopores for a SBA-15 material calcined in air at 823 K.[60]

Thickness Equations. The initial intent in examining adsorbed layer thickness was to provide an accounting for the adsorbed layer on pore walls when calculating pore size distributions (e.g. by the BJH method) as described in the next section. The most generally applicable and most frequently employed are the methods of Harkins and Jura, Halsey and Broekhoff-de

Boer.[47] For this work the empirical Harkins-Jura multilayer thickness equation was being used which is determined for nonporous reference materials:

For a hydrophobic, non porous silica reference material (LiChrospher Si 1000 modified with octyldimethylsilyl groups):[157]

$$t/nm = 0.1[8.873/(0.08004 - \log(p/p_0)]^{0.6147}$$ Eq. 7.10.

and

for a pure non porous silica material (LiChrospher Si 1000):[158]

$$t/nm = 0.1[60.65/(0.03071 - \log(p/p_0))^{0.3968}$$ Eq. 7.11.

Computation of the Mesopore Size Distribution by the BJH Method[159]. A number of mathematical models, all relying on the application of the Kelvin equation, have been used to derive the mesopore size distribution from nitrogen sorption isotherms. The procedure for calculating pore size distributions using the Kelvin equation involves an imaginary emptying of condensed adsorptive in the pores in a stepwise manner as the relative pressure is likewise decreased. The mathematics of the technique is equally applicable whether following the adsorption branch of the isotherm downward from high to low pressure or following the desorption branch. One of the most popular of these 'classical' computational procedures is that proposed by Barrett, Joyner and Halenda, which is generally known as the BJH method. The BJH mesopore size distributions for this work were calculated applying the empirical Harkins-Jura multilayer thickness equations (see above).

Nitrogen adsorption-desorption isotherms were determined at 77 K using an adsorption porosimeter (Micromeritics, ASAP 2010/2020). Samples were outgassed for 6 h in the degas unit of the adsorption apparatus at 473 K under vacuum prior to analysis. The BET surface area was evaluated using adsorption data in a relative pressure range from 0.05-0.2 (S^{BET}). Pore volumes where estimated by the t-plot method, using the empirical Harkins-Jura multilayer thickness equation. The silica wall pore volumes (P^{wall}) have been calculated as the sum of micro- and small mesopores from the linear part of the t-plot in the region between 0.55-0.85 nm, the volume of the ordered mesopore-system (P^{meso}) from the region between 1.25-1.55 nm. The mesopore size distribution was calculated on the basis of adsorption or desorption branches using the BJH model, applying the Harkins-Jura multilayer thickness

equation (D^{BJH}). The pore wall thickness was calculated by $2d_{10}(SAXS)/\sqrt{3} - D^{BJH}$ for 2D hexagonal mesophases.

7.1.3. Mercury Porosimetry

Mercury porosimetry is a method for the characterization of porous structures in a pore size range between 3 nm and 0.4 mm. Informations about the pore size distribution, specific surface area and skeletal density can be obtained. Mercury porosimetry is based on the principle of capillary depression: applying pressure, a non wetting fluid (Hg) is forced into the pores. The relation between pressure p and pore size R is given by the Washburn Equation:

Washburn Equation:

$$p = -2 \cdot \sigma \cdot \cos\theta/R \qquad \text{Eq. 7.12.}$$

p...pressure

σ...surface tension of Hg (480 dyn/cm, 20° C)

R...pore radius

θ...contact angle (130°, 20° C)

With increasing pressure, smaller pores are being filled and the volume increase of mercury indruded is being determined. In this way, a pore volume distribution of the sample can be obtained. Measurement: under atmospheric pressure (ca. 0.1 MPa), pores with a radius >7.5 µm are filled with Hg. To be able to access also larger pores, measurements are carried out in a low pressure unit starting from vacuum conditions up to pressures of 0.3 MPa. Then, the sample vessel is transferred to a high pressure unit. Normally, intrusion and extrusion curves are determined, which, in general, show a deviation in form of a hysteresis due to: contact angle hysteresis (intrusion and extrusion contact angle are different), pore-blocking (bottleneck pores) and thermodynamic barriers in connection with Hg-extrusion.

Mercury-porosimetry was applied to determine the macropore volume (V^{Hg}) and macropore size distribution (Pascal 140/440 porosimeter), assuming a contact angle of 130° for the pore diameter (D^{Hg}) calculations.

7.1.4. Transmission - and Scanning Electron Microscopy (TEM and SEM)

Electron microscopy was applied in order to obtain information on the pore structure in the meso- and macropore range and on the morphology of the samples. The morphology of the monoliths was investigated by scanning electron microscopy (SEM), which was carried out on a JSM 6400 Jeol operating at 15kV or on a FEGSEM JEOL 6330 fitted with a secondary electron detector at an accelerating voltage of 10kV. Samples were coated with a 15 nm thick layer of Pt/Pd using an Agar High Resolution Sputter Coater. The transmission electron microscopy (TEM) investigations were performed on a JEOL 100 CX TEM with a tungsten filament operating at 100kV in the bright field mode. TEM on a Tecnai F20 operated at 200 kV).

7.1.5. Nuclear Magnetic Resonance (NMR) Spectroscopy (Solution, Solid State Magic Angle Spinning (MAS))

Solution. The ^{1}H-, ^{29}Si- and ^{13}C-NMR spectra of the liquid precursors were recorded on a Bruker DRX Avance 300 spectrometer at 300.13, 59.62, and 75.43 MHz, respectively. To get a better signal for the glycol-modified silane precursors ^{29}Si(H)-HMBC-NMR measurements were carried out.

Solid State. ^{29}Si MAS NMR spectroscopy was conducted in order to obtain additional information on the structure and crosslinking of the silica network and for the hybrid materials to obtain quantitative information of the extent of modification with organic moieties covalently linked to the silica network via Si-C bonds. The spectrum of amorphous silica exhibits three overlapping broad peaks with chemical shifts δ of -91, -101, -109 ppm. They represent framework Q^4, silanol Q^3, and disilanol Q^2 species (see Figure 7.5.). Broadness of the peaks attests to the non-crystalline structure. The inclusion of organosiloxane units T^m in the framework can be seen by the occurrence of an additional two to three overlapping broad peaks in the ^{29}Si NMR spectrum. Exchange of one Si-O bond for a Si-C bond (Q$\rightarrow$T silicon) causes a shift of approximately 45 ppm. The crosslinking parameters Q^n and T^m correspond to the structures $Si(OSi)_n(OR)_{4-n}$ (pure silica), $R'Si(OSi)_m(OR)_{3-m}$ (organo-silica hybrid networks) and mixed forms of these two (not fully substituted organo-silica hybrid networks), wherein R may be H or $CH_3/CH_2CH_3/CH_2CH_2OH$ and n=0-4 and m=0-3. M^1 units are found.

Si
|
O
|
Si—O—Si—O—R
|
O
|
R

Q^2

Si
|
O
|
Si—O—Si—O—R
|
O
|
Si

Q^3

Si
|
O
|
Si—O—Si—O—Si
|
O
|
Si

Q^4

Si
|
O
|
R'—Si—O—R
|
O
|
R

T^1

Si
|
O
|
R'—Si—O—Si
|
O
|
R

T^2

Si
|
O
|
R'—Si—O—Si
|
O
|
Si

T^3

R'
|
R'—Si—R'
|
O
|
Si

M^1
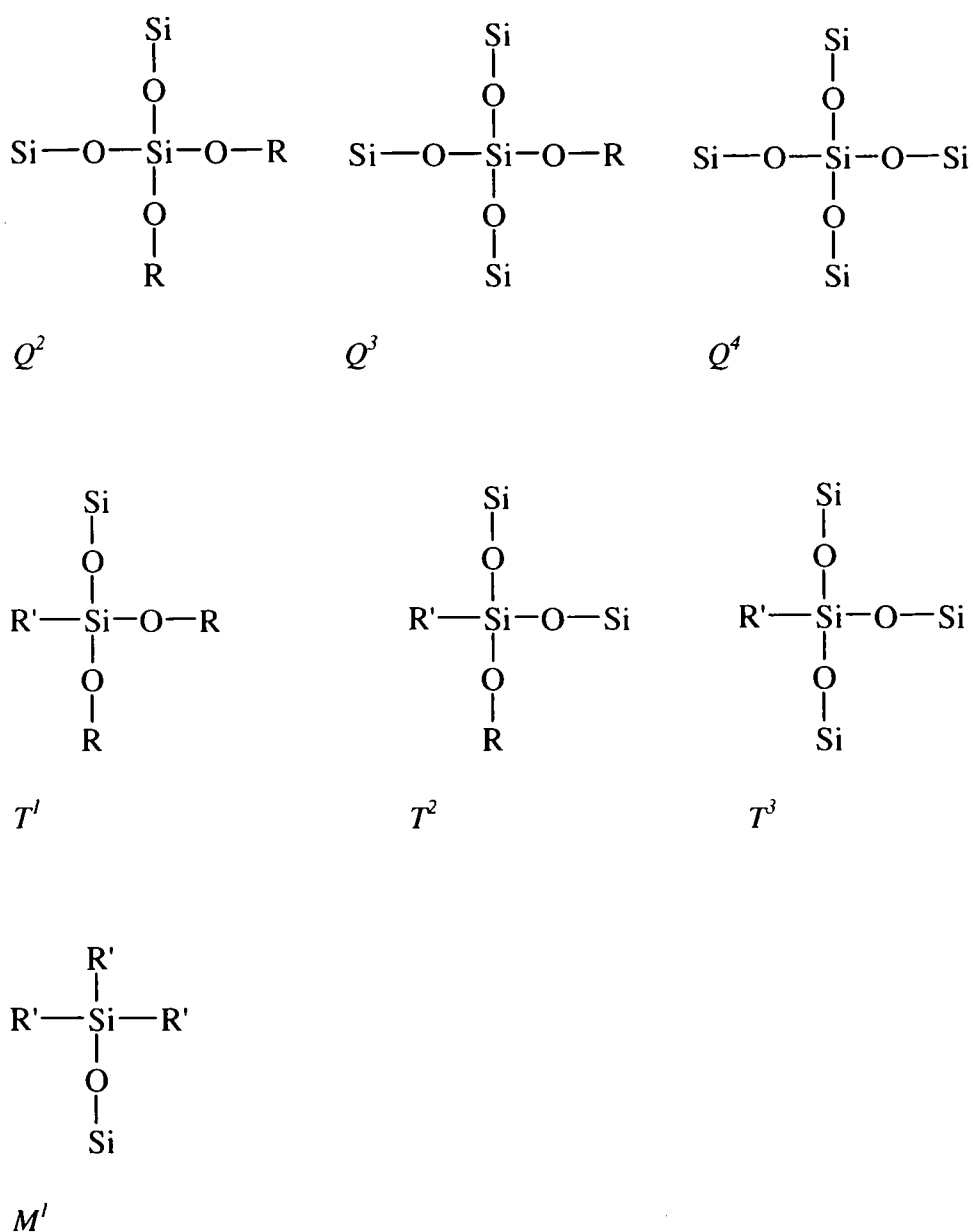
Figure 7.5. Silicon species relevant to this work.

After deconvolution and quantification of the peak areas the degree of condensation of the network can be calculated with the following formula:[160]

$$DC / \% = 100 \cdot \frac{[I(Q^4) + 0.75 \cdot I(Q^3) + 0.5 \cdot I(Q^2) + I(T^3) + 0.66 \cdot I(T^2) + 0.33 \cdot I(T^1)]}{\sum I(Q^n, T^m)} \qquad \text{Eq. 7.13.}$$

DC...degree of condensation of the network

I...area under each Q^n and T^m peak.

Surface loadings of surface silanized silica materials were calculated as amount of organic moieties per amount of SiO_2 (mmol·g^{-1}) and also as number of organic moieties per surface area determined by nitrogen sorption S^{BET} (n·nm^{-2}) according to the following formulas:

$$surface\,loading\,/\,mmol \cdot g^{-1} = 1000 \cdot \frac{I(M^1)}{\sum[I(Q^n) \cdot MW(SiO_2)]}$$ Eq. 7.14.

$$n\,/\,nm^2 = \frac{I(M^1) \cdot N_A}{S^{BET} \cdot 10^6 \cdot \sum I(X^y) \cdot \sum[I(X^y) \cdot MW(X^y)]}$$ Eq. 7.15.

Solid state ^{13}C cross polarizing (CP) MAS NMR spectroscopy was performed for further investigation of the chemical composition, e.g. concerning the presence of residual surfactant in the porous structure, methoxy units due to the methanol exchange before supercritical drying, and the presence and nature of the organic functional groups attached to the silica surface or incorporated into the silica framework.

The ^{13}C CP- and ^{29}Si CP/SP MAS NMR spectra were recorded at a spinning speed of 4 or 10 kHz on a Bruker DRX 300 spectrometer at 100.58 MHz (^{13}C) and 79.49 MHz (^{29}Si). For the ^{29}Si SP MAS NMR spectra a D1 delay of 300 s was applied.

7.1.6. Thermogravimetric Analysis

The composition of the surface modified gels was determined by elemental analyses of C,H,N, and S. The silicon content of the glycol-modified precursors and the composition of the wet, dried and calcined gels were determined by thermogravimetric analyses on a Netzsch TG 209 C in air with a heating ramp of 5 K/ min under a flow of synthetic air. The silicon content was calculated from the residual weight at 900° C which was assumed to be pure SiO_2.

7.1.7. Titration of Double Bonds and Amino Groups

Double bonds of mps and the aminogroups of aza were quantified by titrations analogous to methods described by Byrne[134] and Etienne[135], respectively.

Aminogroups were quantified by pH-metric titration with 0.01 M HCl using a pH-electrode. Monolithic samples were finely ground before titration, and typically 50 mg sample were suspended in 20 mL distilled water. The pH of this suspension was measured after allowing

30 min of equilibration. 1 mL HCl was added every 30 min, taking each point of the titration curve directly before addition of the next portion of HCl until a pH of ~2.5 was reached. The amount of amino groups was calculated from amount HCl consumed to reach the first equivalent point (pH 6.8). The second equivalent point (pH 3.9) corresponds to the protonation of Si-O⁻ (^+H_3NR) species. Surface loadings were calculated as amount of amino groups with respect to the SiO_2 content of the sample ($mmol \cdot g(SiO_2)^{-1}$). The SiO_2 content of the samples was determined by thermogravimetric analysis.

Doublebonds were quantified by reacting them with bromine and subsequent determination of the bromine consumption by iodometric titratration. For better statistics, the titration was carried out three times for each sample. Typically, 3 g NaBr and 0.2 g of finely ground sample or blind were placed in screw necked flasks. 10 mL of freshly prepared solution of Br_2 in methanol (0.4 M) was added and then stirred for 6 h. Unreacted Br_2 was then reduced by addition of KI solution (15 %) before titration with 0.0992 N Sodiumthiosulfate $Na_2S_2O_3$ solution until the yellow colour of I_2 vanished. The titration is based on the following reactions:

$$= \; + Br_2 \rightarrow \quad Br \diagup\hspace{-0.3em}\diagdown\hspace{-0.8em}\diagup Br$$

$$Br_2 + 2\,KI \rightarrow 2\,BrI + I_2$$

$$I_2 + 2\,Na_2S_2O_3 \rightarrow NaI + Na_2S_4O_6$$
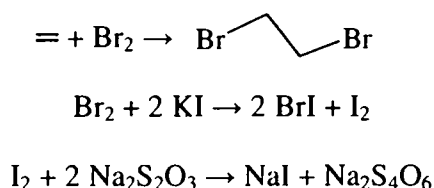
Contents of double bonds were calculated by subtraction of the amount $Na_2S_2O_3$ solution used for the sample titrations from the amount used for the blind, multiplication with the normality of the $Na_2S_2O_3$ solution (0.0992 N) and the stoichiometric factor (0.5). Surface loadings were calculated as amount of double bonds with respect to the SiO_2 content of the sample ($mmol \cdot g(SiO_2)^{-1}$). The SiO_2 content was determined by thermogravimetric analysis.

7.1.8. Elemental Analysis

The composition of the wet gels was determined by elemental analyses of C,H,N, and S in the Microanalytical Laboratory (University of Vienna).

7.2. Sample Preparation

7.2.1. Materials

Glycols: Ethylene glycol (EG, Aldrich), propane-1,2-diol (PG, Aldrich), and glycerol (GL, Acros), all termed glycols throughout this work, as modifying agents were purified by distillation from Na_2SO_4.

Surfactants: As the surfactant and phase separation agent Pluronic P123 (M_{av} = 5800), (ethylene oxide)EO_{20}(propylene oxide)PO_{70}(ethylene oxide)EO_{20} (BASF) was applied without any purification.

Silanes: As silanes, tetramethyl orthosilicate (TMOS), tetraethylorthosilicate (TEOS), trimethylchlorosilane (tmcs), mercaptopropyl-trimethoxysilane (mpts) (both from Fluka), methyltriethoxysilane (mtes), phenyltrimethoxysilane (ptms) (both from Aldrich), vinyldimethylchlorosilane (vdcs), (chloromethyl)dimethylchlorosilane (cdcs), 3-[(2,2-dimethyl-1-aza-2-silacyclopent-1-yl)dimethylsilyl]-1-propaneamine, a cyclic silazane (azas), (methylmethacryloyl) dimethylmethoxysilane (mmds), trimethylphenylsilane (tmps), 1,2-bis(triethoxysilyl)ethane (all from Wacker), were used without further purification. The α-aminoacid functional silane rac-3-(dimethyl(phenyl)silyl)alanineester (rac-34) used for surface modification of silica materials was synthesized in the laboratory of Prof. R. Tacke (University of Würzburg).

Synthesis of 1,4-bis(triethoxysilyl)benzene: 1,4-dibromobenzene (p.a., Merck) and Mg turnings (purum, for Grignard reactions, ≥99.5% , Aldrich) were used as received.

Silica Materials: As mesoporous reference material, Nucleosil® 100-10 (NUC), a spherical silica gel (10 μm) (Macherey-Nagel) was used as received. All other materials were synthesized according to the procedures described in this chapter.

7.2.2. Preparation of Glycol-Modified Silanes

Ethylene Glycol-, Propane-1,2-Diol-, Glycerol-Modified Silane (GlyMS).

Ethylene Glycol-Modified Methyl-, Phenyl, Ethylene-Bridged, Phenylene-Bridged Silane (OrEGMS).

Table 7.1. Glycol-modified silanes.

Notation	Silane	Glycol	Silane: glycol / mol	Si content (theor.) /wt%
EGMS	tetraethyl-orthosilicate	ethylene glycol	1 : 4	9.8 (10)
PGMS	tetraethyl-orthosilicate	propane-1,2-diol	1 : 4	7.5 (8.5)
GLMS	tetraethyl-orthosilicate	glycerol	1 : 4	7.7 (7.2)
MeGMS	methyltrimethoxysilane	ethylene glycol	1 : 3	8.4 (12.3)
PhGMS	phenyltriethoxysilane	ethylene glycol	1 : 3	9.6 (9.7)
bEtGMS	1,2-bis(triethoxysilyl)ethane	ethylene glycol	1 : 6	12 (12.5)
bPhGMS	1,4-bis(triethoxysilyl)benzene	ethylene glycol	1 : 6	11 (11)

For substitution of ethoxy- or methoxy groups with glycols, silane and glycol were reacted in a certain molar ratio in an argon atmosphere at 413 K according to the synthesis published by Mehrotra.[116] Ethanol or methanol, which is produced during the transesterification reaction was continuously removed by distillation over a Vigreux column. When no more progress in the reaction could be observed, excess of ethanol or methanol and unmodified silane was removed in vacuo. ^{29}Si(H)-HMBC-NMR investigations using CDCl$_3$ as solvent showed one peak at about -83 ppm (EGMS, PGMS, GLMS), -92 ppm (MeGMS), -109 ppm (PhGMS) indicative of a single Si-species. bEtGMS and bPhGMS could not be characterized by NMR due to their low solubility in any other solvent than alcohols or water.

1,4-Bis(triethoxysilyl)benzene was synthesized by Grignard reaction from 1,4-Dibrombenzene as described by Shea *et al.*[53] An Ar-purged three-necked round-bottomed flask with a stirrer bar and magnesium turnings (15 g, 0.62 mol) was flame-dried before adding TEOS (450 mL, 2 mol), dry tetrahydrofuran (THF, 250 mL), and a few crystals of iodine. The solution was brought to reflux (65 °C) and 1,4-dibromobenzene (48 g, 0.2 mol) in THF (125 mL) was added dropwise to the flask during a 2h period. This solution was allowed to reflux for another 1.5 h, becoming light yellow. Cooling to room temperature, THF was

removed by vacuum evaporation and about 200 mL petroleum ether was added to precipitate MgBr; it was removed by vacuum filtration. The liquor was condensed by rotary evaporation and subjected to vacuum distillation to remove excess TEOS (65 °C, 0.5 Torr). The product appeared as a colourless oil (35 g, recovered yield 43 %). ^{1}H NMR (300.13 MHz, CDCl$_3$/TMS, δ 7.67 (s, 4H), 3.85 (q, 12H), 1.24 (t, 18H). ^{13}C NMR (75.43 MHz, CDCl$_3$/TMS, δ 134.1, 133.3, 58.7, 18.1).

7.2.3. Preparation of Monolithic Gels

Hexagonal Mesophases Using P123: Variation of Composition, Glycol, and pH. Wet gels were prepared by adding EGMS, PGMS or GLMS to a homogenous mixture of P123 and aqueous HCl in the concentration range of 0-5 M, resulting in a composition (by weight fraction) of SiO$_2$/P123/HCl = 10-20/30/70. The mixture was homogenized for 1 min using a vortex stirrer. The liquid mixtures were allowed to gel in a closed PP cylinder at 313 K and the gels were kept at this temperature for 7 days for aging. The theoretical density of the final dry gels corresponds to approximately 0.07-0.1 gcm^{-3}. Gels are in the following denoted as GlyMSm(SiO$_2$), with GlyMS describing the type of glycol-modified silane used (EGMS, PGMS or GLMS) and m(SiO$_2$) being the weight fraction of SiO$_2$ in relation to P123/HCl = 30/70 which was kept constant.

Drying of the wet gel monoliths was performed by silanization of the whole monolith body with a solution of 10 wt% trimethylchlorosilane in petroleum ether for 24 h, leading to an immediate, visible extraction of the surfactant and aqueous pore liquid (see also chapter below, Surface modification and drying). After washing with petroleum ether (three times within 24 h) and ethanol (three times within 24 h), the wet gel bodies were dried by heating them to 200 °C (heating rate of 1 °C/h) at ambient pressure.

Table 7.2. Composition, pH and gelation times of gels prepared with EGMS

EGMS						
Sample	Composition / weight fractions				pH	Gelation
	Si (SiO₂)	P123	EG	H₂O		time /
E10	4.7 (10)	30	42	70	6	2
	"	"	"	"	3.5	3
	"	"	"	"	3.0	200
	"	"	"	"	2.5	260
	"	"	"	"	1.5	320
	"	"	"	"	1.0	180
	"	"	"	"	0.7	120
E13	6.1 (13)	"	55	"	2.5	255
E17	8.0 (17)	"	71	"	2.5	250
	"	"	"	"	1.0	120
	"	"	"	"	0.7	10
E20	9.4 (20)	"	84	"	2.5	245

Table 7.3. Composition, pH and gelation times of gels prepared with PGMS

PGMS						
Sample	Composition / weight fractions				pH	Gelation
	Si (SiO₂)	P123	PG	H₂O		time / min
P10	4.7 (10)	30	58	70	6	15
	"	"	"	"	3.5	18
	"	"	"	"	3.0	2000
	"	"	"	"	2.5	2500
	"	"	"	"	1.5	2600
	"	"	"	"	1.0	250
	"	"	"	"	0.7	150

Table 7.4. Composition, pH and gelation times of gels prepared with GLMS

GLMS						
Sample	Composition / weight fractions				pH	Gelation
	Si (SiO₂)	P123	PG	H₂O		time / min
G10	4.7 (10)	30	56	70	6	0.2
	"	"	"	"	3.5	0.5
	"	"	"	"	3.0	450
	"	"	"	"	2.5	480
	"	"	"	"	1.5	540
	"	"	"	"	1.0	250
	"	"	"	"	0.7	20

Preparation of Organosilica Monoliths with Hexagonal Mesophases Using P123: Variation of Organic Moietiy, Content of Organic Moieties and pH. Wet gels were prepared using Pluronic P123 as surfactant in the pH range from 0.7-8 (adjusted with HCl/NH_3). The organo-silanes were mixed with EGMS (except for bPhGMS) and added to aqueous LC-phases of P123, resulting in compositions (by mass) of $Si/P123/H_2O$ = 5.8-8.0/30/70. The substitution of EGMS with OrGMS is denoted as content of silicon resulting from OrGMS (Si^{Or}) and lies in the range of 10-100 mol%. Gels are in the following denoted as Orx with x being the degree of substitution with OrGMS in mol%. For gels prepared only from bEtGMS or bPhGMS at pH 2.5, the Si content was varied with $Si/P123/H_2O$ = 5.8, 7.0, 8.0/30/70. The gels are denoted as Or_a, b and c with decreasing Si content.

Drying and surfactant extraction was carried out by supercritical drying with carbon dioxide (see also chapter below, Surface modification and drying) or soft calcination (3 h at 350 °C, heating rate 1°/h up to 200 °C, 1°/min up to 350 °C).

Table 7.5. Composition, pH and gelation times of gels prepared with MeGMS and EGMS.

MeGMS							
Sample	Si^{Me} / mol%	Composition / weight fractions				pH	Gelation
		Si	P123	EG	H_2O		times / min
Me10	10	8.0	30	69	70	6	3
"	"	"	"	"	"	2.5	720
"	"	"	"	"	"	1	80
"	"	"	"	"	"	0.7	5
Me25	25	"	"	68	"	6.5	6
"	"	"	"	"	"	6	10
"	"	"	"	"	"	2.5	1050
Me50	50	"	"	66	"	6.5	6
"	"	"	"	"	"	6	60
"	"	"	"	"	"	2.5	2160*
Me75	75	"	"	64	"	6.5	60
"	"	"	"	"	"	6	120
"	"	"	"	"	"	2.5	2400*
Me100	100	"	"	62	"	8	45
						6.5	120
"	"	"	"	"	"	6	180
"	"	"	"	"	"	2.5	1440*

Table 7.6. Composition, pH and gelation times of gels prepared with PhGMS and EGMS.

PhGMS

Sample	Si^{Ph} / mol%	Composition / weight fractions				pH	Gelation
		Si	P123	EG	H_2O		times / min
Ph10	10	8.0	30	70	70	6.5	2
"	"	"	"	"	"	6	3
"	"	"	"	"	"	2.5	180
Ph25	25	"	"	67	"	6	3
"	"	"	"	"	"	2.5	660
Ph50	50	"	"	62	"	6.5	60*
"	"	"	"	"	"	6	180
"	"	"	"	"	"	2.5	-
Ph75	75	"	"	58	"	6.5	120*
"	"	"	"	"	"	6	360
"	"	"	"	"	"	2.5	-
Ph100	100	"	"	53	"	6.5	180*
"	"	"	"	"	"	6	420
"	"	"	"	"	"	2.5	-

*Precipitation instead of gelation

Table 7.7. Composition, pH and gelation times of gels prepared with bEtGMS and EGMS.

bEtGMS

Sample	Si^{bEt} / mol%	Composition / weight fractions				pH	Gelation
		Si	P123	EG	H_2O		times / min
bEt10	10	8.0	30	70	70	6	0
"	"	"	"	"	"	2.5	150
bEt25	25	"	"	67	"	6	0
"	"	"	"	"	"	2.5	300
bEt50	50	"	"	63	"	6	0
"	"	"	"	"	"	2.5	480
bEt75	75	"	"	58	"	6	0
"	"	"	"	"	"	2.5	900
bEt100	100	"	"	54	"	6	0
bEt c	"	"	"	"	"	2.5	2160
bEt b	"	7	"	47	"	"	"
bEt_a	"	5.8	"	39	"	"	"

Table 7.8. Composition, pH and gelation times of gels prepared with bPhGMS and EGMS.

bPhGMS							
Sample	Si^{bPh} / mol%	Composition / weight fractions				pH	Gelation
		Si	P123	EG	H_2O		times / min
bPh10	10	8.0	30	70	70	2.5	75
bPh25	25	"	"	67	"	"	120
bPh50	50	"	"	63	"	"	150
bPh75	75	"	"	58	"	"	210
bPh100	100	"	"	54	"	"	300
=bPh_c							
bPh_b	"	7	"	47	"	"	"
bPh_a	"	5.8	"	39	"	"	"

7.2.4. Surface Modification and Drying

Supercritical Drying with Carbon Dioxide vs. Ambient Pressure Drying after Surface Silylation with Trimethylchlorosilane. Drying of wet E10 gels prepared at pH 6 was performed by different routes:

a. Drying at ambient pressure by slowly heating the sample from room temperature to 150 °C for seven days. (samples TUW –d).

b. By extraction with ethanol or petroleum ether for eight times followed by careful heat treatment as described in a), (samples TUW –ed and –pd, respectively).

c. Via supercritical extraction: For supercritical drying with CO_2 (p_c=7.36 MPa, T_c=304 K) the pore liquid in the gel is exchanged to first methanol then to liquid CO_2. After complete solvent exchange, the material is heated in a closed pressure vessel to a temperature above the critical point with simultaneous increase of the pressure to prevent boiling (TUW –scf).

d. By treatment of the surface with trimethylchlorosilane (TUW –tms). Treatment with trimethylchlorosilane (tmcs) was performed by immersing the whole gel body in a tmcs/petroleum ether (1/10 w/w) solution for 10 hours. After washing with petroleum ether (three times) and ethanol (five times), the wet gel bodies were dried following the same procedure as for the untreated gels.

In addition, all gels were subjected to calcination at 450°C in air for three hours; these samples are denoted as –c.

Ambient Pressure Drying after Surface Silylation/Surfactant Extraction with Organofunctional Silanes. For the following set of experiments E17 gels prepared at pH 1 were used.

Surface silanization of the wet gel monoliths:

For chlorosilanes (trimethylchlorosilane (tms), vinyldimethyl)chlorosilane (vdcs), (chloromethyl)dimethylchlorosilane (cdcs)) the wet gels were reacted by immersing the whole monolith body in a solution of 10 wt% of the silane in petroleum ether (PE) for 24 h, and then washed with petroleum ether (three times within 12 h) and ethanol (five times within 24 h) to remove unreacted silane species.

For organo-alkoxysilanes (phs, mps, mms), the wet gels were reacted directly by immersing the whole monolith body in pure silane for 24 h, and then washed with ethanol (eight times within 48 h) to remove unreacted silane species.

For 3-[(2,2-dimethyl-1-aza-2-silacyclopent-1-yl)dimethylsilyl]-1-propanamine (aza), the wet silica gels were immersed in a 10^{-3} M NH_3 solution, the NH_3 concentration was increased up to 1 M within a period of 12 h, and the gels washed with water for three times within 12 h to convert aminohydrochloride-groups to free aminogroups. Silylation was done by treating the monoliths with a solution of 3 wt% aza in PE for 24 h and subsequent washing with PE (three times within 12 h) and ethanol (five times within 36 h) to remove unreacted silane species.

Drying: All surface modified samples were dried by vacuum evaporation of the solvent at 60 °C.

Amino Acid Surface-functionalisation of Different Silica Model Materials with rac-3-(dimethylphenylsilyl)alaninethylester (rac-34).

Synthesis of monolithic silica gels:

Aerogel *(AER):* Tetramethyl-orthosilicate, methanol, and 0.01 M NH_3 were mixed in a ratio (by weight) of 53:21.5:25.5. The liquid mixture was stirred for 30min and then kept in closed PP-cylinders (∅ 1.25 cm, l 3.5 cm) for gelation (3 h) and aging (7 days) at 40 °C. The theoretical density of the final gels corresponds to 0.20 g cm^{-3}.

Gels with hierarchical build-up *(E17):* Wet gels were prepared by adding EGMS to a homogenous mixture of P123 and 1 M HCl, resulting in a composition (by mass) of SiO_2/P123/HCl = 17/30/70 assuming complete conversion of EGMS to silica. The mixture

was homogenized for 1 min using a vortex stirrer and allowed to gel closed PP cylinders (∅ 1.25 cm, l 3.5 cm) at 40 °C and the gels were kept at this temperature for 7 days after gelation for aging. The theoretical density of the final gels corresponds to $0.10\ \mathrm{g\ cm^{-3}}$.

Functionalization:

Nucleosil *(NUC)*

NUC_ala: NUC (1.14 g) was modified with rac-34 (0.44 g, 1.75 mmol) by hydrolysing the ester of the aminoacid-functionality and the phenylsilyl moiety with 10 mL 6 *M* HCl under reflux for 2h. After cooling to room temperature the solvent was removed under reduced pressure. 5 mL of ethanol and 5 mL of propyleneoxide were added to the solid, and the mixture heated under reflux for 10 min. The residual solid was separated by centrifugation and washed twice each with 5 mL ethanol, and twice each with 5 mL diethylether. The solid powder was dried at 60 °C under a vacuum of 10^{-2} mbar.

NUC_blind and *NUC_tmps:* for comparative purposes, NUC was treated exactly like NUC_ala without the presence of rac-34 *(NUC_blind)*, and with trimethylphenylsilane instead of rac-34 *(NUC_tmps)*, respectively.

Monoliths *(AER* and *E17)*

Considering the monolithic structure of the silica gels, some changes of the functionalization procedure had to be made: first, the times of modification and washing steps were increased, second, solvent evaporation from the monolithic gel body during the modification procedure was avoided by using larger liquid volumes and by removing liquid phases only by decanting instead of evaporation. Finally, supercritical drying with carbon dioxide was implemented to avoid collapse of the porous structure of the *AER*-samples. For supercritical drying (scf) with CO_2 (p_c=7.36 MPa, T_c=304 K) the pore liquid in the gels was exchanged to first methanol then to liquid CO_2. After complete solvent exchange, the materials were heated in a closed pressure vessel to a temperature above the critical point with simultaneous increase of the pressure to prevent boiling. For samples *E17*, supercritical drying was not necessary and the monolithic gels were simply dried as described for *NUC_ala* at 60° C under a vacuum of 10^{-2} mbar.

AER_ala and *E17as_ala*: A mixture of 5.43 g wet gel *AER* or 11.4 g wet gel *E17* (corresponding to 1.14 g SiO_2), 0.440 g rac-34, and 30 mL 6 *M* HCl were heated under reflux for 24 h (*AER/E17as_ala*), respectively. After cooling to room temperature, the liquid phase was decanted and the solid washed three times with each 15 mL of ethanol at intervals of 1 h. Subsequently, 15 mL ethanol and 15 mL propyleneoxide were added to the remaining gel and the resulting mixture heated under reflux for 12 h. The liquid phase was decanted and the gels washed twice each with 15 mL ethanol, and twice each with 15 mL diethylether, all steps at intervals of 1 h.

E17ex_ala: To investigate the effect of the presence of surfactant in the mesopores of samples E17 on the efficiency of surface modification an *E17* gel was surfactant-extracted by treatment with acidic ethanol before the above described modification treatment. For this purpose, the wet gel was refluxed for 12 h with a mixture of 15 mL ethanol and 15 mL 12 *M* HCl, renewing the acidic ethanol mixture after 6h. After cooling to room temperature, the gel was washed three times each with 15 mL of 6 *M* HCl at intervals of 1 h. Modification and drying was implemented as described for sample *E17as_ala*.

AER_scf: As reference for the structural and chemical composition of AER, a wet gel *AER* was supercritically dried with carbon dioxide as described above.

E17_tms: As reference for the structural and chemical composition of *E17*, a sample treated with trimethylchlorosilane was chosen, a process that has already been studied intensively by our group for this material. Wet gels were reacted by immsersing the whole monolith body in a solution of 10 wt% of the silane in petroleum ether (PE) for 24 h, and then washed with petroleum ether (three times within 12 h) and ethanol (five times within 24 h) to remove unreacted silane species. Drying was implemented as described for sample *NUC_ala* at 60° C under a vacuum of 10^{-2} mbar.

7.2.5. Testing of the E17 Monolith as Column Material for High Performance Liquid Chromatography (HPLC)

Wet gels were prepared by adding EGMS to a homogenous mixture of P123 and aqueous HCl (1 M), resulting in a composition (by weight fraction) of SiO_2/P123/HCl = 17/30/70. The mixture was homogenized for 1 min using a vortex stirrer. The mixture was centrifuged at low speed for 1-2 min to remove bubbles from the liquid. The liquid mixture was allowed to

gel in a closed PMMA cylinder ($\varnothing$ = 0.62 cm, l = 15 cm) at 313 K and the gels were kept at this temperature for 5 days for aging. The theoretical density of the final dry gels corresponds to approximately 0.1 $g \cdot cm^{-3}$. To increase the mechanical stability of the gels, the gels were refluxed in an ethanol/HCl_{conc} (1/1 v/v) solution for 10 hours. After washing with ethanol (three times) and petroleum ether (three times) the wet monoliths were silanized with trimethylchlorosilane (tmcs) by immersing them in a tmcs/petroleum ether (1/10 w/w) solution for 10 hours. After washing with petroleum ether (three times) and ethanol (five times), the wet gel bodies were dried at ambient pressure by slowly heating the sample from room temperature to 200 °C within seven days. This way, crack free monoliths with a density of 0.2 $g \cdot cm^{-3}$ and linear shrinkage (with respect to the diameter of the PMMA cylinder) of 13 % were obtained.

These monoliths were tested as columns for HPLC in collaboration with an industrial partner.

8 Conclusions

This work presents the sol-gel synthesis of a new type of monolithic meso- and macroporous silica and organosilica materials with a structural organization on several hierarchical levels from the molecular to the macroworld:

Molecular Level   Integrating organic functionality into the amorphous silica framework either distributed within the silica network or grafted onto the surface.

Nanometer Level   Periodically ordered mesopore-system in the fashion of SBA-materials.

Micrometer Level   Macroporous framework.

Millimeter Level   Monolithic shape.

The novel aspect of this work is the highly periodic arrangement of the mesopores embedded within macroporous scaffolds with different morphologies and macropore sizes, and especially the fact that monolithic materials can be prepared. Furthermore, the surface- and also the network chemistry of the materials was modified with a wide range of organic functionalities.

This was achieved by using a new type of precursor – glycolate-substituted tetraalkoxysilanes and organo(-bridged)trialkoxysilanes – in a true liquid-crystal templating (TLCT) approach with the non-ionic poly(ethylene oxide)-based block copolymeric surfactant P123 in aqueous (neutral) and acidic conditions. In particular, ethylene glycol, propylene glycol and glycerol substituted tetraalkoxysilane and ethylene glycol substituted methyl-, phenyl-, ethylene-bridged and phenylene-bridged trialkoxysilane, were applied. The macroscopic gel morphology and periodic ordering of the mesopore structure can be significantly influenced by the choice of pH, organic functionality (type and content) and the Si/P123 ratio. For each system, the optimal synthesis parameters have to be fine-tuned to get optimal results with respect to long-range periodicity of the mesostructure.

The advantage of the new precursors is based on the additional –OH functionality and therefore higher hydrophilicity of the glycols compared to the – for alkoxysilanes – conventional monoalcohols like methanol and ethanol. Two for this work important consequences are 1) the high water-solubilty of the glycolate-substituted (organo-) silanes and 2) the exceptional compatibility of the glycols with lyotropic surfactant phases in water, both

in contrast to the conventional alkoxysilanes. The water-soluble glycol-modified derivatives can be processed without co-solvents, even under neutral conditions (no catalyst is required to start the sol-gel reactions) and periodic mesostructures can be obtained without the addition of swelling agents such as 1,3,5-trimethylbenzene, making the synthesis of hierarchically structured silica and also organosilica monoliths a facile, rapid and environmentally benign process. The presented materials have great potential for several applications e.g. chromatographic or separation purposes, support materials or catalysis. The potential of application of a material developed in the course of this work as stationary phase for high performance liquid chromatography (HPLC) has been tested in cooperation with an industrial partner and showed first, promising results.

Another topic presented in this work is the processing and chemical modification of the wet, as synthesized monolithic (organo-)silica gels. In order to remove the template and pore fluid from the porous structure while preserving the monolith shape and organic moieties (in case of organosilica materials), several methods have been investigated and developed.

Simple heat treatment at 350-450 °C (calcination) to evaporate the pore fluid and combust the organic mesopore-template is the easiest method and can only be applied for the pure silica materials, as it leads to oxidative cleavage of Si-C bonds of the organosilica hybrid frameworks. The meso- and macroporous structure and also the monolithic shape can be maintained, but only in association with a high shrinkage.

Lower shrinkage can be achieved by supercritical drying with carbon dioxide. By this method, also the mesopore-template is extracted with an efficiency of up to 96 %. Furthermore, it can be applied to all organosilica materials presented in this work, including the materials modified with alaninedimethylsilyl-functionality. Calcination of the supercritically dried materials leads to complete template removal and a much lower shrinkage than simple drying and calcination.

As an alternative to supercritical drying, which is an expensive and time consuming technique, an ambient pressure drying technique relying on a simple surface modification treatment with trimethylchlorosilane was developed. Silylation with trimethylchlorosilanes allowed to simultaneously extract the templating agent from the wet gel monoliths and facilitate simple drying at ambient pressure of the large monoliths. Very good results i.e. low shrinkage, high template extraction, high integrity of the porous structure and low shrinkage

upon calcination were obtained by this method. Furthermore, this method was successfully extended to a variety of organofunctional silanes such as 3-mercaptopropyltrimethoxysilane, phenyltrimethoxysilane, 3-[(2,2-dimethyl-1-aza-2-silacyclopent-1-yl)dimethylsilyl]-1-propane amine, a cyclic silazane resulting in aminopropyldimethylsilyl groups on the silica surface, and (methylmethacryloyl) dimethylmethoxysilane. The post-synthesis surface modification procedure does not only reduce the number of synthetic steps in the synthesis of functional mesoscopically organized silica monoliths, since it combines three processing steps into one, such as surface functionalisation resulting in high surface loadings, extraction of the template and facilitation of drying, but also opens access to a wide range of ordered hybrid inorganic-organic monolithic frameworks.

A novel amino acid-functional silane (rac-3-(dimethyl(phenyl)silyl)alanineester) has been successfully applied to modify various porous silica model materials with alanine-dimethyl silyl groups. The phenylsilyl moiety of this molecule showed a high reactivity towards acidic hydrolysis to form a silanol group which could be used for covalent coupling to silica surfaces yielding high surface coverages with amino acid functionality. The different porous structures were completely retained during the process of functionalization via grafting to the intrachannel hydroxyls. Again, this post-synthesis modification procedure did not only lead to surface functionalization, but also surfactant extraction from a templated material was achieved. Furthermore, it facilitates drying and increases the mechanical strength of monoliths with a bimodal pore structure.

In summary, this work presents the synthesis, characterization and application of hierarchically structured (organo-) silica monoliths starting from the synthesis of specifically designed molecular precursors via the monolith preparation by TLCT, monolith processing and modification of the surface chemistry to the prospect of application of the materials as stationary phase in HPLC.

9 References

1.   Mann, S. *Biomineralization: Principles and Concepts in Bioinorganic Materials Chemistry* (2002).

2.   Mann, S. & Editor. *Biomimetic Materials Chemistry* (1996).

3.   Mann, S., Webb, J., Williams, R. J. P. & Editors. *Biomineralization. Chemical and Biochemical Perspectives* (1989).

4.   Yang, P., Rizvi, A. H., Messer, B., Chmelka, B. F., Whitesides, G. M. & Stucky, G. D. Patterning porous oxides within microchannel networks. *Advanced Materials (Weinheim, Germany)* **13**, 427-431 (2001).

5.   Shenton, W., Pum, D., Sleytr, U. B. & Mann, S. Synthesis of cadmium sulfide superlattices using self-assembled bacterial S-layers. *Nature (London)* **389**, 585-587 (1997).

6.   Murray, C. B., Kagan, C. R. & Bawendi, M. G. Self-organization of CdSe nanocrystallites into three-dimensional quantum dot superlattices. *Science (Washington, D. C.)* **270**, 1335-8 (1995).

7.   Wang, Z. L. Structural analysis of self-assembling nanocrystal superlattices. *Advanced Materials (Weinheim, Germany)* **10**, 13-30 (1998).

8.   Andres, R. P., Bein, T., Dorogi, M., Feng, S., Henderson, J. I., Kubiak, C. P., Mahoney, W., Osifchin, R. G. & Reifenberger, R. \"Coulomb staircase\" at room temperature in a self-assembled molecular nanostructure. *Science (Washington, D. C.)* **272**, 1323-1325 (1996).

9.   Galow, T. H., Boal, A. K. & Rotello, V. M. A \"building block\" approach to mixed-colloid systems through electrostatic self-organization. *Advanced Materials (Weinheim, Germany)* **12**, 576-579 (2000).

10.   Mirkin, C. A., Letsinger, R. L., Mucic, R. C. & Storhoff, J. J. A DNA-based method for rationally assembling nanoparticles into macroscopic materials. *Nature (London)* **382**, 607-609 (1996).

11. Mann, S., Shenton, W., Li, M., Connolly, S. & Fitzmaurice, D. Biologically programmed nanoparticle assembly. *Advanced Materials (Weinheim, Germany)* **12**, 147-150 (2000).

12. Sanchez, C., Arribart, H., Madeleine, M. & Guille, G. Biomimetism and bioinspiration as tools for the design of innovative materials and systems. *Nature Materials* **4**, 277-288 (2005).

13. Brinker, C. & Scherer, G. *Sol-Gel Science: The Physics and Chemistry of Sol-Gel Processing* (1990).

14. Beck, J. S., Vartuli, J. C., Roth, W. J., Leonowicz, M. E., Kresge, C. T., Schmitt, K. D., Chu, C. T. W., Olson, D. H., Sheppard, E. W. & et al. A new family of mesoporous molecular sieves prepared with liquid crystal templates. *Journal of the American Chemical Society* **114**, 10834-43 (1992).

15. Asefa, T., MacLachlan, M. J., Coombs, N. & Ozin, G. A. Periodic mesoporous organosilicas with organic groups inside the channel walls. *Nature (London)* **402**, 867-871 (1999).

16. Brinker, C. J., Lu, Y., Sellinger, A. & Fan, H. Evaporation-induced self-assembly. Nanostructures made easy. *Advanced Materials (Weinheim, Germany)* **11**, 579-585 (1999).

17. Yoshina-Ishii, C., Asefa, T., Coombs, N., MacLachlan, M. J. & Ozin, G. A. Periodic mesoporous organosilicas, PMOs: fusion of organic and inorganic chemistry 'inside' the channel walls of hexagonal mesoporous silica. *Chemical Communications (Cambridge)*, 2539-2540 (1999).

18. Inagaki, S., Guan, S., Fukushima, Y., Ohsuna, T. & Terasaki, O. Novel Mesoporous Materials with a Uniform Distribution of Organic Groups and Inorganic Oxide in Their Frameworks. *Journal of the American Chemical Society* **121**, 9611-9614 (1999).

19. Zhao, D., Huo, Q., Feng, J., Chmelka, B. F. & Stucky, G. D. Nonionic triblock and star diblock copolymer and oligomeric surfactant syntheses of highly ordered, hydrothermally stable, mesoporous silica structures. *Journal of the American Chemical Society* **120**, 6024-6036 (1998).

20. Bagshaw, S. A., Prouzet, E. & Pinnavaia, T. J. Templating of mesoporous molecular sieves by nonionic polyethylene oxide surfactants. *Science (Washington, D. C.)* **269**, 1242-4 (1995).

21. Brandhuber, D., Torma, V., Raab, C., Peterlik, H., Kulak, A. & Huesing, N. Glycol-Modified Silanes in the Synthesis of Mesoscopically Organized Silica Monoliths with Hierarchical Porosity. *Chemistry of Materials* **17**, 4262-4271 (2005).

22. Landskron, K. & Ozin, G. A. Periodic mesoporous dendrisilicas. *Science (Washington, DC, United States)* **306**, 1529-1532 (2004).

23. Yu, C., Fan, J., Tian, B., Zhao, D. & Stucky, G. D. High-yield synthesis of periodic mesoporous silica rods and their replication to mesoporous carbon rods. *Advanced Materials (Weinheim, Germany)* **14**, 1742-1745 (2002).

24. Attard, G. S., Glyde, J. C. & Goltner, C. G. Liquid-crystalline phases as templates for the synthesis of mesoporous silica. *Nature (London)* **378**, 366-8 (1995).

25. Amatani, T., Nakanishi, K., Hirao, K. & Kodaira, T. Monolithic Periodic Mesoporous Silica with Well-Defined Macropores. *Chemistry of Materials* **17**, 2114-2119 (2005).

26. Nakanishi, K., Kobayashi, Y., Amatani, T., Hirao, K. & Kodaira, T. Spontaneous Formation of Hierarchical Macro-Mesoporous Ethane-Silica Monolith. *Chemistry of Materials* **16**, 3652-3658 (2004).

27. Smtt, J.-H., Schunk, S. & Linden, M. Versatile Double-Templating Synthesis Route to Silica Monoliths Exhibiting a Multimodal Hierarchical Porosity. *Chemistry of Materials* **15**, 2354-2361 (2003).

28. Coppens, M. O., Sun, J. & Maschmeyer, T. Synthesis of hierarchical porous silicas with a controlled pore size distribution at various length scales. *Catalysis Today* **69**, 331-335 (2001).

29. Nakanishi, K. Porous gels made by phase separation: recent progress and future directions. *Journal of Sol-Gel Science and Technology* **19**, 65-70 (2000).

30. Nakanishi, K. Pore structure control of silica gels based on phase separation. *Journal of Porous Materials* **4**, 67-112 (1997).

31. Zhao, D., Feng, J., Huo, Q., Melosh, N., Frederickson, G. H., Chmelka, B. F. & Stucky, G. D. Triblock copolymer syntheses of mesoporous silica with periodic 50 to 300 angstrom pores. *Science (Washington, D. C.)* **279**, 548-552 (1998).

32. Antochshuk, V. & Jaroniec, M. Functionalized Mesoporous Materials Obtained via Interfacial Reactions in Self-Assembled Silica-Surfactant Systems. *Chemistry of Materials* **12**, 2496-2501 (2000).

33. Antochshuk, V. & Jaroniec, M. Simultaneous modification of mesopores and extraction of template molecules from MCM-41 with trialkylchlorosilanes. *Chemical Communications (Cambridge)*, 2373-2374 (1999).

34. Antochshuk, V. & Jaroniec, M. Adsorption, Thermogravimetric, and NMR Studies of FSM-16 Material Functionalized with Alkylmonochlorosilanes. *Journal of Physical Chemistry B* **103**, 6252-6261 (1999).

35. Ballard, C. P. & Fanelli, A. J. Sol-gel route for materials synthesis. *Chem. Adv. Mater.*, 1-17 (1993).

36. Hench, L. L. & West, J. K. The sol-gel process. *Chemical Reviews (Washington, DC, United States)* **90**, 33-72 (1990).

37. Zelinski, B. J. J., Brinker, C. J., Clark, D. E., Ulrich, D. R. & Editors. *Materials Research Society Symposium Proceedings, Vol. 180: Better Ceramics Through Chemistry IV. Symposium Held April 16-20, 1990, San Francisco, Calif., U.S.A* (1990).

38. Iler, R. K. *The Chemistry of Silica: Solubility, Polymerization, Colloid and Surface Properties and Biochemistry* (1979).

39. Morse, D. E. Silicon biotechnology: harnessing biological silica production to construct new materials. *Trends in Biotechnology* **17**, 230-232 (1999).

40. Vrieling, E. G., Beelen, T. P. M., van Santen, R. A. & Gieskes, W. W. C. Diatom silicon biomineralization as an inspirational source of new approaches to silica production. *Journal of Biotechnology* **70**, 39-51 (1999).

41. Mann, S. Biomineralization and biomimetic materials chemistry. *Journal of Materials Chemistry* **5**, 935-46 (1995).

42.   Cha, J. N., Stucky, G. D., Morse, D. E. & Deming, T. J. Biomimetic synthesis of ordered silica structures mediated by block copolypeptides. *Nature (London)* **403**, 289-292 (2000).

43.   Husing, N. & Schubert, U. Porous inorganic-organic hybrid materials. *Functional Hybrid Materials*, 86-121 (2004).

44.   Rao, A. V., Kulkarni, M. M., Amalnerkar, D. P. & Seth, T. Surface chemical modification of silica aerogels using various alkyl-alkoxy/chloro silanes. *Applied Surface Science* **206**, 262-270 (2003).

45.   Huesing, N., Schubert, U., Misof, K. & Fratzl, P. Formation and Structure of Porous Gel Networks from Si(OMe)4 in the Presence of A(CH2)nSi(OR)3 (A = Functional Group). *Chemistry of Materials* **10**, 3024-3032 (1998).

46.   Huesing, N., Schubert, U., Mezei, R., Fratzl, P., Riegel, B., Kiefer, W., Kohler, D. & Mader, W. Formation and Structure of Gel Networks from Si(OEt)4/(MeO)3Si(CH2)3NR'2 Mixtures (NR'2 = NH2 or NHCH2CH2NH2). *Chemistry of Materials* **11**, 451-457 (1999).

47.   Schuth, F., Sing, K. S. W. & Weitkamp, J. *Handbook of Porous Solids* (2002).

48.   Comez-Romero, P., Sanchez, C. & Editors. *Functional Hybrid Materials* (2004).

49.   Moller, K. & Bein, T. Inclusion Chemistry in Periodic Mesoporous Hosts. *Chemistry of Materials* **10**, 2950-2963 (1998).

50.   Burkett, S. L., Sims, S. D. & Mann, S. Synthesis of hybrid inorganic-organic mesoporous silica by co-condensation of siloxane and organosiloxane precursors. *Chemical Communications (Cambridge)*, 1367-1368 (1996).

51.   Fowler, C. E., Burkett, S. L. & Mann, S. Synthesis and characterization of ordered organosilica-surfactant mesophases with functionalized MCM-41-type architecture. *Chemical Communications (Cambridge)*, 1769-1770 (1997).

52.   Husing, N. & Schubert, U. Organofunctional silica aerogels. *Journal of Sol-Gel Science and Technology* **8**, 807-812 (1997).

53.   Shea, K. J., Loy, D. A. & Webster, O. Arylsilsesquioxane gels and related materials. New hybrids of organic and inorganic networks. *Journal of the American Chemical Society* **114**, 6700-10 (1992).

54. Shea, K. J., Moreau, J., Loy, D. A., Corriu, R. J. P. & Boury, B. Bridged polysilsesquioxanes. Molecular-engineering nanostructured hybrid organic-inorganic materials. *Functional Hybrid Materials*, 50-85 (2004).

55. Schwertfeger, F., Glaubitt, W. & Schubert, U. Hydrophobic aerogels from tetramethoxysilane/methyltrimethoxysilane mixtures. *Journal of Non-Crystalline Solids* **145**, 85-9 (1992).

56. Schwertfeger, F., Huesing, N. & Schubert, U. Influence of the nature of organic groups on the properties of organically modified silica aerogels. *Journal of Sol-Gel Science and Technology* **2**, 103-8 (1994).

57. Inagaki, S., Fukushima, Y. & Kuroda, K. Synthesis of highly ordered mesoporous materials from a layered polysilicate. *Journal of the Chemical Society, Chemical Communications*, 680-2 (1993).

58. Flodstroem, K., Teixeira, C. V., Amenitsch, H., Alfredsson, V. & Linden, M. In Situ Synchrotron Small-Angle X-ray Scattering/X-ray Diffraction Study of the Formation of SBA-15 Mesoporous Silica. *Langmuir* **20**, 4885-4891 (2004).

59. Huesing, N., Raab, C., Torma, V., Roig, A. & Peterlik, H. Periodically Mesostructured Silica Monoliths from Diol-Modified Silanes. *Chemistry of Materials* **15**, 2690-2692 (2003).

60. Van Grieken, R., Calleja, G., Stucky, G. D., Melero, J. A., Garcia, R. A. & Iglesias, J. Supercritical Fluid Extraction of a Nonionic Surfactant Template from SBA-15 Materials and Consequences on the Porous Structure. *Langmuir* **19**, 3966-3973 (2003).

61. Miyazawa, K. & Inagaki, S. Control of the microporosity within the pore walls of ordered mesoporous silica SBA-15. *Chemical Communications (Cambridge)*, 2121-2122 (2000).

62. Zhao, D., Sun, J., Li, Q. & Stucky, G. D. Morphological Control of Highly Ordered Mesoporous Silica SBA-15. *Chemistry of Materials* **12**, 275-279 (2000).

63. Kruk, M., Jaroniec, M., Ko, C. H. & Ryoo, R. Characterization of the Porous Structure of SBA-15. *Chemistry of Materials* **12**, 1961-1968 (2000).

64. Ryoo, R., Ko, C. H., Kruk, M., Antochshuk, V. & Jaroniec, M. Block-Copolymer-Templated Ordered Mesoporous Silica: Array of Uniform Mesopores or Mesopore-Micropore Network? *Journal of Physical Chemistry B* **104**, 11465-11471 (2000).

65. Yang, P., Zhao, D., Chmelka, B. F. & Stucky, G. D. Triblock-Copolymer-Directed Syntheses of Large-Pore Mesoporous Silica Fibers. *Chemistry of Materials* **10**, 2033-2036 (1998).

66. Kipkemboi, P., Fogden, A., Alfredsson, V. & Flodstroem, K. Triblock Copolymers as Templates in Mesoporous Silica Formation: Structural Dependence on Polymer Chain Length and Synthesis Temperature. *Langmuir* **17**, 5398-5402 (2001).

67. Flodstroem, K., Alfredsson, V. & Kaellrot, N. Formation of a New Ia.hivin.3d Cubic Meso-Structured Silica via Triblock Copolymer-Assisted Synthesis. *Journal of the American Chemical Society* **125**, 4402-4403 (2003).

68. Kleitz, F., Choi, S. H. & Ryoo, R. Cubic Ia3d large mesoporous silica: synthesis and replication to platinum nanowires, carbon nanorods and carbon nanotubes. *Chemical Communications (Cambridge, United Kingdom)*, 2136-2137 (2003).

69. Matos, J. R., Kruk, M., Mercuri, L. P., Jaroniec, M., Zhao, L., Kamiyama, T., Terasaki, O., Pinnavaia, T. J. & Liu, Y. Ordered Mesoporous Silica with Large Cage-Like Pores: Structural Identification and Pore Connectivity Design by Controlling the Synthesis Temperature and Time. *Journal of the American Chemical Society* **125**, 821-829 (2003).

70. Liu, X., Tian, B., Yu, C., Gao, F., Xie, S., Tu, B., Che, R., Peng, L.-M. & Zhao, D. Room-temperature synthesis in acidic media of large-pore three-dimensional bicontinuous mesoporous silica with Ia3d symmetry. *Angewandte Chemie, International Edition* **41**, 3876-3878 (2002).

71. Goeltner, C. G., Smarsly, B., Berton, B. & Antonietti, M. On the Microporous Nature of Mesoporous Molecular Sieves. *Chemistry of Materials* **13**, 1617-1624 (2001).

72. Lu, Y., Ganguli, R., Drewien, C. A., Anderson, M. T., Brinker, C. J., Gong, W., Guo, Y., Soyez, H., Dunn, B., Huang, M. H. & Zink, J. I. Continuous formation of supported cubic and hexagonal mesoporous films by sol-gel dip-coating. *Nature (London)* **389**, 364-368 (1997).

73. El-Safty, S. A. & Hanaoka, T. Monolithic nanostructured silicate family templated by lyotropic liquid-crystalline nonionic surfactant mesophases. *Chemistry of Materials* **15**, 2892-2902 (2003).

74. Melosh, N. A., Davidson, P. & Chmelka, B. F. Monolithic mesophase silica with large ordering domains. *Journal of the American Chemical Society* **122**, 823-829 (2000).

75. Kapoor, M. P., Yang, Q. & Inagaki, S. Organization of Phenylene-Bridged Hybrid Mesoporous Silisesquioxane with a Crystal-like Pore Wall from a Precursor with Nonlinear Symmetry. *Chemistry of Materials* **16**, 1209-1213 (2004).

76. Landskron, K., Hatton, B. D., Perovic, D. D. & Ozin, G. A. Periodic Mesoporous Organosilicas Containing Interconnected [Si(CH2)]3 Rings. *Science (Washington, DC, United States)* **302**, 266-269 (2003).

77. Inagaki, S., Guan, S., Ohsuna, T. & Terasaki, O. An ordered mesoporous organosilica hybrid material with a crystal-like wall structure. *Nature (London, United Kingdom)* **416**, 304-307 (2002).

78. Goto, Y. & Inagaki, S. Synthesis of large-pore phenylene-bridged mesoporous organosilica using triblock copolymer surfactant. *Chemical Communications (Cambridge, United Kingdom)*, 2410-2411 (2002).

79. Matos, J. R., Kruk, M., Mercuri, L. P., Jaroniec, M., Asefa, T., Coombs, N., Ozin, G. A., Kamiyama, T. & Terasaki, O. Periodic Mesoporous Organosilica with Large Cagelike Pores. *Chemistry of Materials* **14**, 1903-1905 (2002).

80. Kuroki, M., Asefa, T., Whitnal, W., Kruk, M., Yoshina-Ishii, C., Jaroniec, M. & Ozin, G. A. Synthesis and Properties of 1,3,5-Benzene Periodic Mesoporous Organosilica (PMO): Novel Aromatic PMO with Three Point Attachments and Unique Thermal Transformations. *Journal of the American Chemical Society* **124**, 13886-13895 (2002).

81. Kapoor, M. P., Yang, Q. & Inagaki, S. Self-Assembly of Biphenylene-Bridged Hybrid Mesoporous Solid with Molecular-Scale Periodicity in the Pore Walls. *Journal of the American Chemical Society* **124**, 15176-15177 (2002).

82. Asefa, T., Kruk, M., MacLachlan, M. J., Coombs, N., Grondey, H., Jaroniec, M. & Ozin, G. A. Novel Bifunctional Periodic Mesoporous Organosilicas, BPMOs: Synthesis, Characterization, Properties and in-Situ Selective Hydroboration-

Alcoholysis Reactions of Functional Groups. *Journal of the American Chemical Society* **123**, 8520-8530 (2001).

83.   Kruk, M., Jaroniec, M., Guan, S. & Inagaki, S. Adsorption and Thermogravimetric Characterization of Mesoporous Materials with Uniform Organic-Inorganic Frameworks. *Journal of Physical Chemistry B* **105**, 681-689 (2001).

84.   Asefa, T., Yoshina-Ishii, C., MacLachlan, M. J. & Ozin, G. A. New nanocomposites: putting organic function \"inside\" the channel walls of periodic mesoporous silica. *Journal of Materials Chemistry* **10**, 1751-1755 (2000).

85.   Huesing, N., Launay, B., Doshi, D. & Kickelbick, G. Mesostructured Silica-Titania Mixed Oxide Thin Films. *Chemistry of Materials* **14**, 2429-2432 (2002).

86.   Yang, P., Zhao, D., Margolese, D. I., Chmelka, B. F. & Stucky, G. D. Block Copolymer Templating Syntheses of Mesoporous Metal Oxides with Large Ordering Lengths and Semicrystalline Framework. *Chemistry of Materials* **11**, 2813-2826 (1999).

87.   Brezesinski, T., Smarsly, B., Iimura, K.-i., Grosso, D., Boissiere, C., Amenitsch, H., Antonietti, M. & Sanchez, C. Self-assembly and crystallization behavior of mesoporous, crystalline HfO2 thin films: A model system for the generation of mesostructured transition-metal oxides. *Small* **1**, 889-898 (2005).

88.   El-Safty, S. A. & Hanaoka, T. Microemulsion Liquid Crystal Templates for Highly Ordered Three-Dimensional Mesoporous Silica Monoliths with Controllable Mesopore Structures. *Chemistry of Materials* **16**, 384-400 (2004).

89.   Feng, P., Bu, X., Stucky, G. D. & Pine, D. J. Monolithic mesoporous silica templated by microemulsion liquid crystals. *Journal of the American Chemical Society* **122**, 994-995 (2000).

90.   Goltner, C. G., Henke, S., Weissenberger, M. C. & Antonietti, M. Mesoporous silica from lyotropic liquid crystal polymer templates. *Angewandte Chemie, International Edition* **37**, 613-616 (1998).

91.   Anderson, M. T., Sawyer, P. S. & Rieker, T. Surfactant-templated silica aerogels. *Microporous and Mesoporous Materials* **20**, 53-65 (1998).

92. Holland, B. T., Abrams, L. & Stein, A. Dual Templating of Macroporous Silicates with Zeolitic Microporous Frameworks. *Journal of the American Chemical Society* **121**, 4308-4309 (1999).

93. Yang, P., Deng, T., Zhao, D., Feng, P., Pine, D., Chmelka, B. F., Whitesides, G. M. & Stucky, G. D. Hierarchically ordered oxides. *Science (Washington, D. C.)* **282**, 2244-2247 (1998).

94. Antonietti, M., Berton, B., Goeltner, C. & Hentze, H. P. Synthesis of mesoporous silica with large pores and bimodal pore size distribution by templating of polymer lattices. *Advanced Materials (Weinheim, Germany)* **10**, 154-159 (1998).

95. Velev, O. D., Jede, T. A., Lobo, R. F. & Lenhoff, A. M. Microstructured porous silica obtained via colloidal crystal templates. *Chemistry of Materials* **10**, 3597-3602 (1998).

96. Wang, H., Huang, L., Wang, Z., Mitra, A. & Yan, Y. Hierarchical zeolite structures with designed shape by gel-casting of colloidal nanocrystal suspensions. *Chemical Communications (Cambridge, United Kingdom)*, 1364-1365 (2001).

97. Liang, C., Dai, S. & Guiochon, G. Use of gel-casting to prepare HPLC monolithic silica columns with uniform mesopores and tunable macrochannels. *Chemical Communications (Cambridge, United Kingdom)*, 2680-2681 (2002).

98. Dong, A., Wang, Y., Tang, Y., Zhang, Y., Ren, N. & Gao, Z. Mechanically stable zeolite monoliths with three-dimensional ordered macropores by the transformation of mesoporous silica spheres. *Advanced Materials (Weinheim, Germany)* **14**, 1506-1510 (2002).

99. Davis, S. A., Burkett, S. L., Mendelson, N. H. & Mann, S. Bacterial templating of ordered macrostructures in silica and silica-surfactant mesophases. *Nature (London)* **385**, 420-423 (1997).

100. Zhao, D., Yang, P., Chmelka, B. F. & Stucky, G. D. Multiphase Assembly of Mesoporous-Macroporous Membranes. *Chemistry of Materials* **11**, 1174-1178 (1999).

101. Ishizuka, N., Minakuchi, H., Nakanishi, K., Soga, N. & Tanaka, N. Designing monolithic double-pore silica for high-speed liquid chromatography. *Journal of Chromatography, A* **797**, 133-137 (1998).

102. Sato, Y., Nakanishi, K., Hirao, K., Jinnai, H., Shibayama, M., Melnichenko, Y. B. & Wignall, G. D. Formation of ordered macropores and templated nanopores in silica sol-gel system incorporated with EO-PO-EO triblock copolymer. *Colloids and Surfaces, A: Physicochemical and Engineering Aspects* **187-188**, 117-122 (2001).

103. Nakanishi, K., Takahashi, R., Nagakane, T., Kitayama, K., Koheiya, N., Shikata, H. & Soga, N. Formation of hierarchical pore structure in silica gel. *Journal of Sol-Gel Science and Technology* **17**, 191-210 (2000).

104. Sattler, K., Gradzielski, M., Mortensen, K. & Hoffmann, H. Influence of surfactant on the gelation of novel ethylene glycol esters of silicic acid. *Berichte der Bunsen-Gesellschaft* **102**, 1544-1547 (1998).

105. Sattler, K. & Hoffmann, H. A novel glycol silicate and its interaction with surfactant for the synthesis of mesoporous silicate. *Progress in Colloid & Polymer Science* **112**, 40-44 (1999).

106. Husing, N. & Schubert, U. Aerogels - airy materials: chemistry, structure, and properties. *Angewandte Chemie, International Edition* **37**, 22-45 (1998).

107. Mukai, S. R., Nishihara, H. & Tamon, H. Formation of monolithic silica gel microhoneycombs (SMHs) using pseudosteady state growth of microstructural ice crystals. *Chemical Communications (Cambridge, United Kingdom)*, 874-875 (2004).

108. Smith, D. M., Stein, D., Anderson, J. M. & Ackerman, W. Preparation of low-density xerogels at ambient pressure. *Journal of Non-Crystalline Solids* **186**, 104-12 (1995).

109. Deshpande, R., Smith, D. M. & Brinker, C. J. 34 pp ((University of New Mexico, USA). Application: WO WO, 1994).

110. Smith, D. M., Deshpande, R. & Brinker, C. J. Preparation of low-density aerogels at ambient pressure. *Materials Research Society Symposium Proceedings* **271**, 567-72 (1992).

111. Smith, D. M., Scherer, G. W. & Anderson, J. M. Shrinkage during drying of silica gel. *Journal of Non-Crystalline Solids* **188**, 191-206 (1995).

112. Goneberg, A. & Verheyden, A. ((Union chimique belge Soc. anon.). BE, 1952).

113. Krimm, H. & Schnell, H. 3 pp ((Farbenfabriken Bayer A.-G.). Application: DE

DE, 1962).

114. Goldberg, E. P. & Powers, E. J. Polycarbonate-siloxane copolymers and blends. *Journal of Polymer Science* **2**, 835-8 (1964).

115. Vaughn, H. A. 6 pp ((General Electric Co.). Application: GB

GB, 1965).

116. Mehrotra, R. C. & Narain, R. P. Reactions of tetramethoxy- and triethoxysilanes with glycols. *Indian Journal of Chemistry* **5**, 444-8 (1967).

117. Gill, I. & Ballesteros, A. Encapsulation of Biologicals within Silicate, Siloxane, and Hybrid Sol-Gel Polymers: An Efficient and Generic Approach. *Journal of the American Chemical Society* **120**, 8587-8598 (1998).

118. Brook, M. A., Brennan, J. D. & Chen, Y. 65 pp ((McMaster University, Can.). Application: WO

WO, 2003).

119. Ivanova, R., Lindman, B. & Alexandridis, P. Evolution in Structural Polymorphism of Pluronic F127 Poly(ethylene oxide)-Poly(propylene oxide) Block Copolymer in Ternary Systems with Water and Pharmaceutically Acceptable Organic Solvents: From \"Glycols\" to \"Oils\". *Langmuir* **16**, 9058-9069 (2000).

120. Alexandridis, P., Ivanova, R. & Lindman, B. Effect of Glycols on the Self-Assembly of Amphiphilic Block Copolymers in Water. 2. Glycol Location in the Microstructure. *Langmuir* **16**, 3676-3689 (2000).

121. Takahashi, R., Sato, S., Sodesawa, T., Suzuki, M. & Ogura, K. Preparation of Microporous Silica Gel by Sol-Gel Process in the Presence of Ethylene Glycol Oligomers. *Bulletin of the Chemical Society of Japan* **73**, 765-774 (2000).

122. Schmidt-Winkel, P., Yang, P., Margolese, D. I., Chmelka, B. F. & Stucky, G. D. Fluoride-induced hierarchical ordering of mesoporous silica in aqueous acid-syntheses. *Advanced Materials (Weinheim, Germany)* **11**, 303-307 (1999).

123. Boissiere, C., Larbot, A., van der Lee, A., Kooyman, P. J. & Prouzet, E. A New Synthesis of Mesoporous MSU-X Silica Controlled by a Two-Step Pathway. *Chemistry of Materials* **12**, 2902-2913 (2000).

124. Liu, Z., Terasaki, O., Ohsuna, T., Hiraga, K., Shin, H. J. & Ryoo, R. An HREM study of channel structures in mesoporous silica SBA-15 and platinum wires produced in the channels. *ChemPhysChem* **2**, 229-231 (2001).

125. Moller, K., Bein, T. & Fischer, R. X. Synthesis of Ordered Mesoporous Methacrylate Hybrid Systems: Hosts for Molecular Polymer Composites. *Chemistry of Materials* **11**, 665-673 (1999).

126. Margolese, D., Melero, J. A., Christiansen, S. C., Chmelka, B. F. & Stucky, G. D. Direct Syntheses of Ordered SBA-15 Mesoporous Silica Containing Sulfonic Acid Groups. *Chemistry of Materials* **12**, 2448-2459 (2000).

127. Yang, C.-M., Zibrowius, B., Schmidt, W. & Schueth, F. Stepwise Removal of the Copolymer Template from Mesopores and Micropores in SBA-15. *Chemistry of Materials* **16**, 2918-2925 (2004).

128. Kawi, S. & Goh, A. H. Supercritical fluid extraction of amine surfactant in hexagonal mesoporous silica (HMS). *Studies in Surface Science and Catalysis* **129**, 131-138 (2000).

129. Kawi, S. Supercritical fluid extraction of surfactant template from MCM-41. *Chemical Communications (Cambridge)*, 1407-1408 (1998).

130. Brandhuber, D., Huesing, N., Raab, C. K., Torma, V. & Peterlik, H. Cellular mesoscopically organized silica monoliths with tailored surface chemistry by one-step drying/extraction/surface modification processes. *Journal of Materials Chemistry* **15**, 1801-1806 (2005).

131. Schwertfeger, F., Frank, D. & Schmidt, M. Hydrophobic waterglass based aerogels without solvent exchange or supercritical drying. *Journal of Non-Crystalline Solids* **225**, 24-29 (1998).

132. Altmann, S. & Pfeiffer, J. Hydrolysis/Condensation Behavior of Alkoxy[(methacryloyloxy)alkyl]silanes: Structure-Reactivity Relations. *Monatshefte fuer Chemie* **134**, 1081-1092 (2003).

133. Anwander, R., Nagl, I., Widenmeyer, M., Engelhardt, G., Groeger, O., Palm, C. & Roeser, T. Surface Characterization and Functionalization of MCM-41 Silicas via Silazane Silylation. *Journal of Physical Chemistry B* **104**, 3532-3544 (2000).

134. Byrne, R. E., Jr. & Johnson, J. B. Unsaturation determination by acid-catalyzed bromination. *Anal. Chem.* **28**, 126-9 (1956).

135. Etienne, M. & Walcarius, A. Analytical investigation of the chemical reactivity and stability of aminopropyl-grafted silica in aqueous medium. *Talanta* **59**, 1173-1188 (2003).

136. Ryu, Y. K., Park, J. K., Lim, H. J. & Park, J. H. Solvatochromic characterization of silica-based stationary phases for liquid chromatography. *Chromatographia* **51**, 567-576 (2000).

137. Nakanishi, K. & Kanamori, K. Organic-inorganic hybrid poly(silsesquioxane) monoliths with controlled macro- and mesopores. *Journal of Materials Chemistry* **15**, 3776-3786 (2005).

138. Brandhuber, D., Peterlik, H. & Huesing, N. Simultaneous drying and chemical modification of hierarchically organized silica monoliths with organofunctional silanes. *Journal of Materials Chemistry* **15**, 3896-3902 (2005).

139. Hatton, B. D., Landskron, K., Whitnall, W., Perovic, D. D. & Ozin, G. A. Spin-coated periodic mesoporous organosilica thin films-towards a new generation of low-dielectric-constant materials. *Advanced Functional Materials* **15**, 823-829 (2005).

140. Landskron, K. & Ozin, G. A. Periodic mesoporous organosilicas: self-assembly from bridged cyclic silsesquioxane precursors. *Angewandte Chemie, International Edition* **44**, 2107-2109 (2005).

141. Wang, W., Zhou, W. & Sayari, A. Synthesis of Periodic Mesoporous Phenylenesilica under Acidic Conditions with Novel Molecular Order in the Pore Walls. *Chemistry of Materials* **15**, 4886-4889 (2003).

142. Asefa, T., Kruk, M., Coombs, N., Grondey, H., MacLachlan, M. J., Jaroniec, M. & Ozin, G. A. Novel Route to Periodic Mesoporous Aminosilicas, PMAs: Ammonolysis of Periodic Mesoporous Organosilicas. *Journal of the American Chemical Society* **125**, 11662-11673 (2003).

143. Kruk, M., Asefa, T., Jaroniec, M. & Ozin, G. A. Metamorphosis of Ordered Mesopores to Micropores: Periodic Silica with Unprecedented Loading of Pendant Reactive Organic Groups Transforms to Periodic Microporous Silica with Tailorable Pore Size. *Journal of the American Chemical Society* **124**, 6383-6392 (2002).

144. Dag, O., Yoshina-Ishii, C., Asefa, T., MacLachlan, M. J., Grondey, H., Coombs, N. & Ozin, G. A. Oriented periodic mesoporous organosilica (PMO) film with organic functionality inside the channel walls. *Advanced Functional Materials* **11**, 213-217 (2001).

145. Asefa, T., Kruk, M., MacLachln, M. J., Coombs, N., Grondey, H., Jaroniec, M. & Ozin, G. A. Sequential hydroboration-alcoholysis and epoxidation-ring opening reactions of vinyl groups in mesoporous vinylsilica. *Advanced Functional Materials* **11**, 447-456 (2001).

146. Guan, S., Inagaki, S., Ohsuna, T. & Terasaki, O. Cubic Hybrid Organic-Inorganic Mesoporous Crystal with a Decaoctahedral Shape. *Journal of the American Chemical Society* **122**, 5660-5661 (2000).

147. Melde, B. J., Holland, B. T., Blanford, C. F. & Stein, A. Mesoporous Sieves with Unified Hybrid Inorganic/Organic Frameworks. *Chemistry of Materials* **11**, 3302-3308 (1999).

148. Lu, Y., Fan, H., Doke, N., Loy, D. A., Assink, R. A., LaVan, D. A. & Brinker, C. J. Evaporation-Induced Self-Assembly of Hybrid Bridged Silsesquioxane Film and Particulate Mesophases with Integral Organic Functionality. *Journal of the American Chemical Society* **122**, 5258-5261 (2000).

149. Ikegami, T. & Tanaka, N. Monolithic columns for high-efficiency HPLC separations. *Current Opinion in Chemical Biology* **8**, 527-533 (2004).

150. Simon, F., Kuzmany, H., Rauf, H., Pichler, T., Bernardi, J., Peterlik, H., Korecz, L., Fulop, F. & Janossy, A. Low temperature fullerene encapsulation in single wall carbon nanotubes: synthesis of NC60SWCNT. *Chemical Physics Letters* **383**, 362-367 (2004).

151. Guinier, A. & Fournet, G. *Small-Angle Scattering of X-rays* (1955).

152. Amenitsch, H., Bernstorff, S. & Laggner, P. High-flux beamline for small-angle x-ray scattering at ELETTRA. *Review of Scientific Instruments* **66**, 1624-6 (1995).

153. Amenitsch, H., Bernstorff, S., Kriechbaum, M., Lombardo, D., Mio, H., Rappolt, M. & Laggner, P. Performance and first results of the ELETTRA high-flux beamline for small-angle X-ray scattering. *Journal of Applied Crystallography* **30**, 872-876 (1997).

154. Steinhart, M., Kriechbaum, M., Pressl, K., Amenitsch, H., Laggner, P. & Bernstorff, S. High-pressure instrument for small- and wide-angle x-ray scattering. II. Time-resolved experiments. *Review of Scientific Instruments* **70**, 1540-1545 (1999).

155. Sing, K. S. W., Everett, D. H., Haul, R. A. W., Moscou, L., Pierotti, R. A., Rouquerol, J. & Siemieniewska, T. Reporting physisorption data for gas/solid systems with special reference to the determination of surface area and porosity (Recommendations 1984). *Pure and Applied Chemistry* **57**, 603-19 (1985).

156. Brunauer, S., Emmett, P. H. & Teller, E. Adsorption of gases in multimolecular layers. *Journal of the American Chemical Society* **60**, 309-19 (1938).

157. Kruk, M., Antochshuk, V., Jaroniec, M. & Sayari, A. New Approach to Evaluate Pore Size Distributions and Surface Areas for Hydrophobic Mesoporous Solids. *Journal of Physical Chemistry B* **103**, 10670-10678 (1999).

158. Jaroniec, M., Kruk, M. & Olivier, J. P. Standard Nitrogen Adsorption Data for Characterization of Nanoporous Silicas. *Langmuir* **15**, 5410-5413 (1999).

159. Barrett, E. P., Joyner, L. G. & Halenda, P. P. The determination of pore volume and area distributions in porous substances. I. Computations from nitrogen isotherms. *Journal of the American Chemical Society* **73**, 373-80 (1951).

160. Ou, D. L. & Seddon, A. B. Structural investigation of ormosils with potential as host photonic materials. *Journal of Sol-Gel Science and Technology* **8**, 139-145 (1997).

Curriculum Vitae

Doris Brandhuber

Alserstrasse 57/12, A-1080 Vienna, Austria

date of birth 22-03-1979 in Wels, Austria

citizenship: Austrian

Higher Education

2003 – 2005 **Studies for the Ph.D. degree in Technical Sciences, Technical Chemistry** at the Vienna University of Technology (TU Vienna), Austria.

Ph.D. thesis on synthesis and characterization of mesoscopically ordered (organo-) silica monoliths with hierarchical pore structures, elaborated at the Institute of Materials Chemistry, TU Vienna, Austria, and at the Department for Inorganic Chemistry I, University of Ulm, Germany, under the guidance of Prof. Nicola Huesing.

1997 – 2003 **Studies for the Diploma Program in Technical Chemistry** at the TU Vienna, with a concentration in Inorganic Chemistry and Technology, graduation with distinction.

Diploma Thesis: "Tubular Inorganic-Lipid Hybrid Structures".

Elaborated at the Center for Organized Matter Chemistry, University of Bristol, UK, supervised by Prof. Stephen Mann in cooperation with Prof. Ulrich Schubert, Institute of Materials Chemistry, TU Vienna. Awarded with a prize for Best Diploma Theses 2003 by the Austrian Chemical Society (GOECH).

School Education

1989 – 1997 **High School** with a focus on languages, BG Schauerstrasse Wels, Austria. Final high school examination passed with distinction.

1985-1989 **Primary School**, VS IV, Wels, Austria.

Professional Experience

2003 to date   **Research Assistant** on a grant of the Volkswagen foundation (05-11/2003), **University Assistant** at the University of Ulm, Germany (05-08/2005) and

Scientific Coworker (wissenschaftliche Mitarbeiterin in Ausbildung) at the TU Vienna (12/2003-04/2005 and 09/2005 to date).

03-06/2003   **Tutor** in the laboratory course for inorganic chemistry at the TU Vienna, Austria.

2000 – 2002   **Scientific Assistant** in the area of mycotoxin analysis for Biomin GTI at the Department for Agrobiotechnology (IFA) Tulln, Austria.

07-08/1999   **Summer Internship**, quality-/production control, Avenarius Agro GmbH Wels, Austria.

Publications

Journal Articles

D. Brandhuber, H. Peterlik, N. Huesing. Small, **2005** in press. *Facile Self-Assembly Processes to Phenylene-bridged Silica Monoliths with Four Levels of Hierarchy.*

D. Brandhuber, V. Torma, C. Raab, H. Peterlik, A. Kulak, N. Huesing, Chem. Mater. **2005**, *17*, 4262-4271. *Glycol-Modified Silanes in the Synthesis of Mesoscopically Organized Silica Monoliths with Hierarchical Porosity.*

D. Brandhuber, H. Peterlik, N. Huesing, *J. Mater. Chem.* **2005**, *15*, 3896-3902. *Simultaneous drying and chemical modification of hierarchically organized silica monoliths with organofunctional silanes.*

D. Brandhuber, N. Huesing, C. K. Raab, V. Torma, H. Peterlik, *J. Mater. Chem.* **2005**, *15*, 1801-1806. *Cellular mesoscopically organized silica monoliths with tailored surface chemistry by one-step drying/extraction/surface modification processes.*

D. Brandhuber, N. Huesing, H. Peterlik, *Mater. Res. Soc. Symp. Proc.* **2005**, *847*, 127-134. *Inorganic-Organic Hybrid Hierarchically Structured Methyl-Modified Silica Monoliths.*

C. Fritscher, N. Huesing, S. Bernstorff, D. Brandhuber. T. Koch, S. Seidler, H. C. Lichtenegger, *J. Synchrotron Radiation* **2005**, *12*, 717-720. *In-situ SAXS study on cationic and non-ionic surfactant liquid crystals using synchrotron radiation.*

M. Elser, T. Berger, J. Bernardi, D. Brandhuber, O. Diwald, E. Knözinger. Submitted to Ang. Chem. Int. Ed. *When nanoparticles come together: electron centers in adjoined TiO$_2$ nanocrystals.*

Talks

Hierarchically Structured Organo-Silica Monoliths.

D. Brandhuber, N. Huesing, 11. Österreichische Chemietage 2005, Leoben, Austria.

Hierarchically Structured Silica Monoliths.

D. Brandhuber, Institute seminar at the Max Planck Institute of Colloids and Interfaces in Golm, Germany, 23-02-2005, invited by G. Garnweitner and Prof. M. Antonietti.

Mesostructured Silica Monoliths.

D. Brandhuber, V. Torma, H. Peterlik, N. Huesing, IMMS Cape Town 2004, Cape Town, South Africa.

Nanostrukturierte Monolithe aus Siliziumdioxid.

D. Brandhuber, WACÖ 2004, Graz, Austria.

Poster Presentations

Periodically Mesostructured Organosilica Monoliths with Hierarchical Build-Up.

D. Brandhuber, N. Huesing, ISOS XIV 2005, Wuerzburg, Germany, awarded with a poster prize.

Periodically Mesostructured Organosilica Monoliths with Hierarchical Build-Up.

D. Brandhuber, N. Huesing, EMRS Spring Meeting 2005, Strasbourg, France.

Templating of Organic/Inorganic Hybrid Materials.

C. Fritscher, H. C. Lichtenegger, J. Stampfl, N. Huesing, R. Liska, R. Infuehr, T. Koch, D. Brandhuber, S. Bernsdorff, S. Seidler, EMRS Spring Meeting 2005, Strasbourg, France.

Hierarchically Structured Silica Monoliths Carrying Organic Functions.

D. Brandhuber, N. Huesing, MRS Fall Meeting 2004, Boston, USA.

In-situ SAXS investigations on the formation of mesostructured spider-web like silica monoliths.

D. Brandhuber, N. Huesing, , V. Torma, H. Peterlik, S. Bernstorff, M. Steinhart, M. Kriechbaum, SAXS-Symposium 2004, Vienna, Austria.

Hierarchically nanostructured silica films carrying a chiral information.

D. Brandhuber, N. Huesing, U. Lavrencic-Stangar, H.-A. Wagenknecht, P. Kaden, 1st International Symposium on Complex Materials by the Volkswagen-Stiftung 2003, Bremen, Germany.

Synthesis of amphiphilic glycosides for the preparation of chirally imprinted nanostructured silica films.

P. Kaden, D. Brandhuber, N. Hüsing, U. Lavrencic-Stangar, H.-A. Wagenknecht, 1st International Symposium on Complex Materials by the Volkswagen-Stiftung 2003, Bremen, Germany.

Diploma Thesis

Tubular Inorganic-Lipid Hybrid Structures. 2003. Awarded with a prize for Best Diploma Theses 2003 by the Austrian Chemical Society (GOECH).

Etc.

N. Hüsing, D. Brandhuber, V. Torma, C. Raab, H. Peterlik, S. Bernstorff, M. Kriechbaum, M. Steinhardt, Elettra Highlight 2003. *In-situ SAXS Investigations on the Formation of Mesostructured Spider-Web Like Silica Monoliths.*

N. Huesing, D. Brandhuber, V. Torma, C. Raab, H. Peterlik. Organosilicon Chemistry VI, Eds. Norbert Auner, Johann Weis, Wiley-VCH, Weinheim, (2005), 955-961. *Polyol-modified silanes as precursors for mesostructured silica monoliths.*

N. Huesing, D. Brandhuber, C. Raab, V. Torma, H. Peterlik, M. Steinhart, M. Kriechbaum, S. Bernstorff. Annual report 2003, Austrian SAXS beamline at Elettra (2004) 104-106. *In-situ investigations on the formation of mesostructured spiderweb like silica monoliths and their drying in supercritical carbon dioxide.*